ALPHA-PARTICLE EXCITED X-RAY ANALYSIS

X-RAY EMISSION ANALYSIS
USING
RADIOISOTOPIC ALPHA-PARTICLE EXCITATION

by

ROBERT ROBERTSON, M.Sc.

A Thesis

Submitted to the School of Graduate Studies
in Partial Fulfilment of the Requirements
for the Degree
Doctor of Philosophy

McMaster University

September 1977

DOCTOR OF PHILOSOPHY (1977) MCMASTER UNIVERSITY

(Chemistry) Hamilton, Ontario.

TITLE: X-Ray Emission Analysis using Radioisotopic Alpha-Particle Excitation

AUTHOR: Robert Robertson
B.Sc. (McMaster University)
M.Sc. (University of Surrey)

SUPERVISOR: Professor K. Fritze

NUMBER OF PAGES: xiv; 169

ABSTRACT

The combined capabilities of alpha-particle emitting isotopic excitation sources and modern semiconductor detectors are investigated with a view to extending the light-element range of radioisotope-based X-ray emission analysis.

The construction and performance of a windowless low-energy X-ray spectrometer designed around a lithium-drifted silicon detector and a ^{210}Po source are discussed. It is shown that under the conditions used low-energy X-ray emission and detection are greatly favoured.

Measurements of relative cross-sections for the production of X-rays by $\sim$5.2 MeV alpha-particles in elements from oxygen to iron are reported. The results for elements of $Z>16$ are in good agreement with those predicted from the scaling of equal velocity proton values but show large positive deviations for elements of $Z<16$.

Investigative applications of the spectrometer to quantitative analyses of blast-furnace slags, iron ores and silicate rocks for oxygen, silicon, sulpher, calcium and iron are described.

The future prospects of radioisotopic alpha-particle X-ray excitation methods are surveyed.

ACKNOWLEDGEMENTS

The author expresses his appreciation to Dr. Klaus Fritze and the members of his Supervisory Committee, Drs. O.E. Hileman, T.J. Kennett and R.H. McNutt for their critical comments and constructive advice throughout this work.

He also thanks Dr. Y. Peng for help in preparing the targets used in the cross-section measurements; and Richard Doelle and Bill Van De Vrande of Dominion Foundries and Steel Limited for providing some of the samples for analysis.

The research was supported financially by the National Research Council of Canada.

TABLE OF CONTENTS

LIST OF FIGURES

LIST OF FIGURES

(cont'd)

LIST OF FIGURES

(cont'd)

LIST OF TABLES

LIST OF TABLES

(cont'd)

LIST OF TABLES

(cont'd)

CHAPTER 1

GENERAL PROPOSALS AND BACKGROUND

1.1 Introduction

Determinations of elemental composition are important in the characterization of materials and are of major interest in analytical chemistry. The required analyses used to be performed almost entirely by chemical means through manual operations; but in response to modern demands an array of instrumental methods based largely on physical phenomena have more recently emerged. Some of the best established and most powerful of the newer procedures are those which fall under the general heading "X-ray Secondary-Emission Spectrometry".* They rely upon measurements of the energies and intensities of characteristic X-rays emitted from materials bombarded by suitable forms of ionizing radiation. It is a particular aspect of these methods, their weakness in the low-energy region of the X-ray spectrum, which is the concern of this thesis.

Over the last two decades the instrumentation associated with X-ray emission analysis has been

---

* Often called "X-ray Fluorescence Spectrometry" (XRF).

extensively developed and is now widely and routinely applied. The present various forms, which differ mainly in their means of X-ray excitation and detection, are capable of fast, sensitive and non-destructive measurements of most elements in the periodic table. However, as a group they tend to be weak towards the low atomic-number region. Especially ineffective in this area are the sub-class of simple and inexpensive instruments based on X-ray excitation by the emissions from radio-isotopes. Although these are useful in many circumstances, with few exceptions they have proven practically useless for the elements below silicon. This is unfortunate, since there are many materials of scientific and commercial interest consisting mainly of light elements. And their analysis through such equipment may be otherwise advantageous.

Some of the reasons for the poor low-energy performances of X-ray spectrometric methods are associated with inefficiencies in the systems used for X-ray production and detection. It is through improvements in these areas that progress in light-element analysis may be expected. For radioisotope-based methods in this regard, alpha-

particle emitting isotopes are attractive for X-ray production, since it is known that heavy charged-particles have substantial advantages over the normally utilised photons and electrons in efficiently stimulating low-energy X-ray emission. But the few attempts in this direction have been greatly hampered by detector-related problems such as inadequate energy-resolution and X-ray attenuation in detector windows. Recent advances in semiconductor X-ray detector technology promise to alleviate these problems and lead to the general proposals of the present work:

1. To investigate the combined capabilities of alpha-particle emitting isotopic excitation sources and modern semiconductor detectors in the low-energy region of the X-ray spectrum.

2. Through various applications of this combination to take steps in extending the light-element range of radioisotope-based X-ray emission analysis.

The remainder of this chapter is written with a view to putting the above proposals and the later described experimental work into context. Much of the

material presented has to do with the basic physics or current practice of X-ray spectrometry and is quite general in nature. When this is the case no specific references are given. At this juncture the reader is recommended to texts dealing with the fundamentals of radiation physics and X-ray analysis; the books by Evans (1), Birks (2), Woldseth (3) and Bertin (4) are especially useful. The latter author also gives an interesting and concise treatment of the history of X-ray spectrometry.

1.2 X-radiation and its production processes

1.2.1 Characteristic X-rays :

Vacancies in inner electron-shells may be created by bombarding atoms with ionizing radiation such as energetic photons, electrons and heavy charged-particles (see Fig. 1). The subsequent filling of the vacancies by electrons cascading from outer shells requires the dissipation of discrete amounts of energy equal to the difference in binding-energies between the two shells involved in electron transfer. There are two competing mechanisms whereby the excess energy may be lost; both

Figure 1. Schematic representation of X-ray excitation.

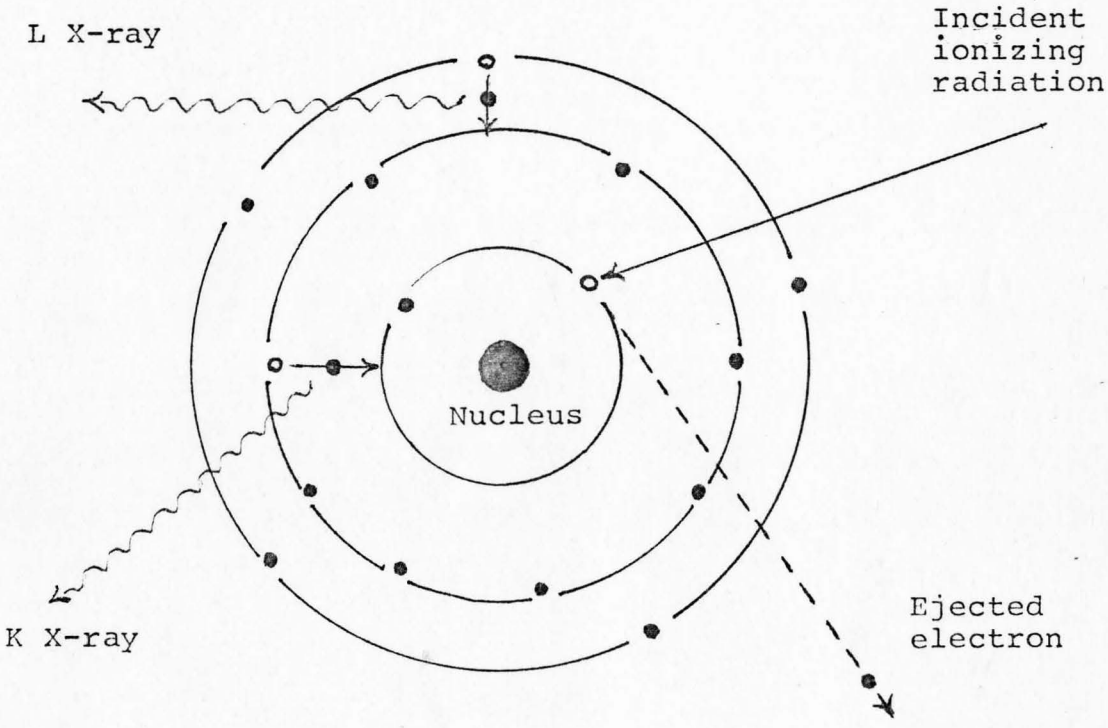

are essentially independent of the means of vacancy formation. One is Auger-electron emission, where an electron, bound in a shell outside that with the vacancy, is ejected with kinetic energy equal to the amount required to be lost minus its binding-energy. The complementary process, which is the one of interest in X-ray spectrometry, is characteristic X-ray emission. The energy of the emitted X-ray photon equals the full amount of excess energy and is identifiable with the element whose atom was originally ionized. Note that neither of the above processes has any directional preference.

The probability of characteristic X-ray emission is a property of the electron-shell in which a vacancy occurs and is called the "fluorescence yield", ω. It approaches unity for the innermost shells of the heavy elements but falls off rapidly with atomic-number and towards the outer shells. For the K shell the atomic-number (Z) dependence is $\sim Z^4$. X-ray emission by the light elements and low-energy X-ray emission in general is not favoured (see Table 1).

TABLE 1

Some X-ray energies (keV) and fluorescence yields*

(adapted from Refs. 3 and 4)

Atomic Number	Element	K series					L series				
		ω_K	$K_{\beta 2}$	$K_{\beta 1}$	$K_{\alpha 1}$	$K_{\alpha 2}$	$\bar{\omega}_L$	$L_{\beta 2}$	$L_{\beta 1}$	$L_{\alpha 1}$	$L_{\alpha 2}$
4	Be	4.5×10^{-4}			0.110						
6	C	2.0×10^{-3}			0.282						
8	O	5.8×10^{-3}			0.523						
9	F	9.0×10^{-3}			0.677						
11	Na	1.9×10^{-2}		1.067	1.041						
12	Mg	2.7×10^{-2}		1.297	1.254						
13	Al	3.6×10^{-2}		1.553	1.487	1.486					
14	Si	4.7×10^{-2}		1.832	1.740	1.739					
15	P	6.0×10^{-2}		2.136	2.015	2.014					
16	S	7.6×10^{-2}		2.464	2.308	2.306					
17	Cl	7.4×10^{-2}		2.815	2.622	2.621					
18	Ar	1.2×10^{-1}		3.192	2.957	2.955					
19	K	1.4×10^{-1}		3.589	3.313	3.310					
20	Ca	1.6×10^{-1}		4.012	3.691	3.688	1×10^{-3}	0.344		0.341	
23	V	2.5×10^{-1}		5.427	4.952	4.944	2×10^{-3}	0.519		0.510	
25	Mn	3.1×10^{-1}		6.490	5.898	5.887	3×10^{-3}	0.647		0.636	
26	Fe	3.5×10^{-1}		7.057	6.403	6.390	3×10^{-3}	0.717		0.704	
47	Ag	8.3×10^{-1}	25.454	24.942	22.988	21.988	6.3×10^{-3}	3.348	3.151	2.984	2.978
79	Au	9.6×10^{-1}	80.165	77.968	68.794	66.980	3.6×10^{-1}	11.582	11.439	9.711	9.625
82	Pb	9.7×10^{-1}	87.343	84.922	74.957	72.794	3.9×10^{-1}	12.620	12.611	10.549	10.448

* The table includes most of the X-rays referred to in this work

There is a well defined relationship between characteristic X-ray energies and the atomic-numbers of the corresponding elements. This relationship was first quantitatively described through the classic researches of Moseley (5) and lays the foundation for X-ray spectroscopy. For the K and L series, which are of most interest here, the energies are approximately proportional to Z^2, and for the stable elements, fall in the 0-90 keV and 0-16 keV ranges respectively (see Table 1). It will be noted that the light elements yield very low-energy X-rays which are easily attenuated in matter, including the materials from which they arise (ie. self-absorption).

The probability of inner-shell ionization of a target atom depends upon the nature and energy (E) of the incident radiation, and the atomic-number (Z) of the atom. For incident photons where the major interaction mode is the photo-electric effect, the probability of ionization in the K and L shells is approximately proportional to $Z^4E^{-3.5}$ (note E must be greater than the electron binding-energies, i.e. absorption edges, of the particular shells of the elements considered). Thus, photons of given energy favour X-ray production in the heavier elements; and for a given shell of a given element, X-ray excitation is favoured by photons close in energy to the absorption edge.

Charged projectiles such as electrons, protons, alpha-particles etc. interact with bound electrons in a more complex way. Theoretical descriptions of the processes are not complete but the main modes of vacancy formation are a) direct coulombic interactions, b) indirect coulombic interactions through secondary electrons, and c) photo-electric ionization through bremsstrahlung production (see subsection 1.2.2). No simple and generally applicable expressions analogous to the one for photons may be given in this case to describe the probabilities of vacancy formation. However, at the energies most effectively used in X-ray emission analysis, a few tens of keV for electrons and a few MeV for heavy ions, they have a direct dependence upon particle energy and a very strong inverse dependence upon target atomic-number (see Fig. 2). In this sense the use of charged particles for X-ray excitation is complementary to that of photons; it offsets the diminishing fluorescence yields and favours low-energy X-ray production.

Figure 2. X-ray production by various kinds of ionizing radiation. *

(a) Ionization cross-sections vs. atomic-number of target.

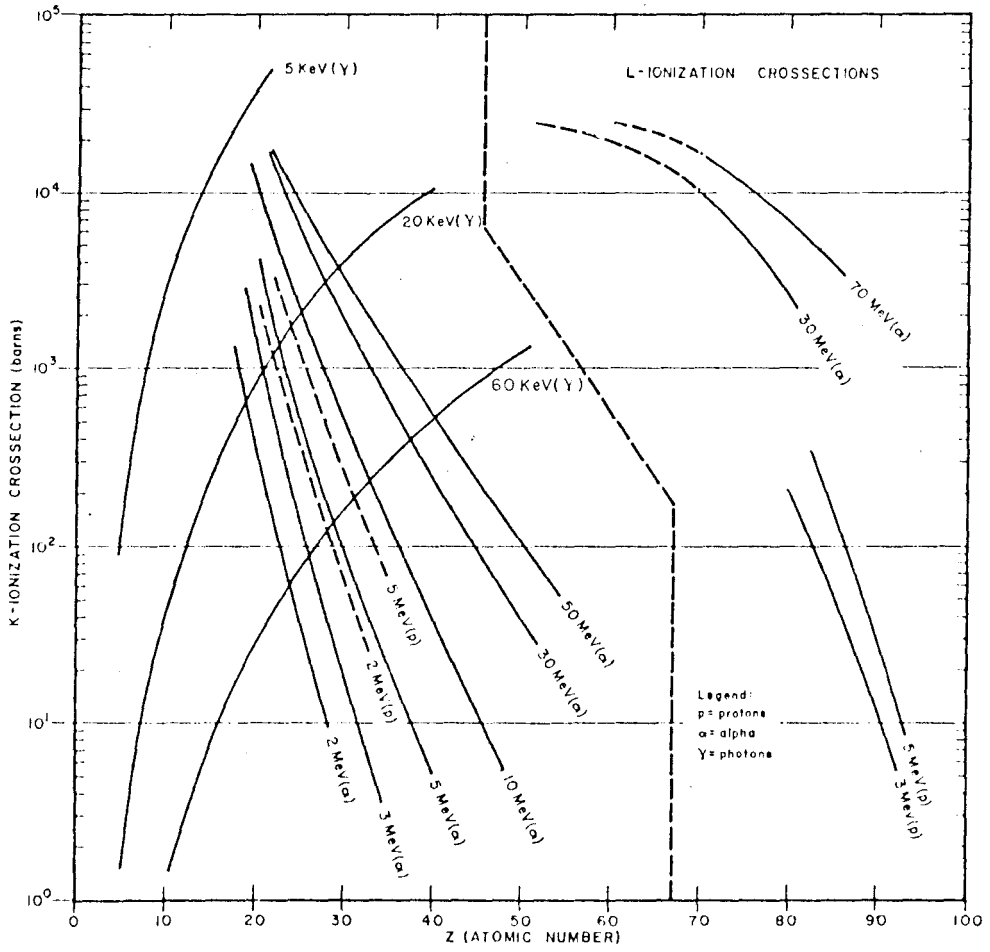

* Adapted from reference (3).

(b) X-ray yields vs. projectile energy.

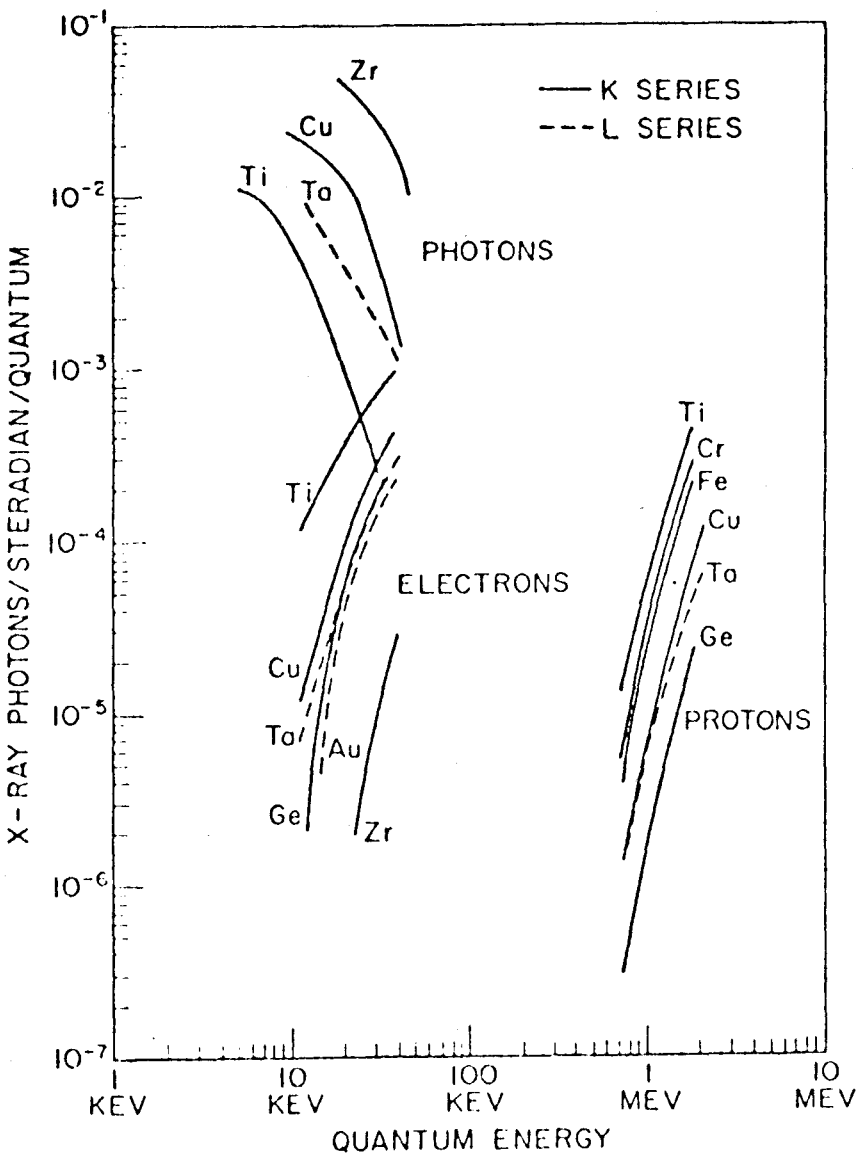

1.2.2 Bremsstrahlung (braking radiation):

This kind of X-radiation, known also as "white" or "continuous" radiation, is observed when materials are irradiated with energetic charged particles. It is generally considered to arise from the acceleration of the particles within the electric fields of atomic nuclei. The continuum ranges from zero energy up to a maximum (end-point energy) defined by the incident particle energy. For very thin targets which do not appreciably degrade the incident particle energy, the intensity distribution of the continuum is virtually flat. For thick targets therefore, the intensity of bremsstrahlung (as produced) is at a maximum at zero energy; but preferential attenuation of the low-energy part of the continuum by the target material results in the emergent radiation having an intensity maximum at some higher energy.

Bremsstrahlung represents a major fraction of the total X-radiation emitted from thick targets when the irradiating particles are electrons and is a significant source of spectral background with conventional X-ray spectrometers where X-ray tubes and electron columns are used as excitation sources. However, the probability of bremsstrahlung production varies with the mass (m) and charge (z) of the incident particle and the atomic-number (Z) of the target material according to $(zZ/m)^2$. It will be seen that energy-

losses to the bremsstrahlung continuum, compared to ionization losses (which may lead to characteristic X-ray emission), are reduced by about 10^6 for heavy particles such as protons and alpha particles relative to electrons of the same velocity. This is of significance in terms of low background in analytical work where heavy particles are used as excitation sources, although in this case bremsstrahlung from secondary electrons is a nuisance at the very low-energy end of the X-ray spectrum (see section 2.4).

1.3 Conventional X-ray emission analysis

By far the greatest number of X-ray emission analyses are carried out through instruments employing electronically produced photon-and electron- excitation radiation such as the outputs from X-ray tubes and electron columns. Although these instruments are in much higher cost and performance categories than radioisotope-based equipment, it will be useful to outline their operations and capabilities; and thereby introduce certain aspects of excitation systems, detection systems and other topics which will be referred to later.

1.3.1 Instrumentation and general performance:

A. Detection systems:

Most X-ray spectrometers as schematically represented in Fig. 3 may be divided into two broad classes, "wavelength-dispersive" and "energy-dispersive",* according to how the secondary X-radiation is spectrally resolved and detected. This classification is independent of the excitation (primary) radiation used.

Wavelength-dispersion is the original method of X-ray spectral analysis having been used since the first decade of this century. It relies upon sequential observation of the various spectral components after their differential angular dispersion by a diffracting crystal according to their wavelengths and the Bragg diffraction law. Backed by scintillation or gas-proportional detectors, which serve mainly to discriminate against high order diffractions, it still serves as the basis for instruments which perform the great majority of X-ray emission analyses.

---

*"energy-dispersive" is poor terminology but is retained here in accordance with current practice; it excludes the small and relatively unimportant class of energy-discriminating devices based on absorption filters.

Figure 3. Schematic diagrams of the main types of analytical X-ray spectrometer.

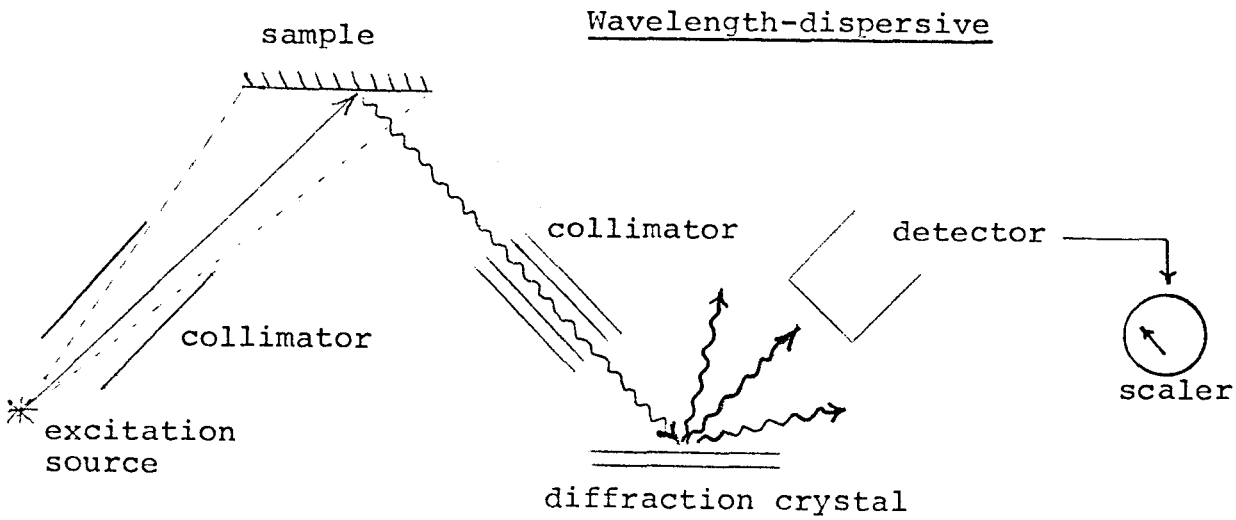

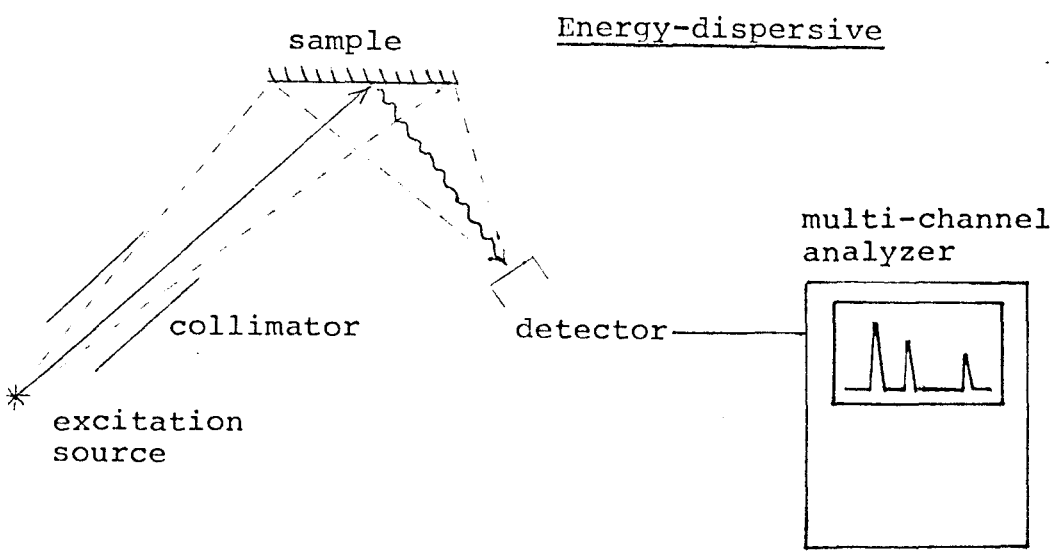

Through appropriate crystal selection these have very good resolving power and are generally analytically superior to alternative types (see Fig. 4). However, because of their sequential nature, they are inherently unsuitable for qualitative analysis or for quantitative analysis which requires the prior identification of sample components. Also, because of the need for X-ray collimation, the poor reflectivity of crystals, and their two component nature, they have poor detection efficiency and need very intense excitation sources. (Their use with radioisotopes is not practical).

Energy-dispersive devices such as gas-proportional, scintillation and semiconductor photon detectors may be used to view the full X-ray spectrum directly without the intervention of a diffraction mechanism. They operate by delivering a pulse proportional in amplitude to the energy absorbed, which ideally corresponds to the total energy of the X-ray photon. Although of inferior resolution and general analytical performance (especially at low X-ray energies), they have certain advantages over wavelength-dispersive systems. They are cheaper, more compact, have no moving parts (i.e. no precise mechanical alignments

Figure 4. Resolutions of energy-dispersive detectors and wavelength-dispersive crystals.*

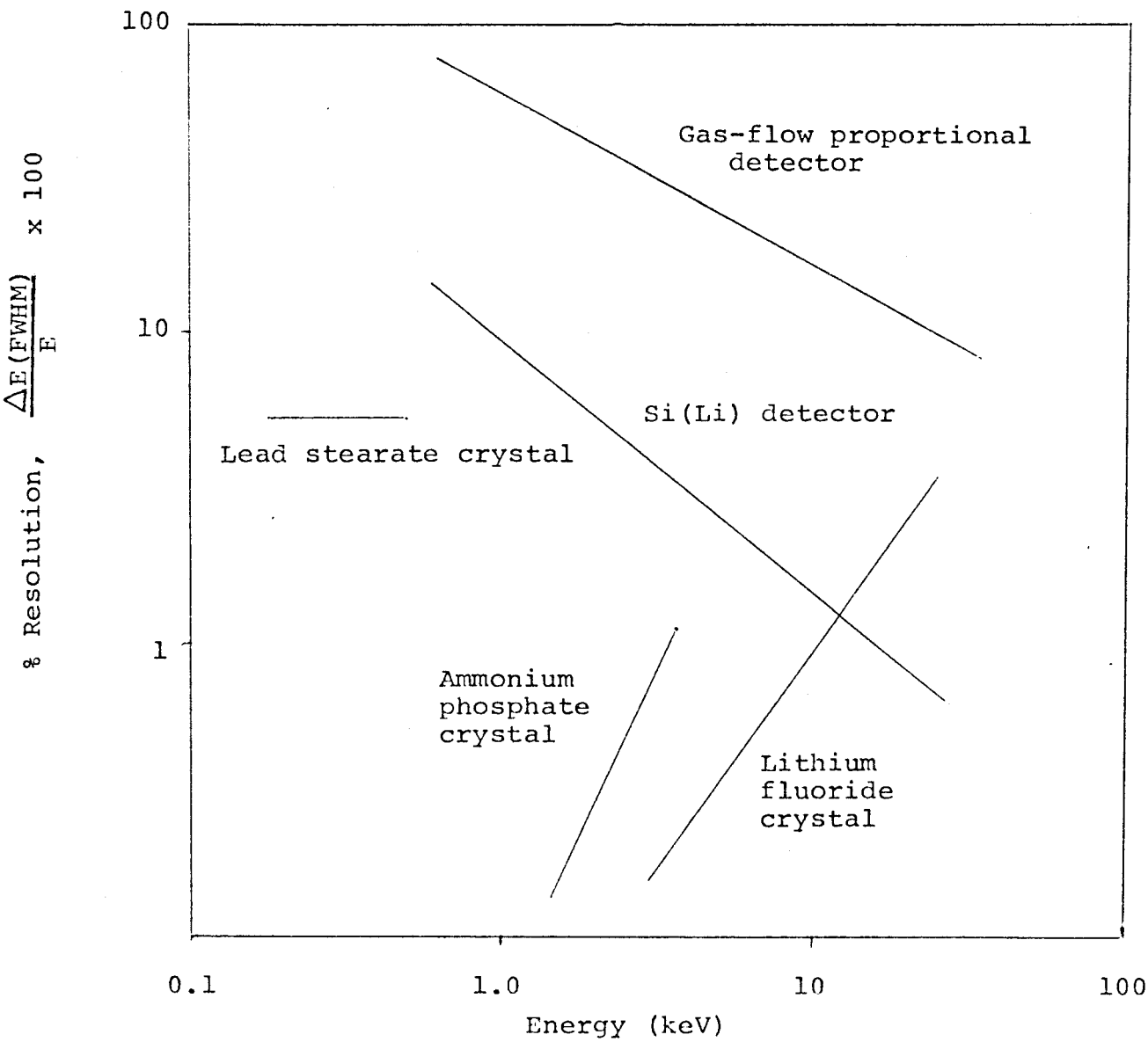

* Adapted from: R. Fitzgerald and P. Gantzel, in Energy-Dispersion X-ray Analysis, ASTM STP 485, pp. 3-35, American society for Testing and Materials, Philadelphia (1971).

needed), in principle permit all regions of the X-ray spectrum to be registered simultaneously, have high intrinsic efficiency (proportional counter excepted), and allow high geometric efficiency. These factors make for low-cost, simple and convenient instrumentation featuring speedy data-acquisition,* reduced intensity requirements on excitation sources and easy identification of unknown sample components.

---

* This point is offset to some degree by the count-rate capabilities of the electronics required for pulse processing in energy-dispersion. Even with pulse pile-up rejectors, the amplifiers and multi-channel analysers used are limited to count-rates from the full spectrum of $\sim$ 50,000 cps (counts per second); and most of the pulses processed are useless in terms of information content. This is to be contrasted to wavelength-dispersive systems requiring simple scaling electronics which may easily handle 100,000 cps attributable to a single spectral peak.

Until 1966, when high resolution semiconductor detectors suitable for X-ray work were first applied by Bowman et al. (6), energy-dispersion was usefully restricted to applications involving simple spectra or the use of low-intensity excitation sources such as radioisotopes. Since then, however, it has been of greatly increasing importance and popularity for more general applications and has had a major impact in reducing instrument costs while maintaining a high standard of performance. Through advances in the design and manufacture of semiconductor detectors and their pre-amplifier circuits, energy-dispersive systems are now competitive in some circumstances with wavelength-dispersive systems, especially for elements of $Z > 25$ (Mn) where resolution requirements are not so stringent (7). Particularly effective, although not yet commercially available, are lithium-drifted silicon (Si(Li)) detectors featuring the anti-coincidence guard-ring invented by Goulding et al. (8).

B. Excitation systems:

Standard X-ray "fluorescence" spectrometers, which primarily are instruments intended for bulk-sample analysis,

employ X-ray tubes for the stimulation of sample X-rays. A typical tube output consists of an intense bremsstrahlung continuum upon which are superimposed the characteristic lines of the anode material. Thus, radiation is produced to cover a wide range of the X-ray spectrum, in the sense that there is usually a component close to the absorption edges of interest. The continuum, besides its positive contribution, also acts as a nuisance through inelastic and elastic scattering events which take place in the sample. It is "reflected" back into the detection system, although distorted and greatly reduced in intensity, and generally is the major source of spectral background.

Despite the detrimental influence of the scattered radiation, X-ray tubes, through proper selection of target-elements, filters and applied voltage and current, offer great analytical sensitivity and elemental range. Determinations at the sub part-per-million level are possible in suitable circumstances, the best results usually being attained with wavelength-dispersive means of spectral analysis.

X-ray stimulation by energetic electrons is the major alternative to photon excitation and is the basis of instruments such as the electron probe micro-analyzer

(electron micro-probe). These instruments allow finely focussed (< 1 μm diameter) intense beams of electrons to be made available at the sample position for X-ray excitation. The electron energies and currents may be selected to optimise sensitivities for particular elements and specimens.

When electron column instruments are operated in their design mode, i.e. micro-analysis, absolute quantities of elements on the order of 10^{-14} to 10^{-12}g may be measured under favourable conditions. For bulk-sample analysis a defocussed beam may be used; but sensitivities in terms of concentration, typically a few-hundred parts-per-million, are generally inferior by a factor of at least ten compared to good X-ray tube excitation systems. The main reason for this is bremsstrahlung background produced directly in the sample. Penetration is also inferior to that obtained using photons and detracts from the quality of the analyses - although at low X-ray energies it may be emergent radiation which is the limiting factor in this respect. The major impact of electron-excitation has been in the study of surfaces and sample micro-features.

1.3.2 Light-element performance:

There are several fundamental and technical factors which militate against good quality analyses towards low X-ray energies: a) diminishing fluorescence yields, b) severe attenuation of soft X-rays within samples and detector windows, and along their optical paths (which often necessitate instrument operation under vacuum), c) with photons - poor excitation efficiency, and d) high spectral background - this is especially troublesome with electron-excitation where the rising bremsstrahlung continuum (at source, within the target) runs against the favourable ionization efficiencies.

The above factors negatively influence signal intensity or signal-to-noise ratio. To make the situation worse there are other considerations which create difficulties - especially at low-energies - in quantitatively relating signal intensity to analyte concentration. Examples of these are particle-size and absorption-enhancement effects (see section 4.3), and the energy-convergence of X-ray lines in the region. The latter puts a premium on detection-system resolution and is especially limiting with energy-dispersive systems.

The result is that systems using photon or electron excitation have analytical performances which progressively and steeply decline with atomic-number of the analyte. Trace analysis is generally difficult for elements lighter than calcium; and sodium, if present in sufficient concentration (generally > 1%), is the lightest element routinely measurable with even the better instruments and most sophisticated means of data analysis. Determinations of elements below sodium may be considered a field apart requiring great care and specialised equipment. References 9-11 point out the problems met in such work and describe some of the exceptional efforts made in accomplishing successful results for elements as light as boron.

1.4 Radioisotope induced X-ray emission*

Certain radioisotopes have proven useful as low-power sources of photons and electrons for purposes of X-ray excitation in bulk-sample X-ray emission analysis. Simple instruments based on these have advantages over other types in terms of low-cost, convenience, portability and reliability. Their designs, properties and applications have been reviewed by Rhodes (12). As a practical necessity all are based on energy-dispersive means of spectral analysis.

The preferred radioisotopes are those which, a) possess a long half-life, b) emit monoenergetic radiation of useful energy, c) decay to a stable or favourable daughter nuclide and, d) are reasonably accessible through convenient nuclear reactions. Needless to say there is no isotope which perfectly fulfils all of these criteria. Rhodes (12) has made a list of those which come close.

---

* The use of alpha-particle emitting isotopes is discussed in section 1.6.

Beta-, gamma- and X-radiation yielding isotopes have been of most service. Direct beta-radiation is not of significant analytical interest, mainly because of background bremsstrahlung production, but also because of the possibility of electrons back-scattering into the detection system (this latter point is of importance at low X-ray energies where thin-windowed detectors must be used). Beta-particle emitters such as ^{3}H and ^{147}Pm have been employed in "miniature X-ray tubes", i.e. to generate secondary photons. Early work was concentrated on this kind of source. They have the disadvantage of producing a continuous scattered background and their use has been generally discontinued in favour of direct photon-emitting isotopes. By far the most popular isotopes are certain gamma-ray and X-ray emitters, especially ^{55}Fe, ^{109}Cd and ^{241}Am whose principle photon emissions are at 5.9, 22 and 60 keV and span most of the energy range of interest. They may directly irradiate samples or be employed in a secondary mode to generate the characteristic X-rays of a target element. Conditions may be thus optimized for the determination of most elements.

Measurements to the trace level may be sometimes made using semiconductor detectors. References 13-15 describe some of the more recent applications of radioisotopes in X-ray emission analysis.

At low X-ray energies the photon and beta-particle emitting isotopes suffer from essentially the same drawbacks as their more conventional counterparts, X-ray tubes and electron columns (see subsection 1.3.3). But unlike these, they lack the power to be used with wavelength-dispersive detection systems which otherwise would help to maintain an acceptable signal-to-noise ratio (in any case this would defeat the advantages of radioisotope-based instruments). The result is that the usual radioisotopic sources rapidly lose their effectiveness with decreasing atomic number of the analyte. Of 116 analyses involving 32 elements cited by Rhodes (12), only one, for aluminum and aided by ^{210}Po alpha-particle excitation, was concerned with an element lighter than silicon. It would seem that a low-energy monochromatic photon-emitter would offer the best prospects in improving the situation. But there is no suitable isotope yielding such radiation below the 5.9 keV manganese K-alpha X-rays from ^{55}Fe.

1.5 Ion induced X-ray emission

It has long been known that X-ray emission can be induced by bombarding materials with heavy charged-particles. Chadwick (16) observed characteristic X-rays in 1912 using alpha-particles*. In 1928 and 1929 Bothe and Franz (17,18) published studies of alpha-particle induced K, L and M X-ray emission for some elements of $Z > 12$. Henneberg (19) did theoretical work on the subject in 1933. Mainly since the early nineteen-fifties a large number of measurements have been made of ion-induced X-ray yields and cross-sections using nuclear-particle accelerators. These have been done chiefly with protons but also with ^{2}H, ^{3}He, ^{4}He and heavier ions. Review articles including theoretical treatments of the ionization process have appeared periodically: by Merzbacher and Lewis (20) in 1958, by Khan et al. (21) in 1965 and by Garcia et al. (22) in 1973. A compilation of cross-sections for K-shell ionization by light-ion impact was made in 1973 by Rutledge and Watson (23).

---

* In this thesis a distinction is made between alpha-particles (from radioisotopic sources) and ^{4}He ions (from accelerators).

In 1975 Crasemann (24) edited an overall view of atomic inner-shell ionization processes including treatments of ion-induced X-ray emission.

All of this work has shown that the inner-shell ionization cross-sections for impact by heavy charged-particles of a few MeV are large and strongly favour low-energy X-ray production. This fact, together with low bremsstrahlung production upon their absorption in matter, makes heavy particles (in contrast to electrons) potentially very useful in low-energy X-ray emission analysis.

During the late nineteen-sixties X-ray emission induced by accelerator-produced ions found some applications to surface and ion-implantation studies, including the estimation of oxide thicknesses. These studies are exemplified by the work of Khan et al. (25), Hart et al. (26) and Cairns et al. (27). They entailed the measurement of fairly simple spectra using proportional detectors.

In 1970 Johansson et al. (28) introduced the combination of nuclear accelerators and semiconductor detectors to elemental analysis. This marked the beginning of a broad application of "particle-induced

X-ray emission (PIXE)" to analytical problems. Most PIXE work has been done with protons and ^{4}He ions and virtually all of it using Si(Li) detectors. Folkmann (29) in 1975 and Johansson and Johansson (30) in 1976 reviewed the field and in August 1976 the first international conference on the subject took place in Sweden (31). The main advantage of PIXE analysis is its excellent absolute sensitivity combined with good concentration sensitivity - a combination of the qualities of standard X-ray fluorescence spectrometers and electron micro-probes - making it a powerful tool for the trace analysis of small samples. Its major disadvantage is the scarcity of accelerators.

Most PIXE applications have been to trace-analysis for the heavier elements in samples of environmental and bio-medical interest. There appears to have been no systematic X-ray analytical work using accelerator-produced ions on elements lighter than sulphur. One probable reason for this is the general problem of dealing with low-energy X-rays. Another is the spectral background at low energies from secondary-electron bremsstrahlung and incomplete charge-collection within detectors. This background

raises sensitivities for the light elements to the point where more readily available methods are competitive.

1.6 Radioisotopic alpha-particle induced X-ray emission

Several authors have recognized the potential of alpha-particle emitting isotopes in X-ray emission elemental analysis. They offer some of the advantages of accelerator-produced ions but at low cost. Although there are special hazards involved in their handling, their use is attractive for problems suitable for simple X-ray emission methods but not amenable to the usually employed radioisotopes.

In 1964 Robert (32) employed ^{210}Po within a general study of radioisotopic excitation methods for the light elements. This work concentrated on the production and detection of X-rays from pure elements or compounds; no quantitative analysis was attempted. Imamura et al. (33) in 1965 described a spectrometer based on excitation simultaneously by alpha-particles from ^{210}Po and secondary photons from $^{3}H/Zr$. Satisfactory results for aluminum

and some heavier elements in preliminary analyses of cement raw-mixes were claimed. The most extensive investigation in the area has been by Sellers et al. (34, 35, 36) from 1966 to 1968. They examined the characteristics of various ^{210}Po and ^{242}Cm sources and suggested several applications. The most interesting one in the present context was a proposal for lunar and planetary surface analysis. This aspect of the work was performed in collaboration with others as part of the American space program. Adler and Trombka (37) elaborated upon it in a general survey of methods of extraterrestrial geochemical exploration. They presented results for magnesium and some heavier elements in a meteorite sample. The accuracy generally was not good but was considered satisfactory for the purpose.

All of the above cited work was carried out with proportional detectors. It was consequently limited by inadequate spectral resolution and by X-ray absorption in detector windows. In 1972 Franzgrote (38) described the use of ^{244}Cm* in the analysis of silicate rocks using

---

* ^{242}Cm and ^{244}Cm are in fact combined alpha-particle and photon emitters.

a beryllium-windowed Si(Li) detector, thereby alleviating the resolution problem. However, because of the window, sodium was the lightest element detectable as shown in a spectrum of pure sodium carbonate. Graphical data (log-log plots) relating "corrected" X-ray intensity to the known corresponding elemental concentration were shown for magnesium and some heavier elements in seventeen rocks. The data points, although fairly scattered, showed a linear relationship. No explicit results of quantitative analysis were presented. In 1974 Hight and Foster (39) analysed evaporated water samples using ^{210}Po alpha-particle excitation and a windowed Si(Li) detector. They were able to detect quantities on the order of micrograms of vanadium and many other heavier elements. Their work did not extend to the low-Z region but L and M X-rays as low in energy as $\sim$ 2 keV were utilised.

1.7 Summary of Chapter 1, and aims of experimental work

The preceding sections of this chapter have introduced topics of interest in providing background to and justifying the general proposals put forward in section 1.1.

The causes of difficulty in low-energy X-ray emission analysis have been outlined and the current state-of-affairs in the area has been surveyed. It has been mentioned that heavy charged-particles are promising in overcoming some of the problems encountered at low energies but have not been thus generally exploited. In particular, the applications of alpha-particle emitting isotopes have been sporadic and for quantitative analysis have been restricted to magnesium and heavier elements.

The body of the thesis, chapters 2, 3 and 4, describes the experimental work done in carrying out the proposals. The main aims of this work were:
a) to construct a windowless low-energy X-ray spectrometer designed around a specially prepared ^{210}Po excitation source and a commercially supplied Si(Li) detector, b) to evaluate the performance of the spectrometer in stimulating and detecting low-energy X-rays, c) to determine the efficiency of the detector, and subsequently apply the spectrometer to the determination of useful low-energy X-ray production cross-sections, and d) to apply the spectrometer to the analysis of complex materials

chosen to represent many other materials composed essentially of light elements.

It was clear from the outset that this approach would not result in a highly sensitive analytical method, but would rather be aimed at determinations of major and minor light-element components of bulk samples.

CHAPTER 2

EXPERIMENTAL APPARATUS - THE SPECTROMETER

2.1 Introduction

2.1.1 General remarks:

The spectrometer used to obtain most of the experimental data in this work was subject to some compromise and improvisation in its design and construction. It should therefore be regarded as having considerable capacity for improvement. Its main features were a Si(Li) detector and cryostat, an annular ^{210}Po excitation source, a facility for presenting samples under a vacuum system common with that of the detector, and electronics for pulse-height analysis.

The fabrication of ^{210}Po sources represented a major experimental effort, but only information on the finished products is given in this chapter. Details of their preparation and testing may be found in Appendix 1.

2.1.2 Choice of detector:

For low-energy X-ray spectrometry, the only energy-discriminating detectors offering close to adequate

energy-resolution are the germanium - and silicon-based semiconductor types. The design, properties and operation of these have been treated by Woldseth (3).

In theory pure germanium (Ge) or lithium-drifted germanium (Ge(Li)) should give better resolution than lithium-drifted silicon (Si(Li))* detectors because of their smaller average energy needed to create an electron-hole pair ($\sim$ 3.0 vs. $\sim$ 3.9 eV). But in practice, for reasons not well understood, the latter are superior (40,41) and have been more generally used in the X-ray energy region. Si(Li) detectors are also less sensitive to background-producing high energy photons, and have less-absorbing dead-layers (regions where charge collection is incomplete) on the entry side resulting in better efficiencies at low energies. In addition, and in common with pure Ge, they may be thermally cycled without damage caused by lithium precipitation; an important consideration here as will be recognized later.

(The above points make it apparent that the Si(Li) detector used in this work and described in subsection 2.2.1 is of the desirable variety for the proposed

---

* Pure silicon detectors have not been successfully made.

experiments. But it should be pointed out that in reality it was the existence of this particular detector that permitted the experiments in the first place).

2.1.3 Choice of excitation source:

There are only three radioisotopes suitable for basic studies of alpha-particle induced X-ray emission. They are ^{210}Po, ^{242}Cm and ^{244}Cm. Of these the readily available ^{210}Po, an essentially pure 5.3 MeV alpha-particle emitter, is to be preferred. The decay schemes of ^{242}Cm and ^{244}Cm are more complex, there being two main groups of alpha-particles split in the ratio $\sim$ 3.1 in both cases. The population of low-level excited states gives rise to gamma-rays upon de-excitation, but more importantly electrons and X-rays from gamma-ray conversion. The use of either of these two isotopes, which in any case are difficult to obtain, would complicate data evaluation. The principle emissions of ^{210}Po, ^{242}Cm and ^{244}Cm are listed in Table 2. All other alpha-particle emitting isotopes may be ruled out on the grounds of inacessibility, too short half-lives, or complex decay schemes with

TABLE 2

^{210}Po, ^{242}Cm and ^{244}Cm decay

		Principle radiations			Daughter properties		
	Half-life	Type	Energy (MeV)	Intensity(%)	Identity	Half-life	Emissions
^{210}Po	138.4 days	α	5.31	100	^{206}Pb	Stable	-
		α	4.50	1.1×10^{-3}			
		γ	0.80	1.1×10^{-3}			
^{242}Cm	162.5 days	α	6.12	74	^{238}Pu	86.4 years	α
		α	6.07	26			U L X-rays
		x	0.014-0.022 (PU - L)	26			
		γ	0.044	4.1×10^{-2}			
^{244}Cm	17.6 years	α	5.81	77	^{240}Pu	6580 years	α
		α	5.77	23			U L X-rays
		x	0.014-0.022 (PU - L)	23			
		γ	0.043	2×10^{-2}			

excessive beta-particle, photon or spontaneous-fission components.

2.2 Spectrometer components

2.2.1 The Si(Li) detector:

The heart of the experimental arrangement was a Kevex* model 3000 system consisting of a surface-passivated 30 mm^2 x 3 mm Si(Li) detector with upright cryostat and resistive feedback preamplifier. The resolution of the system as supplied was 180 eV at 5.9 keV. Unless otherwise noted, it was always operated at - 1000 V bias. Its installation into the spectrometer required removal of the original beryllium-windowed cap. The exposed detector assembly is shown in Fig. 5.

2.2.2 ^{210}Po excitation sources (see Appendix 1):

Two sources (I and II) were at different times employed as indicated at appropriate points in the text. These consisted of ^{210}Po spontaneously electro-deposited in a ring (o.d. 22 mm, i.d. 16 mm) on a polished beryllium

---

* Kevex Corporation, Burlingame, California, U.S.A.

Figure 5. Exposed Si(Li) detector.

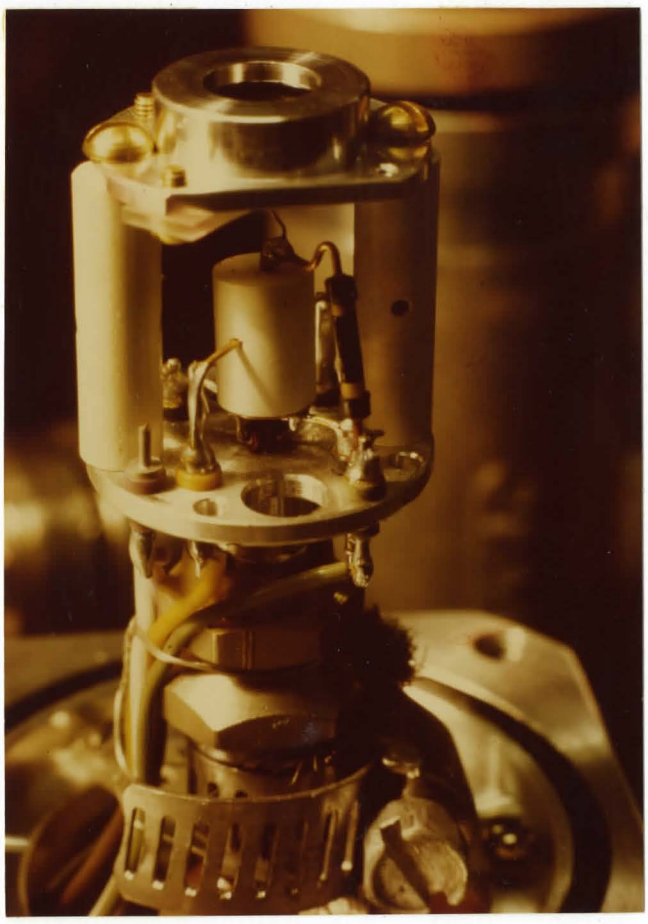

disc 30 mm in diameter and 2 mm thick with a 10 mm concentric aperture for X-ray transmission. A carbon film was used for sealing.

Source I at time of preparation was ∿ 800 μCi (as determined by gamma-ray counting) ^{210}Po sealed with ∿ 120 μg cm^{-2} carbon. The spectral distributions of its radiative outputs are shown in Figs. 6 and 7 and its annular activity distribution is indicated by Fig. 8. The modal alpha-particle energy was 5.20 MeV with a full-width-at-half-maximum (FWHM) of 90 keV. It is estimated that with the exception of Be and C X-rays the total photon output was < 0.1% of the alpha-particle output. This source was installed in the spectrometer for the primary stages of experimentation and was initially used with a thin window (90 μg cm^{-2} aluminised mylar* or 10 μg cm^{-2} formvar*) across the aperture. There were some early doubts with respect to its integrity; the purpose of the windows was to prevent any leaking ^{210}Po from depositing on the detector surface. Subsequent experience showed that ^{210}Po loss from liquid-nitrogen cooled (the conditions

---

* Mylar - a phthalate polyester, trade name of E.I. duPont de Nemours and Co., U.S.A.

Formvar- a polyvinyl formate, trade name of Shawinigan Resins Corp., U.S.A.

Figure 6. Photon outputs of ^{210}Po source.

(a) Source I, ~400 μCi; X-ray spectrum taken with Si(Li) detector at ~1 cm through 0.0025 cm Be window. Gain ~ 50 keV per channel. No peaks above 16 keV. Count-time 1000s.

(b) Source I, ~800 μCi; γ-ray spectrum taken with 3"x 3" NaI(Tl) detector (on surface). Gain ~9.9 keV per channel. Count-time 1000s.

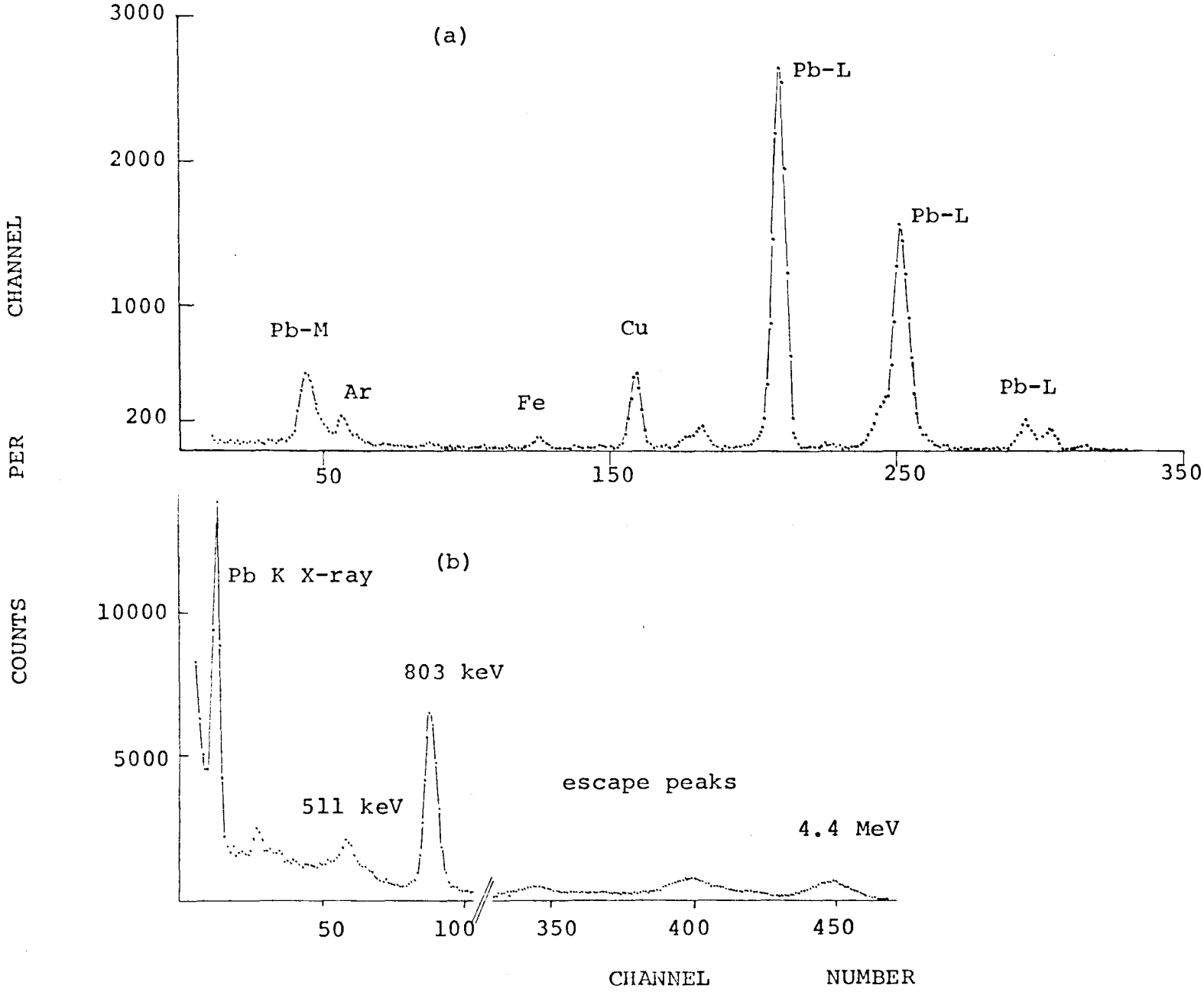
(a)
3000
2000
1000
200
CHANNEL
PER
Pb-M
Ar
Fe
Cu
Pb-L
Pb-L
Pb-L
50
150
250
350
(b)
10000
5000
COUNTS
Pb K X-ray
803 keV
511 keV
escape peaks
4.4 MeV
50
100
350
400
450
CHANNEL NUMBER

41(b)

Figure 7. Alpha-particle energy-distributions of ^{210}Po sources.

(Weak sources prepared identically to Sources I and II. Spectra taken with silicon surface-barrier detector; system gain $\sim$ 9.8 keV per channel. Vacuum path.)

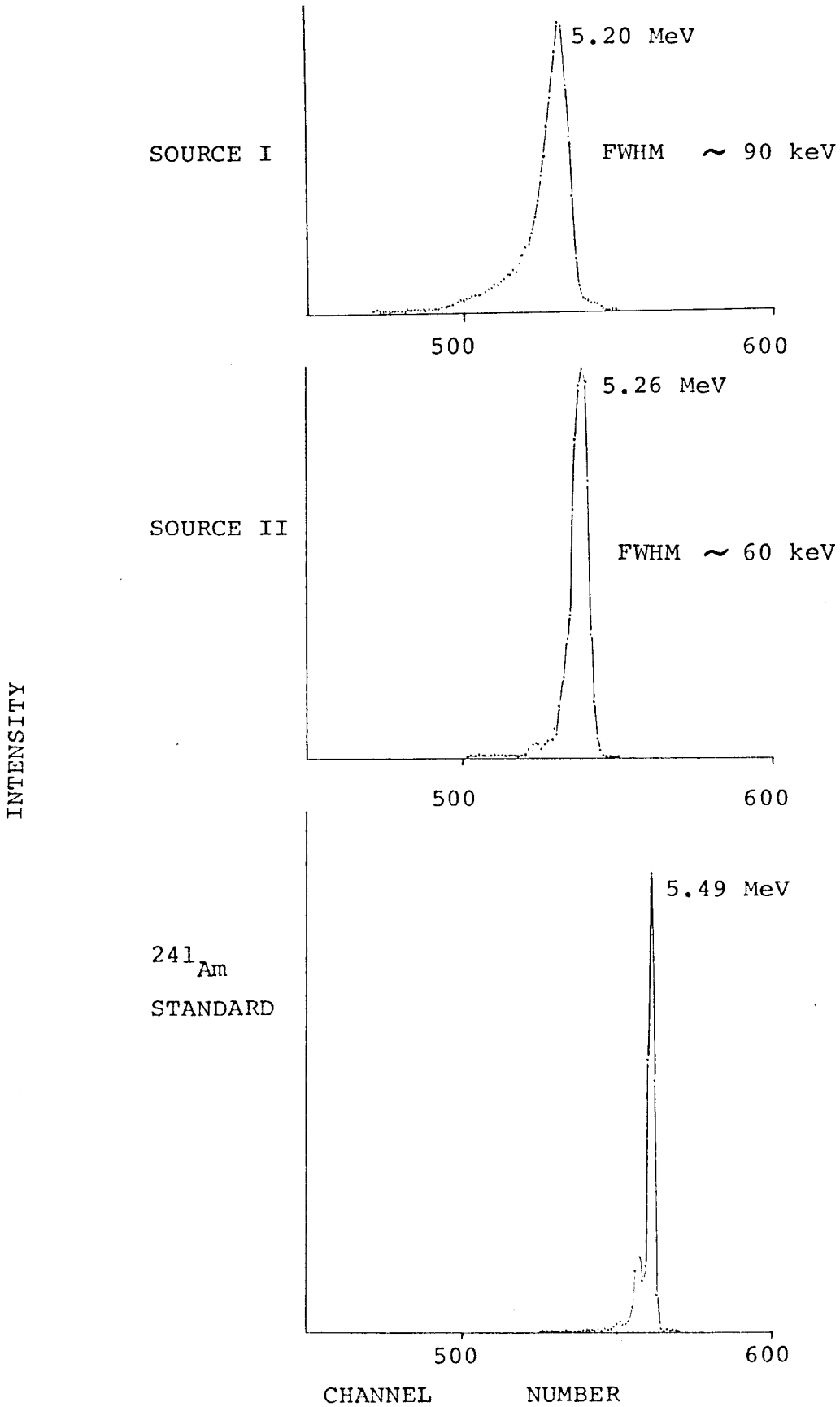
5.20 MeV
SOURCE I
FWHM ~ 90 keV
500
600
5.26 MeV
SOURCE II
FWHM ~ 60 keV
500
600
INTENSITY
5.49 MeV
241Am
STANDARD
500
600
CHANNEL NUMBER

Figure 8. Annular activity distributions of ^{210}Po sources.

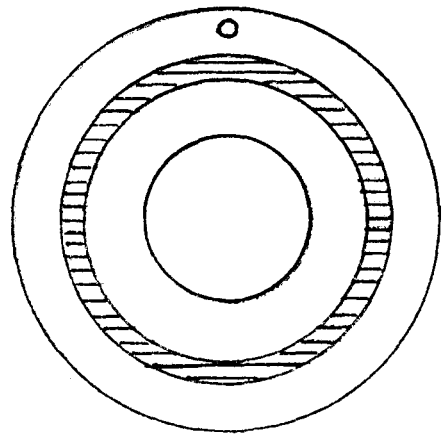

(Weak sources prepared identically to Sources I and II. Counts in four 45 degree sectors in orientations shown. Proportional counter used.)

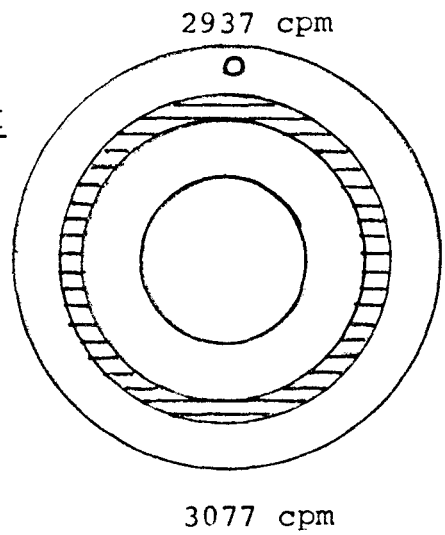

Figure 9. ^{210}Po source in holder (Source II)

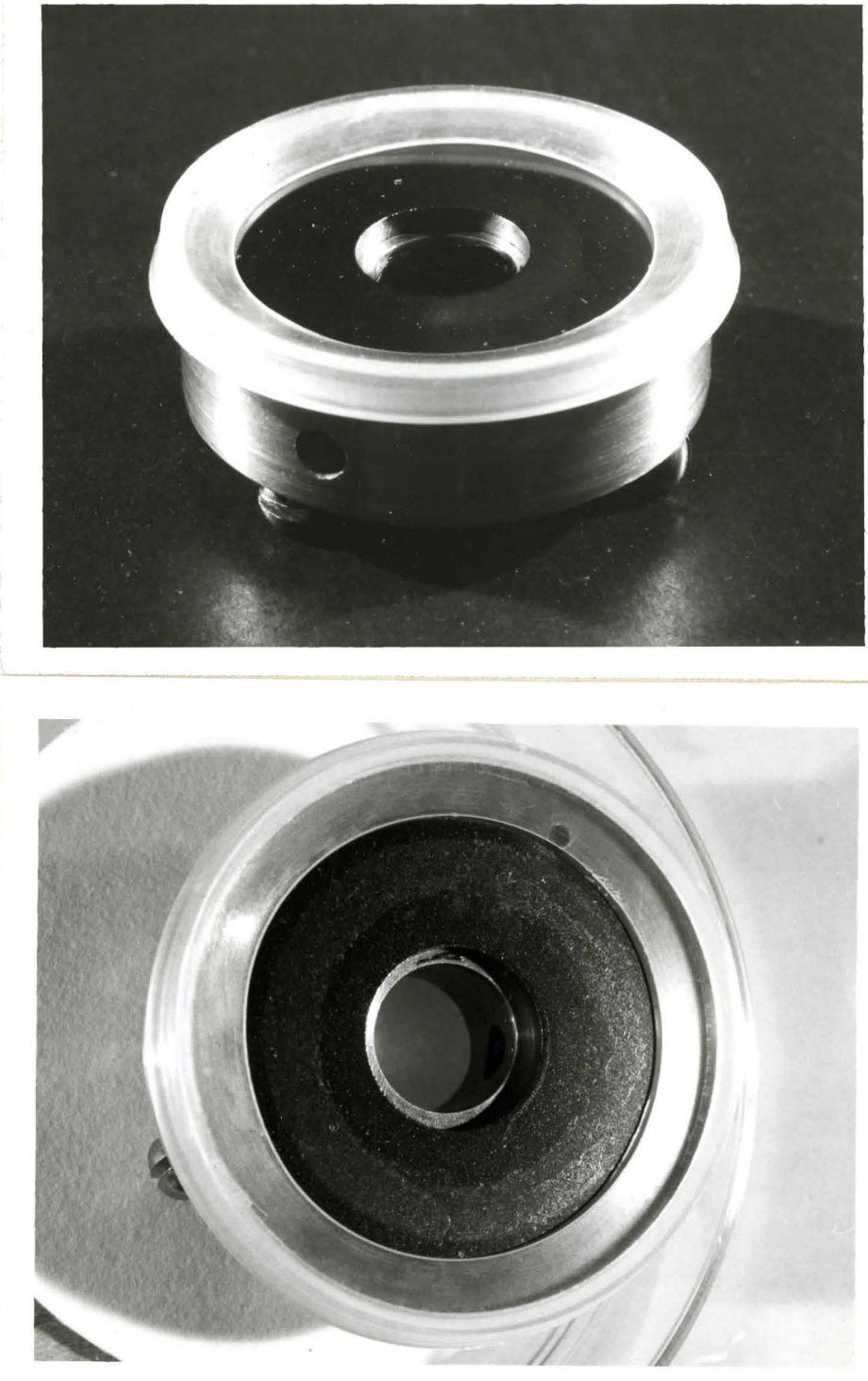

of end use, see subsection 2.2.3) sources to be practically negligible.

Source II at time of preparation consisted of $\sim$ 1.5 mCi ^{210}Po co-deposited with 10 µg copper and sealed with $\sim$ 80 µg carbon. Its alpha-particle output energy distribution is shown in Fig. 7. The modal energy was 5.26 MeV with FWHM 60 keV. The distribution of activity as determined by alpha-counting of a weak source prepared in an identical way is indicated by Fig. 8. Source II in its holder after 4 months of service is shown in Fig. 9. It was always used in the completely windowless mode.

2.2.3 Source-sample-detector configuration:

The geometrical arrangement of the excitation source, sample and detector and other details are shown in Fig. 10. The $\sim$ 150^{o} geometry was chosen because, a) it was as close as practically possible to the 180^{o} geometry desirable in minimising alpha-particle back-scattering, b) it was compact, and c) it facilitated cooling of the excitation source via the detector cryostatic system (this is desirable in the interests

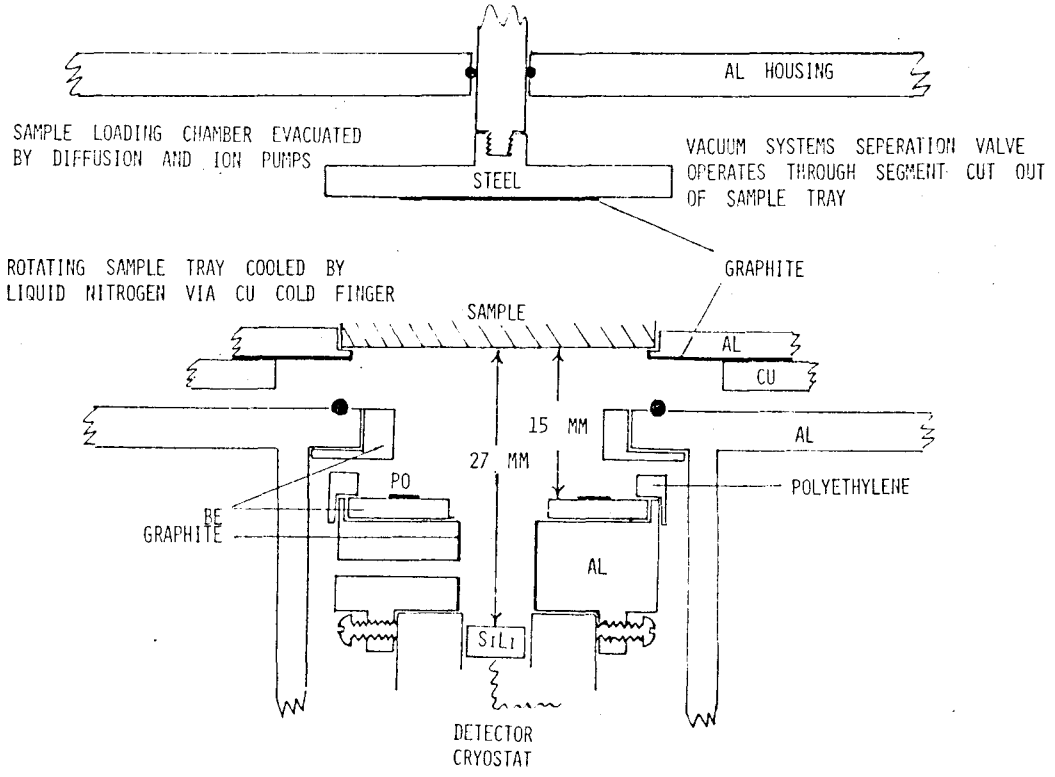

Figure 10. The source-sample-detector arrangement.

of source stability, see Appendix 1). Materials other than samples exposed to an alpha-particle flux were chosen to be of low atomic-number, to minimise both alpha-particle back-scattering and the production of interfering X-rays able to enter the detector after scattering events. The aluminum source-holder cum collimator was designed to, a) restrict the line-of-sight of the detector to a sampling area corresponding to a $\sim$ 30 mm diameter target and b) to shield the detector from X-rays originating in the source.

2.2.4 The sample-chamber:

An overall view of the spectrometer and the sample-changing mechanism are shown in Fig. 11. The sample-chamber parts were: a) a 25 cm diameter aluminum base plate with appendages for housing the detector-excitation source assembly, for sample cooling, and for pumping, b) a 20 cm diameter aluminum turntable with twelve 32 mm diameter sample positions; of the twelve, two were redundant because of restricted turntable rotation, six had apertures, (i.e. diameters exposed to alpha-particle flux) of 30 mm, and four had apertures of 25 mm. c) a 15 cm diameter x 3 mm

Figure 11. The spectrometer and sample-chamber.

a) Overall schematic view of spectrometer

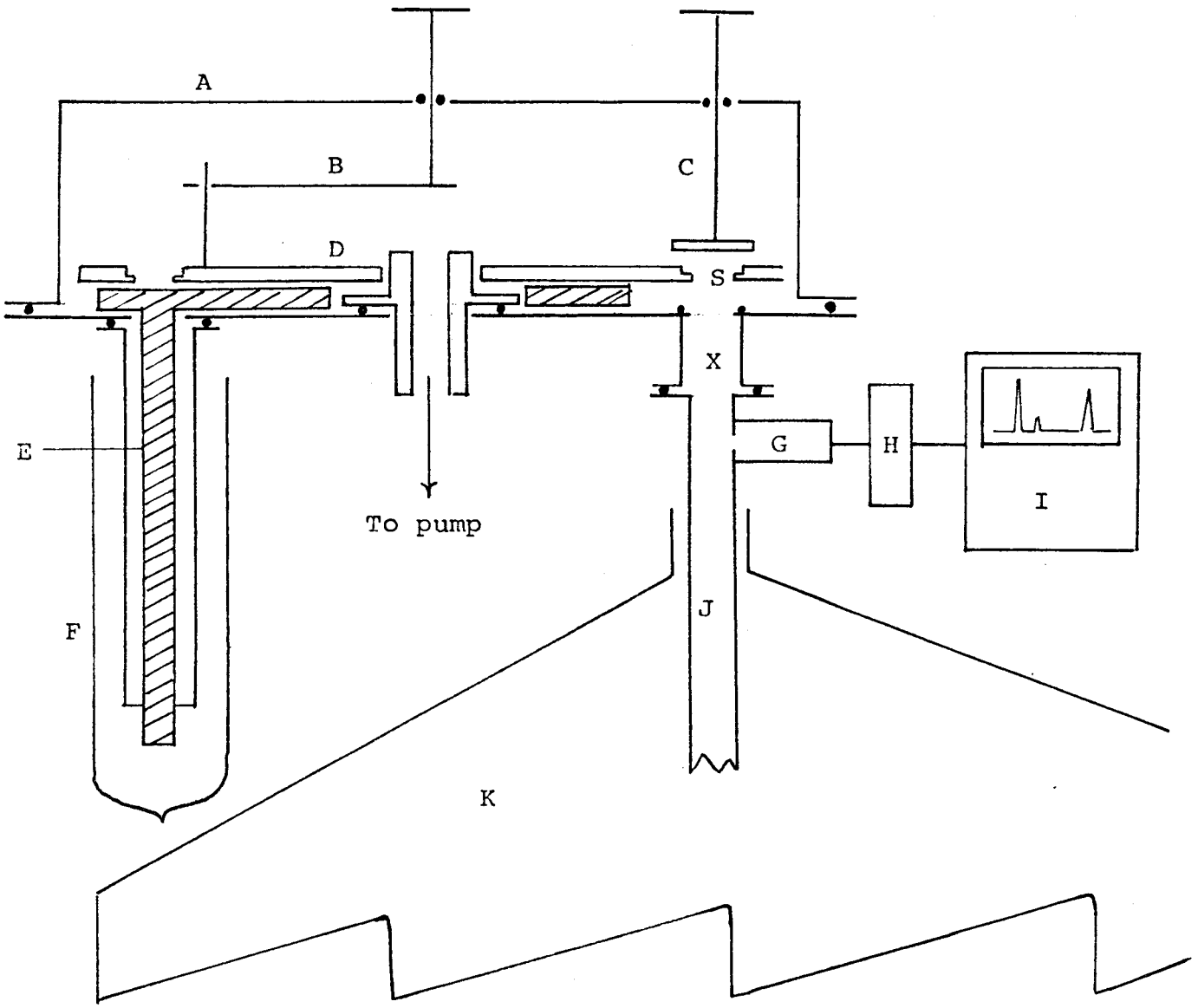

A: Aluminum bell cover. B: Mechanism for rotating sample tray.

C: Vacuum systems separation valve. D: Aluminum sample tray.

E: Copper rod for cooling sample tray. F: Glass dewar for LN_2.

G: Preamplifier. H: Amplifier. I: Multi-channel analyzer.

J: Detector cryostat. K: Detector LN_2 reservoir.

S: Sample position. X: Detector and excitation-source position.

b) The spectrometer sample-chamber

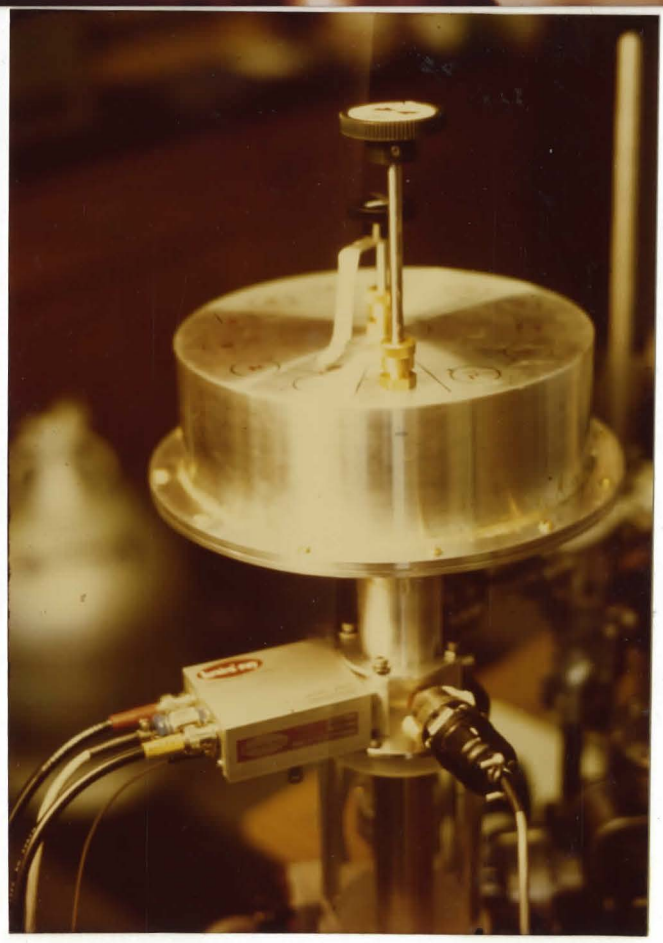

thick copper plate on which the turntable rested and rotated, d) a vacuum-jacketed 2 cm diameter copper rod which extended outside the chamber and which cooled the copper plate and sample-tray by means of liquid-nitrogen through conduction, e) a bell-type aluminum cover with rotary 'O'-ring seals through which the turn-table and vacuum systems separation valve were manually operated via steel rods.

The McMaster University "Engineering Machine Shop" undertook most of the machining involved in making the above items.

2.2.5 Electronics:

Besides the detector, the spectrometer electronics used for pulse-height analysis consisted of, a) a model 2000 Kevex resistive-feedback preamplifier with its first stage cooled by the detector cryostatic system, b) a model 4600 Kevex detector bias supply, c) a model 1413 Canberra* spectroscopy amplifier operated with 8 μs time constants and, d) a model 8100 Canberra multichannel analyser with 4096 channel capacity and teletype output.

---

* Canberra Industries, Meriden, Connecticut, U.S.A.

2.3 Spectrometer assembly and operation

The assembly of the spectrometer components and many subsequent manipulations required bringing the detector to room temperature and exposing it to the atmosphere for short periods. After removal of its liquid-N_2 supply, the detector was allowed to warm up while pumped upon by an oil-diffusion pump with liquid-N_2 trap. After admission of the atmosphere and performance of the required operations, the system was re-evacuated, sealed and recooled. The full cycle, "cold-warm-atmosphere-vacuum-cold" was always carried out as quickly as possible to minimise lithium precipitation and changes in the silicon dead-layer thickness. During the process, which usually took $\sim$ 4 hours and in all needed to be repeated $\sim$ 20 times, there was always concern about chemical attack (oxidation etc.) of the detector surface and damage to the preamplifier circuit through expansion and contraction. However, despite these treatments, which no doubt amounted to abuse according to its design specifications, the

---

* After the initial assembly the spectrometer sample-tray cooling system was used as the cold trap.

Kevex 3000 system suffered no degradation in performance during the course of this work.

In operation the sample-chamber was always evacuated to $< 5 \times 10^{-7}$ mm Hg before the valving mechanism connecting it to the detector vacuum system was withdrawn. A roughing pump and oil-diffusion pump were used down to 10^{-4} mm Hg at which point they were isolated. Further pressure reduction was achieved by cooling the chamber interior with liquid-nitrogen via the copper rod, and switching in an 8 litre s^{-1} ion pump.

The cold copper plate and sample tray presented a large sink for condensable gaseous species and reduced the volatilization and outgassing of certain samples; in this way the detector surface and preamplifier circuit were protected.

Sample-loading and pumpdown time was usually 2-3 hours.

2.4 Spectrometer performance

2.4.1 Energy resolution and noise:

The resolution (FWHM)* of the Kevex 3000 unit as supplied was 180 eV at 5.9 keV. This was in accord with

---

*In X-ray energy spectrometry, spectral energy-resolution is usually defined as the "full-width-at half-maximum" height of a peak at a given energy.

specifications and was confirmed experimentally using a ^{55}Fe source. After the modifications carried out for spectrometer operation the resolution at the same energy lay in the range 180 - 190 eV, the figure varying between detector warm-ups. This was obtained consistently both by alpha-particle excitation of Mn - K X-rays and by direct observation of the same X-rays from the ^{55}Fe source. The slight degradation in resolution was probably caused by increased noise due to less effective detector cooling, since it returned to the 180 eV specified value when the unit was returned to its normal operating mode.

The noise contribution to the observed resolution may be calculated from:

$$FWHM_{observed} = \sqrt{(FWHM)^2_{noise} + (2.35\sqrt{Fe\ E})^2}$$

where E is the energy of the observed X-ray, e is the energy per electron-hole pair for silicon (3.8 - 3.9)*, and F is the Fano factor for silicon (0.10 - 0.13)*.

---

* Taken from reference (3).

An observed resolution of 185 eV at 5.9 keV therefore corresponds to a noise FWHM in the range 133-148 eV; and this was confirmed through the use of a high-precision pulser which gave a peak width of 145 eV.

The resolutions for Si - K (1740 eV) and O - K (525 eV) X-rays, using the above expression and the calculated noise range, should lie within the intervals 146-164 and 137-153 eV respectively. The best observed resolutions for these two X-rays were 165 and 160 eV, both values being outside and above the expected ranges. It has been pointed out by Johansson and Johansson (30) that heavy-ion bombardment of high X-ray production cross-section target atoms may result in multiple ionization with a consequent line broadening due to changes in electron energy-levels. Presumably it was this effect which caused the poorer than expected resolution of low-energy X-rays; although no accompanying shifts in X-ray energies or changes in peak shape were discernible. Fig. 12 is a plot of the best observed vs. expected resolutions for X-rays between 0.5 and 8.0 keV.

The "noise cut-off" for the Kevex 3000 system as supplied was $\sim$ 330 eV. This was the point below which

Figure 12. Expected and observed energy-resolution of the Si(Li) detector.

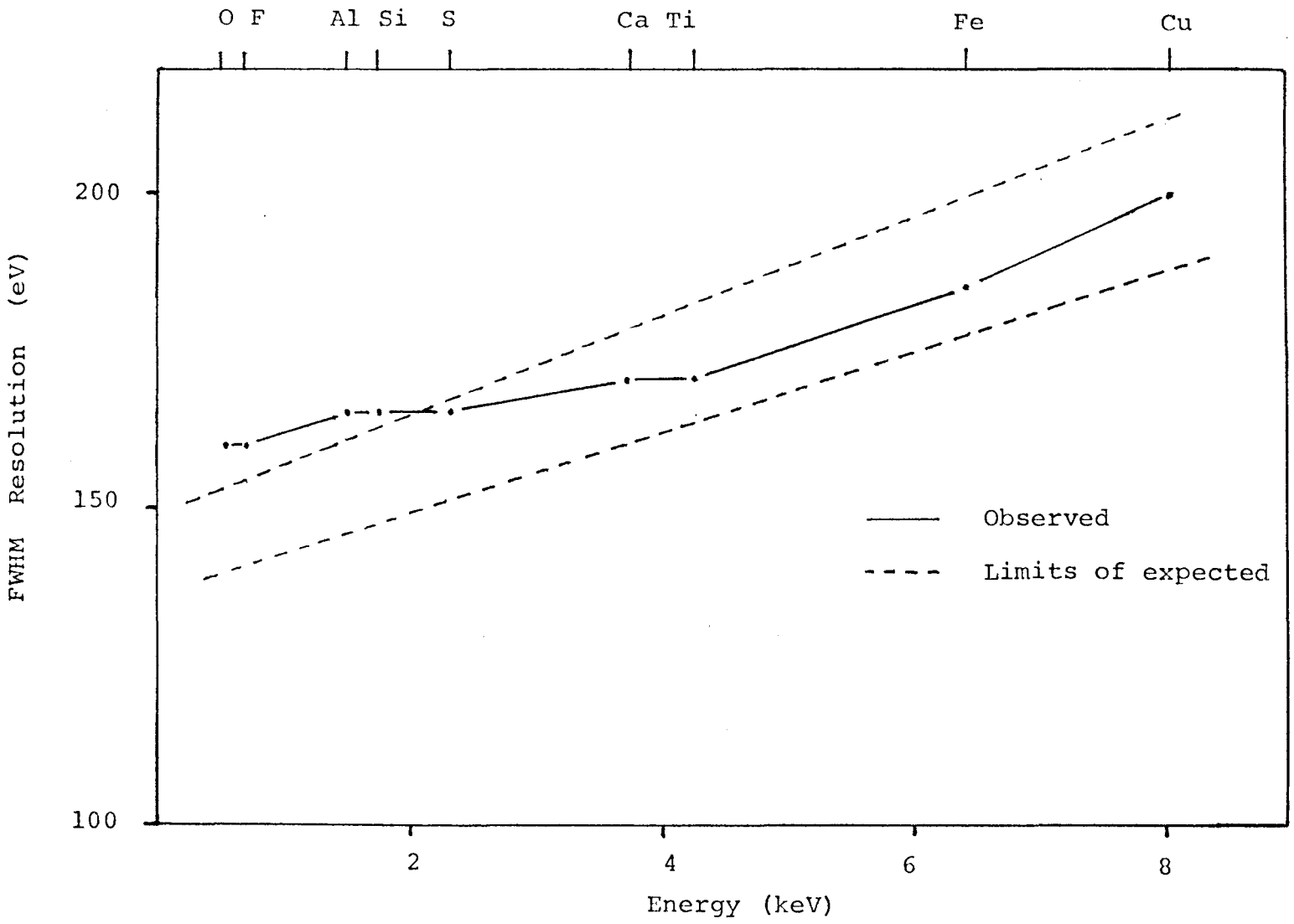

X-ray detection was impractical and was arbitrarily defined by extrapolating the fast-rising low-energy region of the "room-background" spectrum to zero intensity. With the spectrometer assembled, and operating with the formvar-windowed source I in position and a polyethylene target, the equivalent point was $\sim$ 430 eV. This allowed only X-rays of energy > 500 eV to be observed and limited the lightest element measurable to oxygen. The higher energy level of the cut-off was in part caused by increased electronic noise, with secondary electron bremsstrahlung and possibly the summing of carbon X-rays also contributing.

2.4.2 Sample position reproducibility and radial response of targets:

It is important in analytical work involving the detection of radiation that the experimental geometry be reproducible. This is especially true when compact arrangements such as the present one are used; in this case relative positional changes of < 1 mm between source, sample and detector could be expected to lead to significant errors.

Table 3 shows the K X-ray count rates obtained from mirror-finish, thick aluminum targets in the ten adjacent usable sample positions. Also shown are the repeated count-rates obtained for a single position with sample-tray rotation and repositioning between counts. The variability in all cases was $\sim$1%, most of which was accountable for by statistical counting errors.

The cumulative count-rates obtained as a function of target radius are shown in Fig. 13. The targets, again mirror-finish, thick aluminum, were centered on the source-detector axis and partially screened as necessary from the alpha-particle flux using filter paper discs with varying diameter apertures. At small radius (r) the curve goes as $\sim r^2$ before entering a linear region and finally levelling out at r $\sim$ 15 mm. The explanation for this behaviour is difficult to quantitate; and any quantitative description would vary according to the nature of the target material. Changes across the target area of alpha-particle flux and penetration, and absorption of X-rays within the target and their access to the detector all play a part.

TABLE 3

Sample position reproducibility, aluminum targets

Sample tray position	Target diameter	Counts per 100 seconds	Standard deviation
1	30 mm	52696	
2		52548	
3		52465	
4		52231	
5		52196	
6		51531	0.79%
7	25 mm	51279	
8		51929	
9		51259	
10		51458	0.61%
6	Screened to 21 mm with filter paper	32867	
		33081	
		31831	
		32190	
		32274	
	(Sample-tray rotation	32669	
	between counts)	32768	
		32513	
		31922	
		32848	1.3%

Figure 13. Cumulative count-rate vs. radius for an aluminum target.

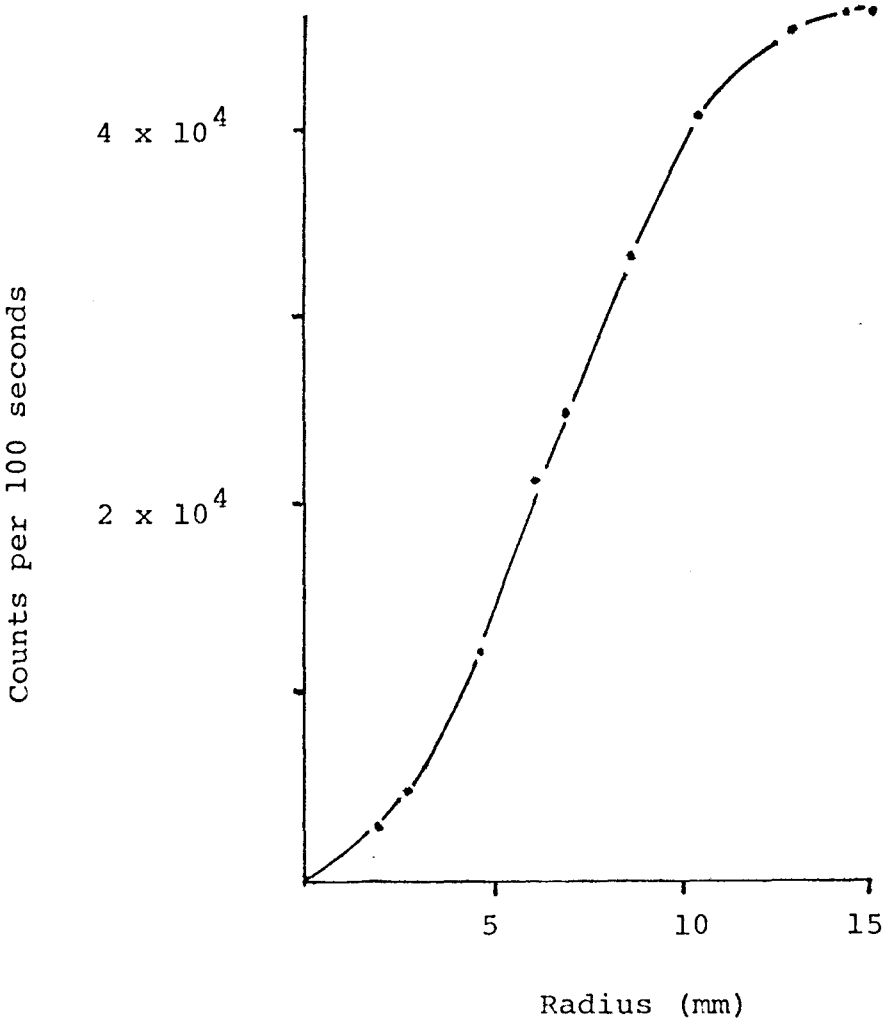

2.4.3 Pure-element target responses:

The K, L and M X-ray total count-rates obtained from 500 or 1000 second counts of thick 25 mm diameter targets of several elements are presented in Fig. 14. Source I (see p.41a) was used with a $\sim$ 10 μg cm^{-2} formvar window across the aperture; the ^{210}Po activity at the time the data were taken was $\sim$ 400 μCi.

The atomic-number dependence of the count-rates for the K X-rays (sum of K_α and K_β) is $\sim Z^{-6}$ in the energy range shown. It is to be expected that this curve would continue to rise below Mg - before reaching a maximum and then falling off because of X-ray attenuation in the formvar window, the detector gold-layer contact and silicon dead-layer. Experimental points were not obtained for the elements oxygen to sodium because of the difficulties in obtaining or handling the pure elements; and the impossibility of correcting for X-ray absorption in mixed-element targets without knowledge of the X-ray production cross-sections as a function of alpha-particle energy. However it may be mentioned that the fluorine K X-ray count-rate from a teflon target was $\sim$ 7% less than

Figure 14. Total X-ray count-rates vs. X-ray energy for pure-element thick targets.

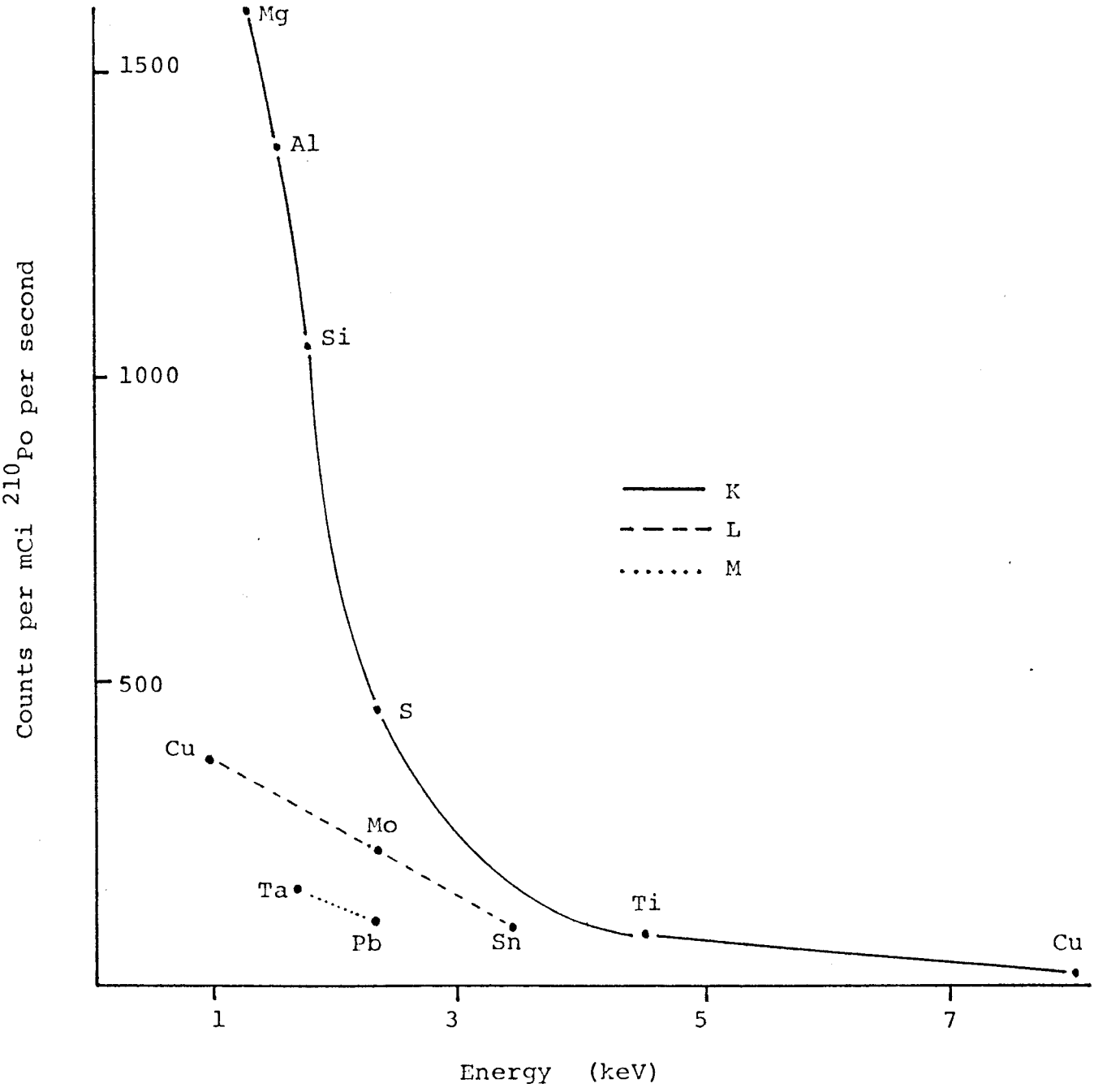

the magnesium count-rate after concentration adjustment.

At given X-ray energy, the cross-sections for L and M X-ray production by heavy particles are generally higher than those for K X-rays. This may be derived from data presented by Johansson et al. (30) and by Thornton et al. (42). The reasons for the reversal shown in Fig. 14 are the increased X-ray absorption in the higher atomic-number targets and the fewer atoms sampled.

A sample spectrum obtained for a thick target of pure silicon is shown in Fig. 15(a). The background plateau below the full absorption peak was caused mainly by X-ray attenuation in the silicon dead-layer of the detector where charge-collection was poor. Fig. 15(b) is a fluorine K X-ray spectrum obtained from a teflon target under identical conditions.

2.4.4 Spectral background:

The sources of spectral background in X-ray work with Si(Li) detectors may be divided into two groups: those which are detector-related and those which are not. The first group includes electronic noise (discussed in

Figure 15. Alpha-particle excited silicon and fluorine K X-ray spectra.

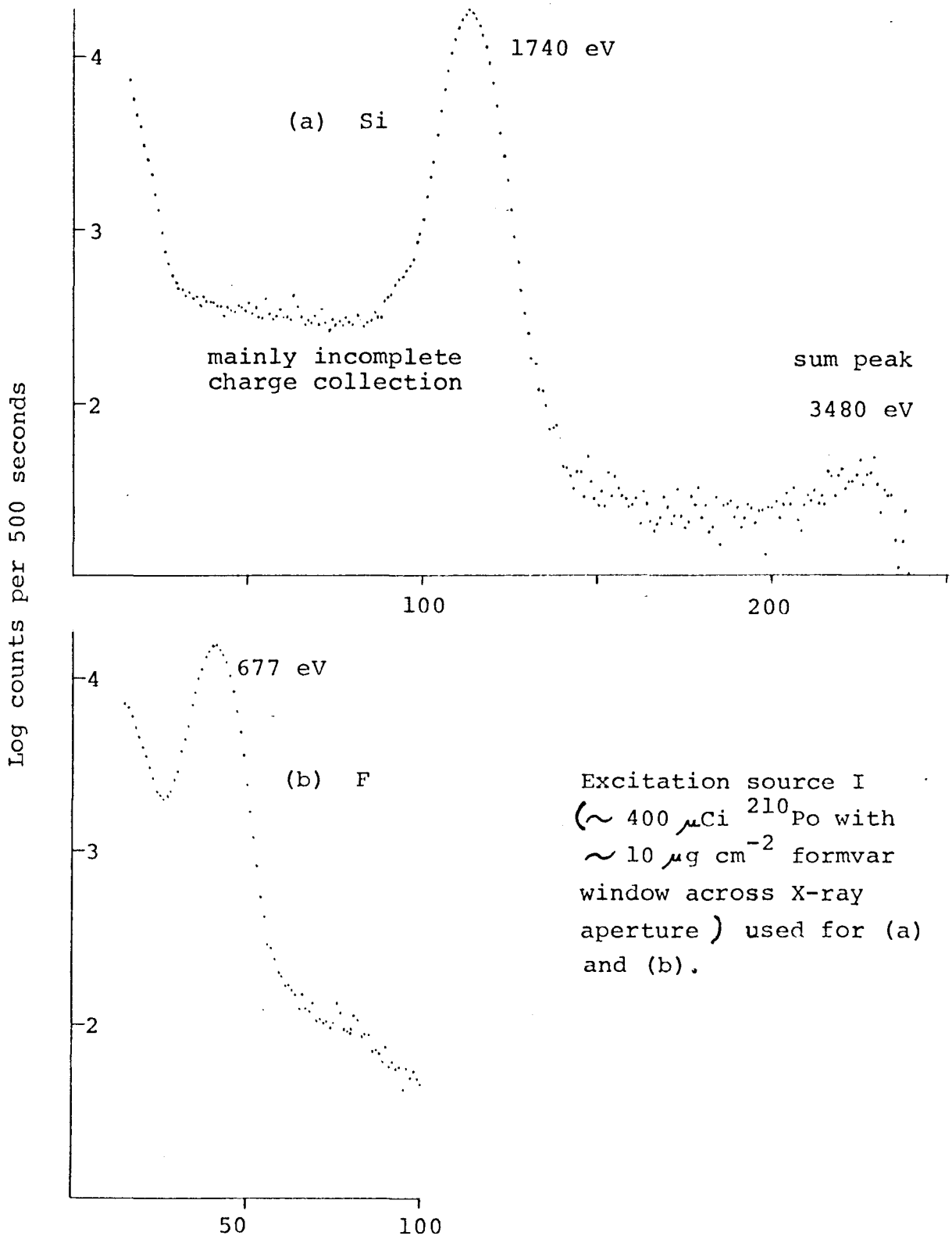

Excitation source I (~ 400 μCi ^{210}Po with ~ 10 μg cm^{-2} formvar window across X-ray aperture) used for (a) and (b).

subsection 2.4.1), Compton-scattering of photons within the detector volume, and incomplete charge-collection. The second group includes "room-background", radiation striking the detector directly from the excitation source, and radiation such as bremsstrahlung and scattered excitation-radiation coming from the sample.

Compton-scattering of photons within the detector and the consequent production of a background continuum is significant in the low-energy region of the X-ray spectrum when higher energy X-rays constitute a major fraction of the detected radiation. It is particularly troublesome when photons are used as excitation-radiation because of their back-scattering by the sample. It is not of significance, as in the present work, when only low-energy X-rays are detected because of the smaller ratios of Compton-scattering to photo-electric cross-sections of the detector material at low energies.

Incomplete charge-collection manifests itself in the X-ray spectrum as a continuum of fractional energy events below total absorption peaks. There are two main

contributors. One is energy deposition near the edge of the active region of the detector where the electric field is distorted. Here, charge may be lost through leakage to the detector surface. This process is important when energy deposition takes place over a large volume, i.e. for high-energy X-rays. It is usually negligible for energies < 5 keV. The other contributor is X-ray absorption in the surface dead-layer on the entry side of the detector. This layer is not completely "dead" but has a high concentration of trapping-centres from which charge-collection is relatively slow and may not occur within the detection system resolving time. This effect is of increasing magnitude towards low X-ray energies and was the major source of spectral background encountered in the present work. An example of it is shown in Fig. 15(a).

A sample spectrum of room-background is given in Fig. 16. This was taken with the spectrometer assembled but in the absence of the ^{210}Po source.

Fig. 17 shows a spectrum of room-background plus the radiation striking the detector directly from

Figure 16. Room-background spectrum, Si(Li) detector

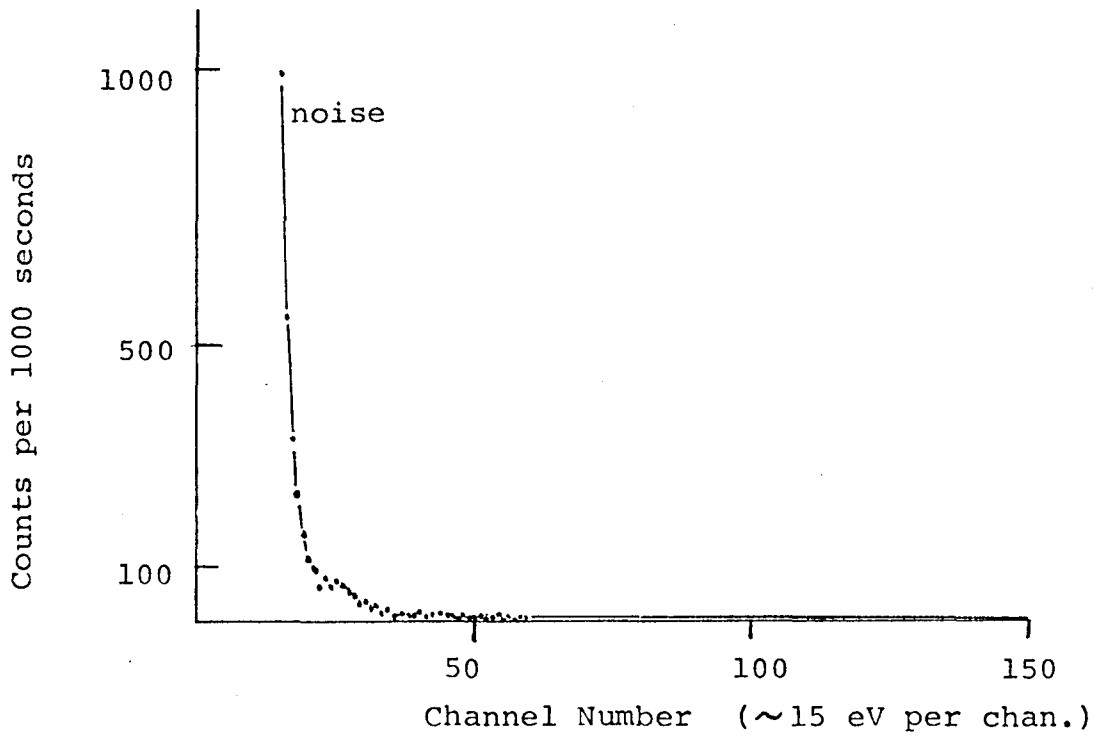

Figure 17. Spectral background direct from ^{210}Po excitation source.

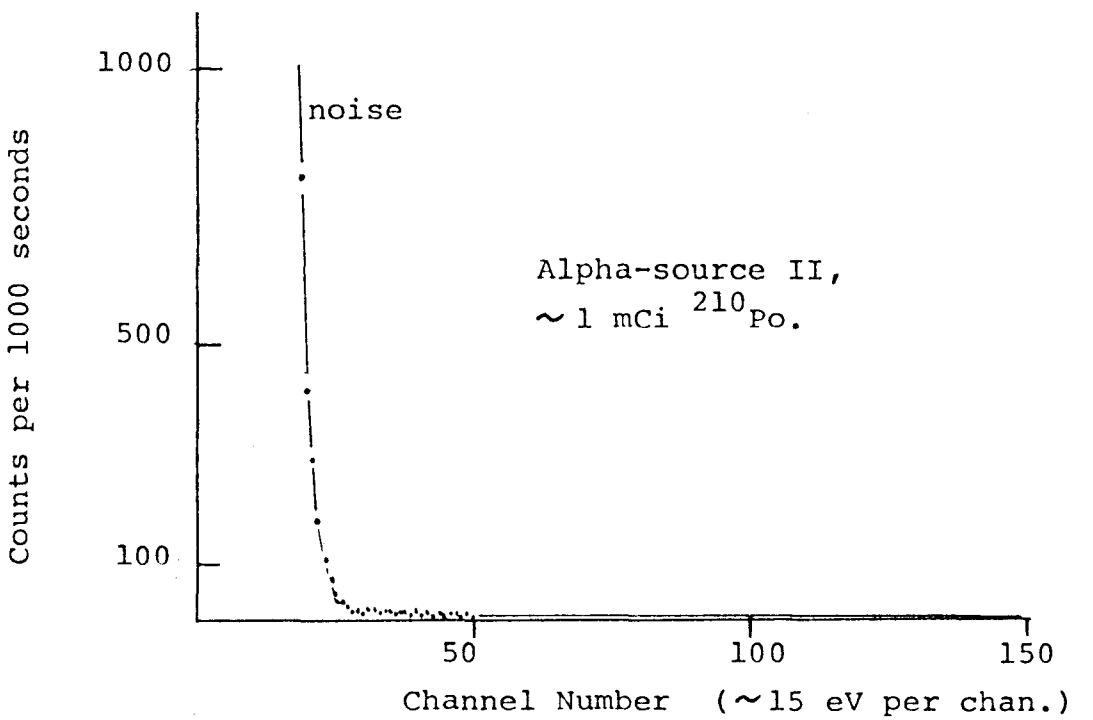

source II (∿ 1 mCi ^{210}Po) in operating position. This spectrum was taken with the spectrometer completely assembled but with the aperture to the detector blocked by a 2 mm thick teflon disc. It includes any contribution from gamma-rays or neutrons produced in the source backing*.

The magnitude of the secondary-electron bremsstrahlung is indicated in Fig. 18. These spectra were taken with source II (∿ 1 mCi) in position. There is no substantial difference between the carbon and manganese spectra despite the atomic-number difference. For practical analytical purposes it seems that bremsstrahlung arising from low - Z targets will usually be less than background arising from the incomplete charge-collection effect outlined above. In theory the maximum energy a heavy charged-particle can impart to a free electron is 4 mE/M, where m is the electron mass, and E and M are the energy and mass of the heavy particle. For 5.2 MeV alpha-particles this corresponds to ∿ 2.8 keV, but there is no obvious discontinuity in either of the spectra at this point.

---

* Approximately one fast neutron and one 4.4 MeV gamma-ray are produced for 10^6 alpha-particles (∿ 5 MeV) incident on a Be target; the reaction is $^{9}Be(\alpha,n)^{12}C$. Also included should be any penetrating radiation produced through nuclear reactions from other materials surrounding the excitation source and from the aluminum target in the sample position.

Figure 18. Secondary-electron bremsstrahlung spectra from carbon and manganese thick targets.

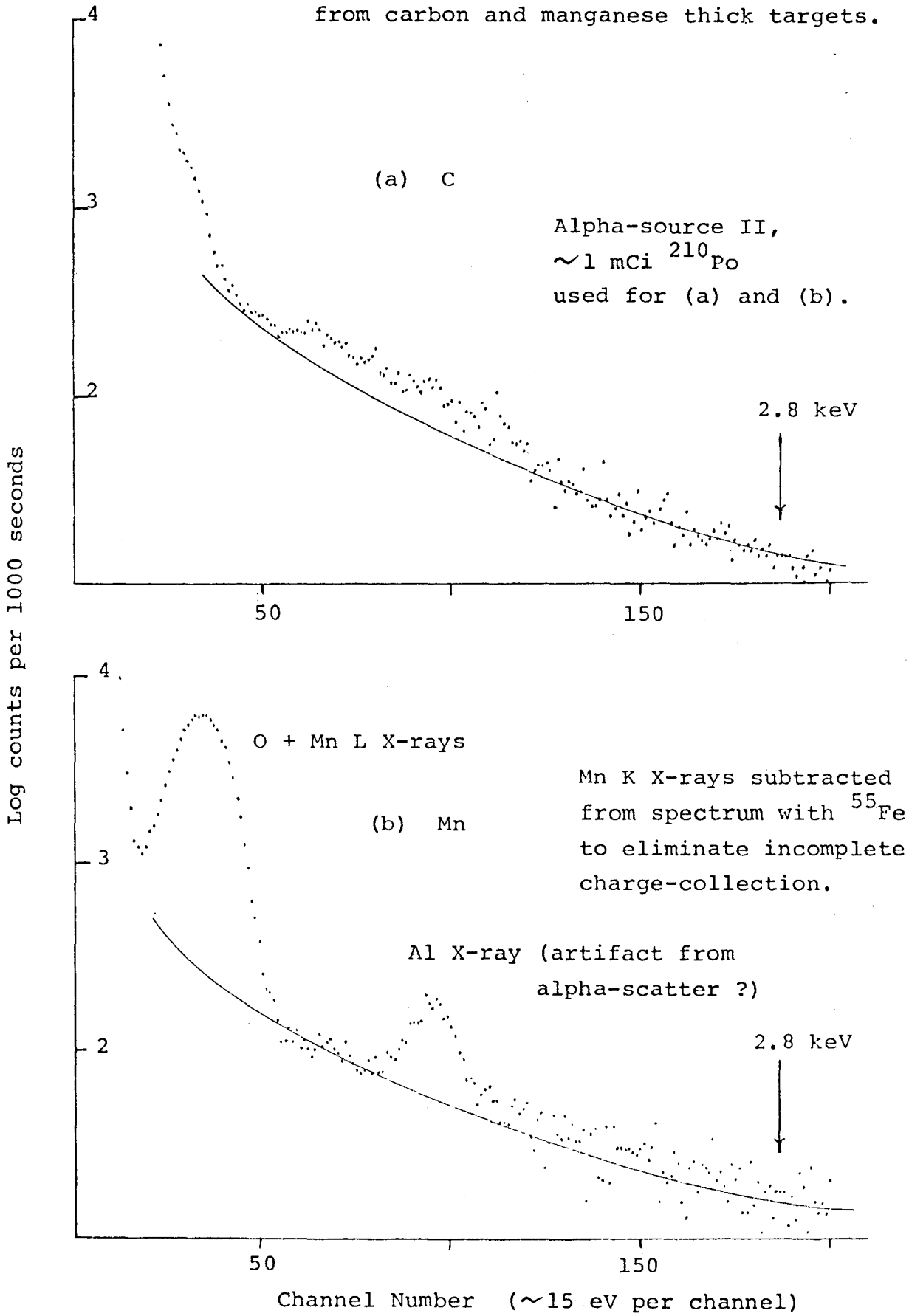

Another potential source of background in the present work was back-scattered alpha-particles. These were observed as very high-energy events which grossly over-loaded the electronics system. It was possible to count them by discriminating against all events below $\sim$ 100 keV. The count-rates obtained for some pure-element targets are shown in Table 4. The "residual" counts were obtained by blocking the aperture to the detector; they presumably arose from ^{210}Po contamination of the detector surface and interior surface of the collimator.* It will be noted that the corrected count-rates within statistical errors have an atomic-number dependence of Z^2 in accordance with the Rutherford scattering theory.

As evidence that the alpha-particles were being correctly counted the following experiment was carried out:

a) the ^{210}Po excitation source was removed from the spectrometer; the residual count-rate under these conditions was 105 cpm (count-time 90 minutes) and represented detector surface contamination.

---

* At this stage of experimentation ^{210}Po sources of at least 300 μCi had been in contact with the detector for $\sim$ 2 years in total; and numerous warm-up cycles had taken place.

TABLE 4

Alpha-particle backscattering from elemental targets *

Target	Z	Alpha-particle count-rates (counts per 100 minutes) observed	Adjusted for "residual counts"
None ("residual counts")	-	18296	-
Be	4	18485	189 ± 234
Al	13	19511	1216 ± 237
Ti	22	22011	3715 ± 242
Cu	29	24997	6701 ± 248

* Source II used; ~ 1.2 mCi ^{210}Po.

b) a weak ^{210}Po source otherwise identical to the excitation source was placed in a target position facing the detector; the count-rate now observed was 213 cpm.

From the known activity of the source, 26844 disintegrations per minute, the detection efficiency was calculated to be 0.36%. The detection efficiency calculated according to the geometry of the arrangement was 0.33%.

Any contribution of alpha-particles to the observed background would be included in both the room-background (Fig. 16) and bremsstrahlung (Fig. 18) spectra because of the detector surface contamination and back-scattering effects mentioned above. But there are no obvious spectral distortions attributable to these factors. However, it should be noted that for best energy resolution it was always found beneficial to run the spectroscopy amplifier in the high count-rate baseline restorer mode to counteract the detrimental effects of the over-load pulses.

2.4.5 Alpha-particle vs. photon excitation:

The major reasonable radioisotopic alternatives to alpha-particle emitters for the direct stimulation of low-energy X-rays are the photon-emitting isotopes ^{55}Fe and ^{109}Cd. These decay by electron-capture and yield mainly the K X-rays of manganese and silver respectively (see Table 5). Experiments were performed with the spectrometer to examine the relative merits of ^{55}Fe, ^{109}Cd and ^{210}Po under similar conditions.

The total K X-ray count rates and peak to background ratios obtained from 30 mm diameter targets of several elements using the three isotopes are shown in Table 6. The ^{210}Po data were obtained using source I in the usual 150^{o} geometry. The measurements for the other two isotopes were made in the geometry shown in Fig. 19 using a commercially supplied source of ^{109}Cd and a specially prepared source of ^{55}Fe, both of very high specific activity (> 5 Ci g^{-1}). The windows on these were 1 mg cm^{-2} mica and 1 mg cm^{-2} mylar respectively and were calculated not to significantly attenuate the photon fluxes. All of the data were obtained with the

TABLE 5

Emissions of ^{55}Fe and ^{109}Cd

	Half-life	Emission	Intensity (%)
^{55}Fe	2.7 years	5.9 keV, Mn K_α X-rays	27
		6.5 keV, Mn K_β X-rays	4
^{109}Cd	453 days	∿22 keV, Ag K_α X-rays	88
		∿25 keV, Ag K_β X-rays	19
		88 keV, γ, ^{109m}Ag daughter	4

TABLE 6

Total K X-ray count-rates and peak/background ratios for ^{210}Po, ^{55}Fe and ^{109}Cd on elemental targets

	Counts mCi^{-1} s^{-1} (peak area/background area)		
	^{210}Po	^{55}Fe	^{109}Cd
F (teflon)	990 (51)	0.08 (1.7)	0.0 (0.0)
Mg	1760 (120)	1. 5 (26)	0.3 (0.5)
Al	1530 (150)	2. 9 (64)	0.5 (0.9)
Ti*	88 (180)	62 (210)	21 (30)
Cu*	11 (28)	-	135 (107)

* For the peak/background ratios in these cases only the K_α peak was considered.

Figure 19. The geometric arrangement used for ^{109}Cd and ^{55}Fe excitations.

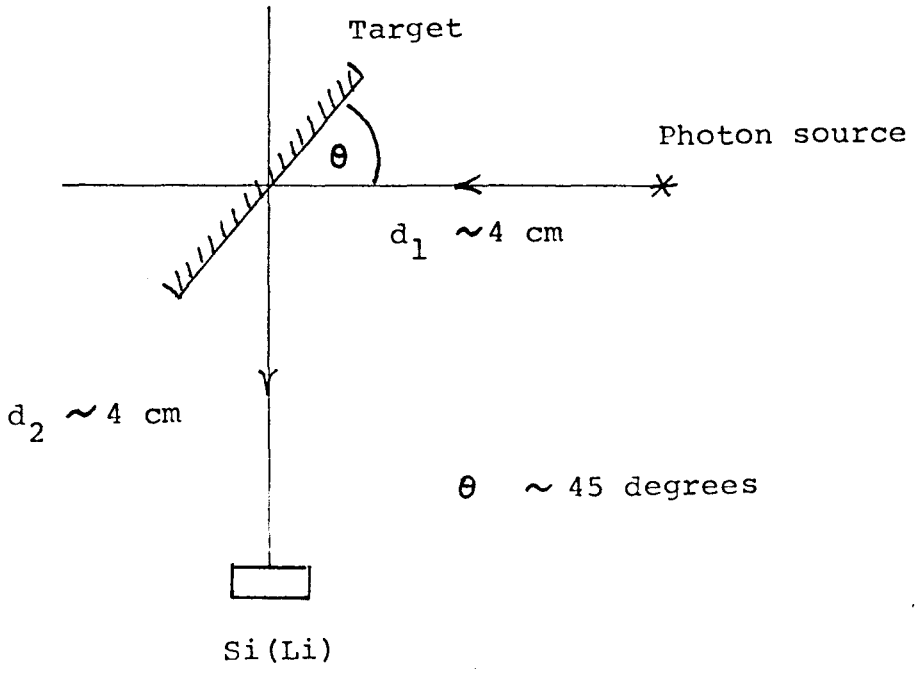

Photon sources : ^{109}Cd ~0.6 mCi

^{55}Fe ~2.0 mCi

spectrometer operating in the totally windowless mode under high vacuum. No corrections were made to the data for geometrical differences, the main points of interest being their trend with target atomic-number and the peak-to-background area ratios.

The spectra obtained with each isotope for a 30 mm diameter pelletized target of the standard rock NIM-D (see subsection 4.3.1) are shown in Fig. 20. Conditions were identical to those described above. The spectra for the photon excitations are almost featureless in the low-energy region.

2.5 Summary

The spectrometer has been demonstrated to be useful for the excitation and detection of low-energy X-rays. Despite certain technical shortcomings, the most notable being that it is "upside-down"*, it may be employed for analytical applications to elements as light as oxygen.

---

* There is a danger with certain sample types of fragments falling onto the detector. An arrangement with the samples facing upwards would be better.

Figure 20. Observed spectra from the standard rock NIM-D for ^{210}Po, ^{109}Cd and ^{55}Fe excitations.

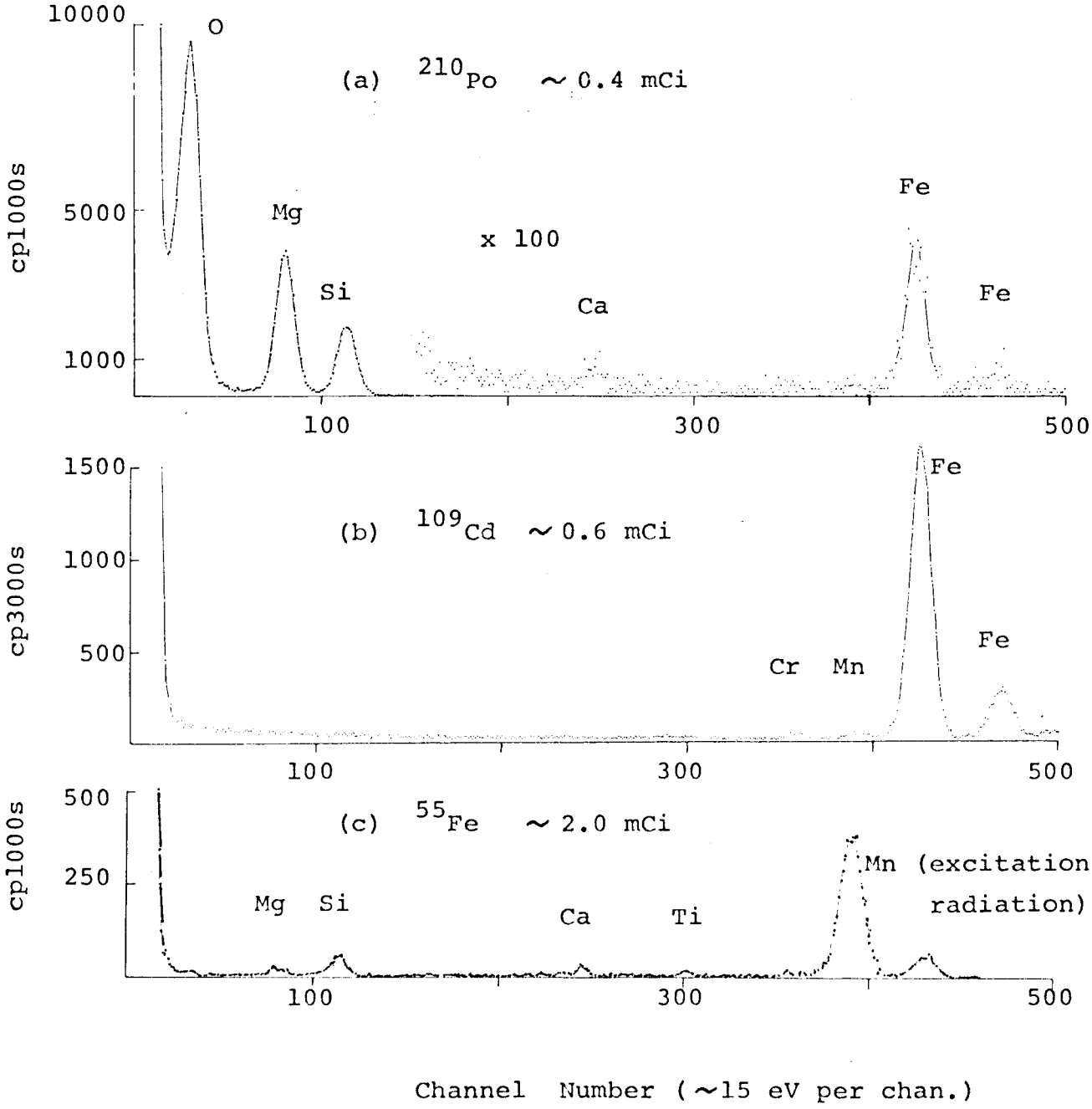

The resolution of the system is poorer than expected below ∿ 2 keV. This may arise from the alpha-particle excitation; peak shapes are well maintained , ruling against imperfect charge collection as the major cause.

The sources of spectral background have been examined. Although secondary-electron bremsstrahlung is significant, poor charge collection is the potential major contribution in analytical applications.

For the light elements, alpha-particle excitation has been shown to be superior to photon excitation under similar conditions.

CHAPTER 3

— EXPERIMENTS I —

X-RAY PRODUCTION CROSS-SECTION MEASUREMENTS

3.1 Introduction

For analytical applications of the spectrometer, values of cross-sections for the production of X-rays by $\sim$ 5 MeV alpha-particles were desirable in correcting for the enhancement effects much in evidence at low X-ray energies. Only relative cross-sections were needed, and the K X-rays of the elements from oxygen to calcium were of most interest. Unfortunately there was a scarcity of published experimental data in this region, and what little did exist was inconsistent between authors and subject to large errors (see subsection 3.4.3).

The experiments of this chapter were designed to provide an internally consistent set of relative cross-sections for elements and X-rays of immediate interest to the analytical work to be described in chapter 4. Although cross-sections as a function of alpha-particle energy are what are ultimately needed, such measurements were not considered practical under present circumstances. All measurements were carried out with the 5.26 MeV alpha-

particle output of source II (see subsection 2.2.2).

3.2 Detector efficiency estimation

3.2.1 Silicon dead-layer thickness:

The partially active layer of silicon on the entry side of Si(Li) detectors presents a barrier to low-energy X-rays. Its exact structure is not known but it is usually considered to be a discrete layer with a high concentration of charge-trapping centres. Its thickness varies from one detector to another, and usually is inversely related to applied detector bias; the normal range is $\sim$ 0.1 - 0.5 μm (3, 43, 44).

Four approaches to thickness determination were tried. The first two were variations of a method used successfully by Jaklevic et al. (43), viz. measurement of the magnitude of the discontinuity in a bremsstrahlung spectrum at the silicon K-absorption edge. The cited authors utilised the bremsstrahlung from electron-gun produced 3.5 keV electrons on a beryllium target. The present attempts were with bremsstrahlung from a 10 mCi ^{3}H source and with the secondary-electron bremsstrahlung from $\sim$ 5 MeV alpha-particles on a carbon target. Neither

of these efforts was successful; no discontinuity was observed even at low applied detector bias. A possible reason for failure was incomplete charge collection from higher energy radiation which would add an unknown constant to the data points in the absorption edge region (1.84 keV), especially for the ^{3}H source where the bremsstrahlung peaked at $\sim$ 5 keV.

The third attempt involved comparisons of calculated and observed escape peak* intensities. The calculated values of escape peak intensity relative to corresponding photopeak intensity were derived from numerical integrations of the expression (see Appendix 2):

$$\frac{F\omega\mu_1}{2} \int_{r=0}^{\infty} \int_{\theta=0}^{\pi/2} e^{-\mu_1 r}\, e^{-\mu_2 \sec\theta (r+d)} \sin\theta\, d\theta\, dr$$

where F is the ratio of K-shell photoelectric to total absorption cross-sections of silicon for the incoming photons, ω is the K-shell fluorescence yield of silicon, μ_1 and μ_2 are the total absorption cross-sections of

---

* Si K X-ray escape

silicon for the incident photons and silicon K X-rays respectively, r is the penetration of the normally incident photons into the active region of the detector, and d is the thickness of the dead-layer. Values of this integral against dead-layer thickness are shown in Table 7; the values of the parameters used were $\omega = 0.047$ (from Ref.45) and $\mu_2 = 340\ cm^2g^{-1}$, $\mu_1 = 145\ cm^2g^{-1}$, $F = 0.91$ (all derived from data presented in Ref. 46). The experimentally found relative escape peak intensities and corresponding derived dead-layer thicknesses vs. applied detector bias are shown in Table 8 for the Mn K X-rays from ^{55}Fe. The incident X-rays were collimated to fall normally upon the 3.5 mm diameter central region of the detector.

The fourth method compared experimentally observed integrated Al K X-ray photopeaks with the corresponding integrated incomplete charge-collection plateaus assumed to extend linearly from the lower energy limits of the photopeaks to zero energy. The Al K X-rays were produced in the spectrometer using the alpha-particle output from source II (see subsection 2.2.2) upon an 8 mm diameter

TABLE 7

Calculated Mn K_α X-ray escape peak intensity vs. silicon dead-layer thickness

Dead-layer thickness ($\mu g\ cm^{-2}$ Si)	20	40	50	70	100	130
Relative escape-peak intensity (%)	0.353	0.348	0.346	0.341	0.325	0.328

TABLE 8

Silicon dead-layer thickness vs. detector bias estimated according to Table 7

Detector bias (volts)	1200	1000	800	500	300
Measured escape-peak relative intensity (%)	0.348	0.349	0.345	0.321	0.305
Estimated dead-layer thickness ($\mu g\ cm^{-2}$)	40	35	55	>130	>130
" (μm)	0.17	0.15	0.24	>0.6	>0.6

TABLE 9

Silicon dead-layer thickness vs. detector bias estimated according to Al K X-ray transmission

Detector bias (volts)	1200	1000	800	600	400
Al X-ray transmission	0.975	0.975	0.963	0.952	0.934
Estimated dead-layer thickness (μm)	0.20	0.20	0.29	0.39	0.53

aluminum target. The detector was screened with a lead collimator so that only the 3.5 mm diameter central region was exposed. Contributions to the spectra by room-background, excitation source background and bremsstrahlung were allowed for by subtracting out a spectrum obtained identically for an 8 mm beryllium target. The transmissions of Al K X-rays through the dead-layer calculated from the experimental data and the corresponding calculated dead-layer thicknesses are shown in Table 9. A mass absorption coefficient of 550 cm^2 g^{-1} derived from Ref. 46 was used.

From Tables 8 and 9 a reasonable estimate of the silicon dead-layer thickness at -1000 v bias is 0.2 ± 0.1 μm. The error estimate is a conservative one based on the obvious discrepancies in the data, uncertainties in the assumed models and errors in the parameters used in calculations. The counting statistical errors were in all cases < ± 2%. Weight has been placed upon the Al K X-ray transmission data, as suggested by Goulding (personal commun. and Ref. 65). The escape peak method serves more as a rough confirmation; there are more uncertain parameters used in its application and with the 5.9 keV X-rays used it is fairly insensitive

to dead-layer thickness variations*.

3.2.2 Gold contact thickness:

Si(Li) detectors usually have an evaporated layer of gold as an electrical contact on the X-ray entry side. The thickness of the layer on the detector used here was quoted by the manufacturer as being nominally 200 Å. For present purposes it was assumed to be a uniform deposit, although there may be doubts about this (43).

Attempts to measure gold layer thicknesses usually depend upon irradiating the operative detector with photons of energy just above one or more of the Au L-absorption edges. This method has been suggested by Hansen et al. (47) and used by Campbell et al. (48). The Au L X-rays are detected superimposed upon a large Compton-scattered background. The layer thickness, x, is calculated absolutely by estimating the intensities of the incident radiations and the Au L X-rays from the observed spectrum and by applying the expression,

---

* Attempts to increase the sensitivity through the use of alpha-particle induced Cl K X-ray were unsuccessful because of high background in the escape peak region.

$$x = \frac{2\ N_{Au}}{\omega\ E_{Au} N_{ex}} \sum_i \left(\frac{E.R}{\mu}\right)_i \quad ;$$

where N_{Au} and N_{ex} are the detected total counts for the Au L X-rays and the excitation radiation photopeaks respectively; ω is the Au L-shell fluorescence yield, E_{Au} is the photopeak efficiency of the detector for Au L X-rays (usually assumed to be unity); and E_i, R_i and μ_i are respectively the photopeak detection efficiency, relative intensity and Au L-shell mass absorption coefficient of the i^{th} component of the incident radiation. The formula as written here assumes all of incident radiations to have energies above the L_1 - absorption edge.

An experiment of the above type was carried out using the Ag K_α and K_β X-ray emissions of ^{109}Cd. The detector was shielded with a steel collimator so that only the 3.5 mm diameter central region was exposed. The source-detector distance was $\sim$ 11 cm. The counting time was 1.03×10^5s. The results of the experiment are summarized as follows:

$$x = \frac{2x5545}{0.39x1.0x(1.56x10^{8})} \left[\frac{0.85x0.84}{33.7} + \frac{0.75x0.16}{25.3} \right]$$

$$= 4.7x10^{-6} \text{ g cm}^{-2}$$

$$\rightarrow \underline{24 \text{ Å} \pm \sim 30\%}$$

The value was less than the expected one by a factor of about eight. As a check, a more empirical approach was devised. Evaporated gold targets on thin polystyrene backings were interposed between the excitation source and detector, and the experiment repeated. The Au X-ray intensities from the target were obtained by difference and x was calculated through applications of the inverse square law and small absorption corrections. The data from two such experiments are presented in Table 10. The results, 23 Å and 26 Å ($\pm \sim 20\%$ and $\sim 40\%$), are in good agreement with the more absolute method.

Reflection upon the above results led to thoughts that the energetic photo-electrons may have been responsible for reducing the contribution to the Au X-ray peaks from the detector contact. The coincident photo-electrons would have energies of $\sim$ 10 keV and Evans (1) has presented evidence indicating that 60-70% of them would travel in the forward direction, ie. into the detector. This would provide some

TABLE 10

Gold contact thickness estimation (secondary Au-target method)*

	^{109}Cd excitation (0.6 mCi)			^{85}Sr excitation (1.0 mCi)		
	(targets)***			(targets)***		
	None	248 Å	2270 Å	None	248 Å	2270 Å
Count-time (seconds)	1.03×10^5	5×10^4	1.5×10^4	2×10^5	8×10^4	10^4
Observed Au-L X-ray counts	5545±1000	5774±680	10069±385	7977±1170	5837±741	4197±268
Counts attributable to detector contact	-	2692	808	-	3191	399
Counts attributable** to target	-	3082	9285	-	2646	3818
Targets counts adjusted**** for geometry and absorption	-	25748	77569	-	22105	31896
Estimated Au contact thickness	-	26Å ± 37%	23Å ± 21%	-	38Å ± 41%	29Å ± 20%

* With ^{109}Cd the Au L_α and L_β lines were used; with ^{85}Sr only the L_α.

** For the 2270Å Au target, allowance has been made for 3% and 5% attenuation of the ^{109}Cd and ^{85}Sr excitation radiations within the target and consequent reduction of detector contact counts.

*** The target thicknesses were determined by neutron activation analysis - the values agreed within ~20% with the values roughly obtained via the quartz oscillator monitor of the evaporator.

**** The target diameters were 2.4 cm, the excitation source distance 3.3 cm and the target detector distance 7.5 cm; the solid angle correction factor was therefore 0.126. The correction factor for absorption of Au X-rays in the air path and Be window was 0.95.

additional charge and result in the disappearance of ∿ two-thirds of the events from the Au X-ray peaks.

To resolve the question, secondary Au-target experiments identical with those for ^{109}Cd were performed with ^{85}Sr. With the latter isotope > 80% of the photoelectrons are < 1.5 keV and should not enter the detector active-volume. The data from these experiments are also presented in Table 10. The results, 29 Å and 38 Å (± ∿ 20% and 40%), are inconclusive however with respect to the effect of the photoelectrons. If it occurs at all, it is evidently too weak to account for the previous low results.

Based on the data in Table 10, a value of 32 Å ± 10 has been used in the detection efficiency calculations below. This figure is the mean of the results obtained using ^{85}Sr (weighted according to the quoted errors), these data being less susceptible to any photo-electron interferences.

3.2.3 Overall efficiency:

For X-rays penetrating the Si dead-layer and Au contact, the intrinsic efficiency of the detector was assumed to be unity upto 8 keV. Attenuations in Si and Au layers of thicknesses 0.2 μm and 32 Å were calculated using the tables of Veigele et al. (46). The efficiency curve is shown in Fig. 21.

Figure 21. Calculated intrinsic Si(Li) detector efficiency

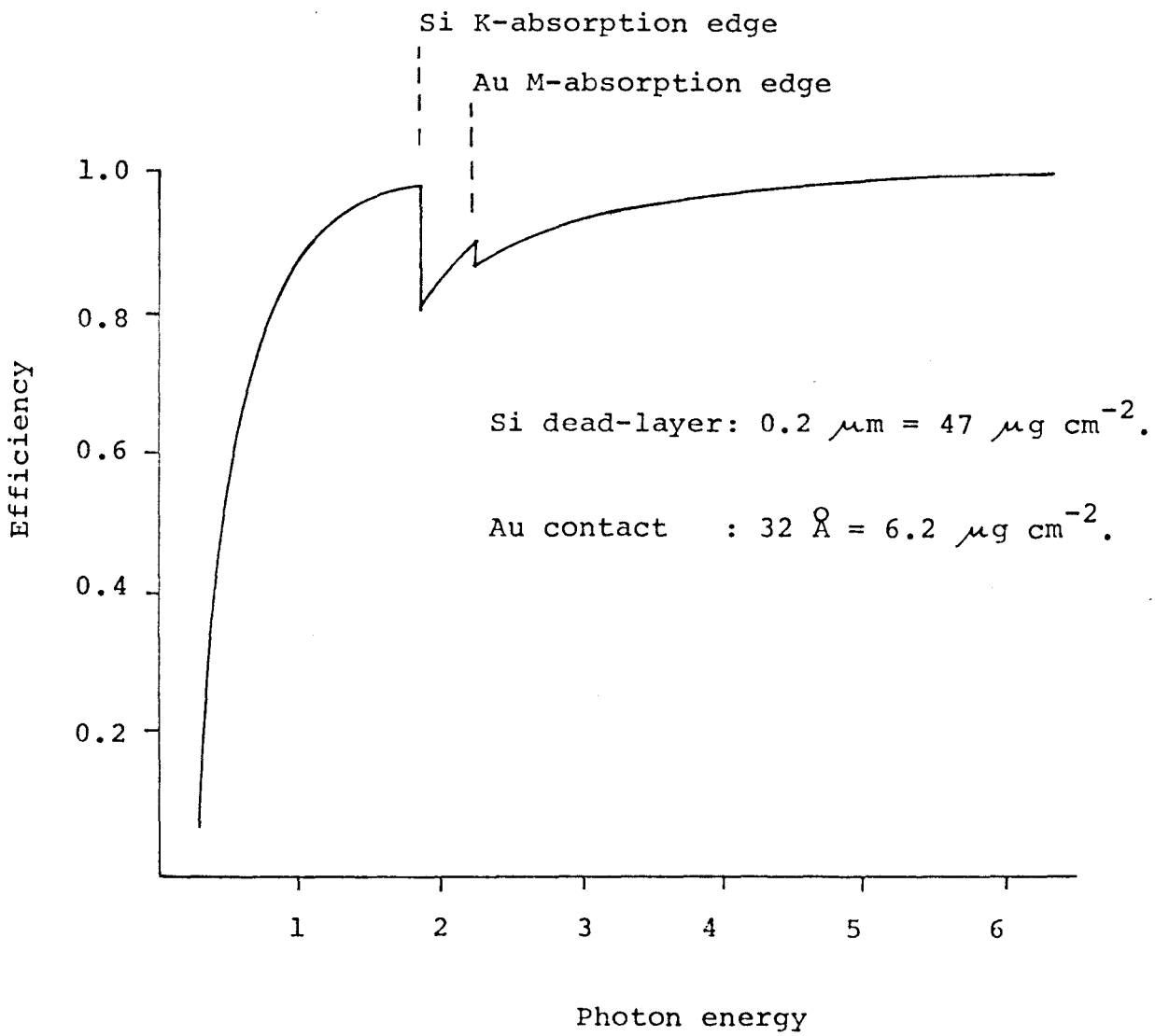

3.3 Targets

3.3.1 Preparation:

Pure elements or compounds were evaporated onto smooth 1 mm thick polystyrene backings (35 mm diameter plastic petrie dishes). The evaporator used was the model 720 of NRC Equipment Corp., Palo Alto, California, U.S.A. Source heating was either by electron-gun on the copper hearth of the evaporator or by resistive heating in tantalum crucibles. A working pressure of $< 10^{-5}$ mm Hg was used. The source to backing distance during the evaporation process was $\sim$ 15 cm, large enough to ensure no significant variation in thickness across individual targets. The target diameters were in all cases 2.40 cm. Thicknesses were always < 400 µg cm^{-2} leading to a $<$ 300 keV loss in energy upon impact by $\sim$ 5 MeV alpha-particles at the experimental angle of incidence (see subsection 3.4.1).

3.3.2 Thickness estimations:

Target thicknesses were measured by standard neutron activation analysis (NAA) procedures after dissolution of the targets from their backings with

dilute acid solutions, either 2 M HF or 2 M HNO_3. Each target material was quantitatively transferred with 2 ml of solution into a 3 ml volume polyethylene vial. The solutions were irradiated in the rabbit system of the McMaster Nuclear Reactor at a neutron flux of $\sim 5 \times 10^{12}$ n $cm^{-2} s^{-1}$. The irradiation, cooling and counting times were chosen to suit the isotope measured. At least two comparator standard solutions of the elements were used for calibration in irradiations immediately before and after the sample irradiation. An exception to the above procedure was the Fe target which needed a 48 hour irradiation. It was transferred to a quartz vial and the solution evaporated to dryness before co-irradiation with a solid Fe_2O_3 comparator. All counting was done with a Ge(Li) gamma-ray spectroscopy system.

The targets, their thicknesses and the corresponding reactions used are listed in Table 11. The errors quoted are a combination of the NAA counting errors plus an arbitrarily assigned 3% error estimated from previous experience with similar measurement procedures.

TABLE 11

Cross-section Measurement Targets

Target	Thickness ($\mu g\ cm^{-2}$)	Nuclear reaction used in thickness measurement
LiF	179 ± 6%	$^{19}F(n,\gamma)^{20}F$
NaCl	211 ± 5%	$^{23}Na(n,\gamma)^{24}Na$
	209 ± 5%	$^{37}Cl(n,\gamma)^{38}Cl$
Mg	124 ± 6%	$^{26}Mg(n,\gamma)^{27}Mg$
Al	48.4± 6%	$^{27}Al(n,\gamma)^{28}Al$
Al_2O_3	127 ± 5%	"
SiO	65.0± 8%	$^{28}Si(n,p)^{28}Al$*
SiO_2	160 ± 7%	"
Sb_2S_3	135 ± 5%	$^{121}Sb(n,\gamma)^{122}Sb$
KBr	392 ± 7%	$^{41}K(n,\gamma)^{42}K$
	382 ± 5%	$^{81}Br(n,\gamma)^{82}Br$
CaO No. 1	120 ± 6%	$^{48}Ca(n,\gamma)^{49}Ca$
CaO No. 2	190 ± 6%	"
V	198 ± 5%	$^{51}V(n,\gamma)^{52}V$
Fe	247 ± 4%	$^{58}Fe(n,\gamma)^{59}Fe$

* Samples and comparator standards were shielded with 1 mm thick cadmium wrapping to suppress the reaction $^{27}Al(n,\gamma)^{28}Al$ on aluminum contamination. The results were confirmed, although with poor statistical precision (± ∿ 20%) through the reaction $^{29}Si(n,p)^{29}Al$ which is free from interference by aluminum.

3.4 Cross-section measurements

3.4.1 Experimental arrangement:

Six of the sample positions of the spectrometer were machined out to accept the 35 mm diameter target backings. The usual alpha source-sample-detector configuration (see subsection 2.2.3) was altered as shown in Fig. 22. The collimators were used to ensure that the targets were essentially homogeneously irradiated and that the emergent X-rays were close to normally incident on the detector to facilitate absorption corrections. Apart from these changes the spectrometer was operated in its usual mode. It was estimated that the average alpha-particle energy used, allowing for attenuation within targets, was 5.2 MeV.

3.4.2 Experimental data and results:

Spectra were acquired over periods ranging from 1000 to 5000 seconds. Some representative examples are shown in Fig. 23. The peaks were integrated between limits defined by the full-width at one-fifth maximum. For the K X-rays of the elements from Cl and above only the K_α peak was used and an adjustment made according to the K_β/K_α

Figure 22. The source-target-detector configuration for cross-section measurements.

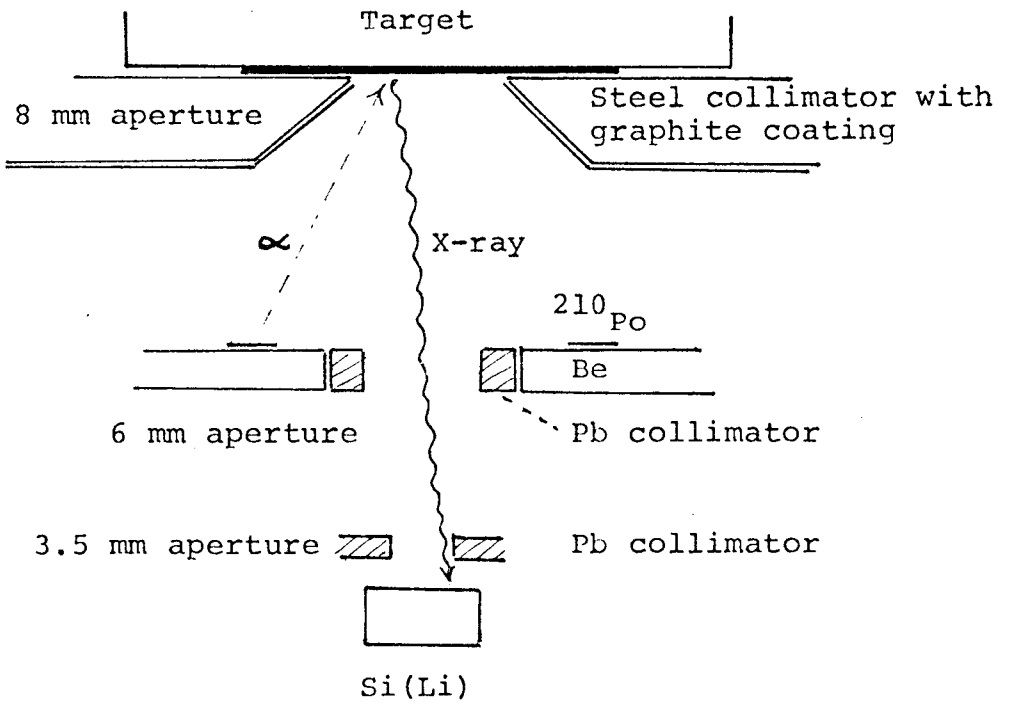

Figure 23. Typical spectra obtained in cross-section measurements.

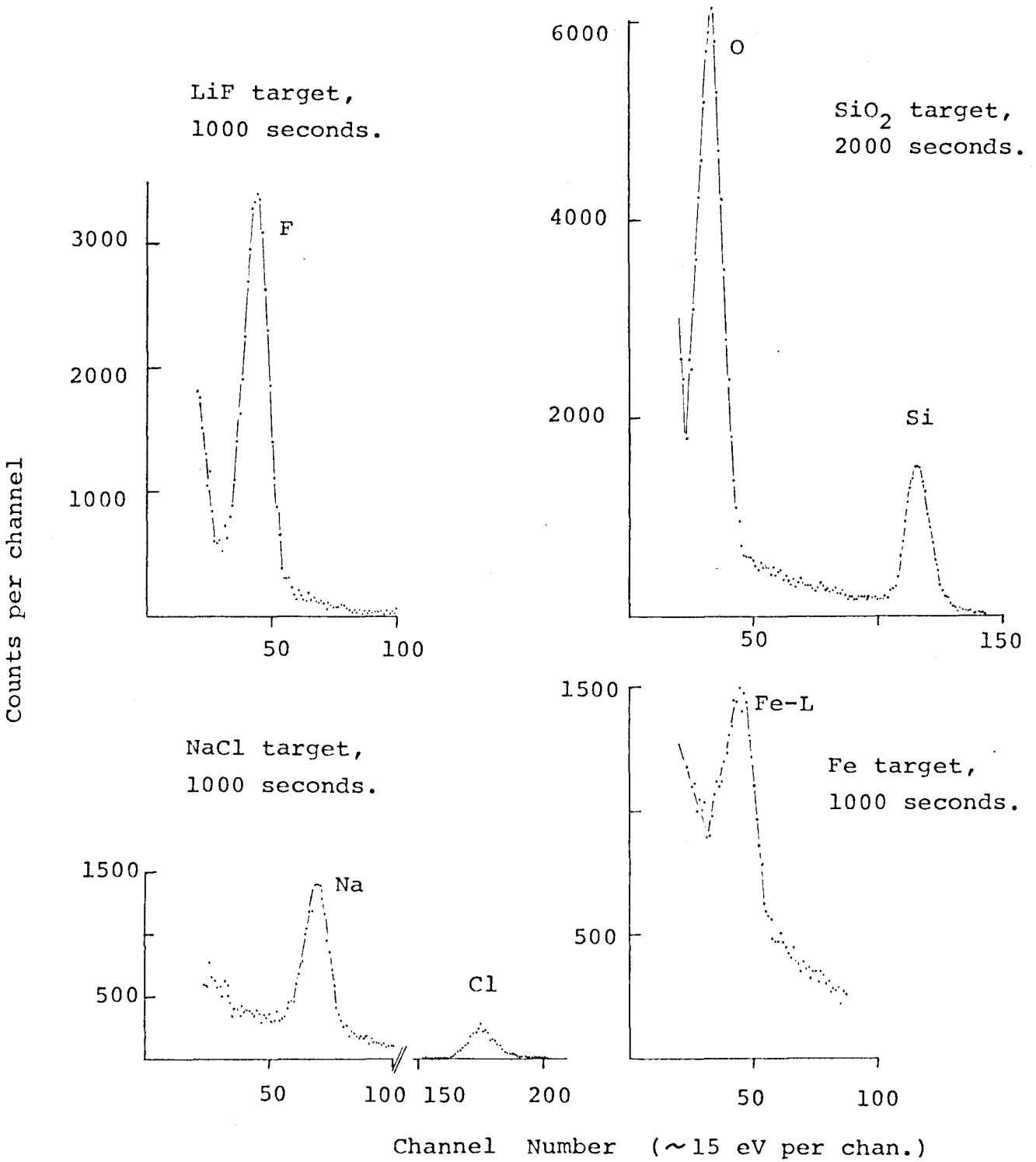

ratios given by Scofield (49).

The integrated net peak areas, the absorption correction factors and reduced data are shown in Table 12. The transmissions through the gold contact and silicon dead-layer of the detector, T_{Au} and T_{Si} respectively, were calculated using the mass absorption coefficient compilation of Veigle (46). The fractional transmission from a homogeneously irradiated target of average mass absorption coefficient μ and thickness t is $T_t = (1 - e^{-\mu t})/\mu t$ (see Appendix 2).

The experimentally obtained cross-sections relative to the K X-ray production cross-section of Fe are presented in Table 13. The values per unit weight are the figures given in the last column of Table 12 divided by the figure for Fe in the same column. The values per atom include a multiplication by the appropriate atomic weights.

3.4.3 Comparisons with literature values:

In 1973 Rutledge and Watson (23) compiled all currently available cross-sections for K shell ionization by light ion impact (i.e. for $Z_1 \leq 2$, where Z_1 is the

TABLE 12

Reduced cross-section data

Element	Target*	Element density (μg cm^{-2})	Count-time (seconds)	Accumulated counts	** T_{Au}	T_{Si}	T_t	Counts/μg element/1000s		
O	Al_2O_3	60.3	1000	16442	0.84	0.66	0.76	1293	1394	±25%
O	SiO_2	85.3	2000	50212	0.84	0.66	0.71	1495		
F	LiF	141	1000	33876	0.91	0.81	0.92		709	±20%
Na	NaCl	82.9	1000	12579	0.96	0.94	0.84		400	±15%
Mg	Mg	124	1000	16146	0.98	0.96	0.97		285	±10%
Al	Al_2O_3	67.3	1000	7113	0.99	0.97	0.94	234	219	±10%
Al	Al	48.4	1000	4686	0.99	0.97	0.99	204		
Si	SiO_2	75.0	2000	15716	0.99	0.98	0.95	227	209	±10%
Si	SiO	41.4	1000	3755	0.99	0.98	0.98	191		
S	Sb_2S_3	38.2	2000	2732	0.98	0.90	0.93		87.2	±15%
Cl	NaCl	127	1000	3110	0.99	0.93	0.95		56.0	±13%
K	KBr	129	1000	1345	0.99	0.96	0.87		25.2	±14%
Ca	CaO (i)	85.8	5000	3630	0.99	0.97	0.99	17.8	17.9	± 8%
Ca	CaO (ii)	136	5000	5825	0.99	0.97	0.99	18.0		
V	V	198	5000	3280	0.99	0.99	0.99		6.83	± 8%
Fe	Fe	247	5000	1932	0.99	0.99	0.99		3.22	± 7%
Fe-L	Fe	247	1000	8729	0.92	0.83	0.40***		231	±20%

* Exposed target diameter = 0.5 cm^2.

** The "T" factors are the transmissions of the detector dead-layers and the targets.

*** In calculating this figure, it has been assumed that ionisation by the alpha-particles is equally probable in all the L subshells; and Coster-Kronig transition probabilities of f_{12}=0.302, f_{13}=0.652 and f_{23}=0.072 have been taken into account (45).

TABLE 13

Measured relative cross-sections
for ∿ 5.2 MeV alpha-particles

Element	Relative cross-sections (per unit weight)	(per atom)	Estimated errors
O	433	124	± 26%
F	220	75	± 21%
Na	124	51	± 17%
Mg	89	38.5	± 12%
Al	68	32.9	± 12%
Si*	65	32.6	± 12%
S	27.1	15.5	± 17%
Cl	17.4	11.0	± 15%
K	7.8	5.5	± 16%
Ca	5.6	3.99	± 11%
V	2.12	1.93	± 11%
Fe	1.00	1.00	
Fe - L	71.7	71.7	± 21%

* The result for silicon appears to be high. It was decreased by 10% for the analytical work described in Chapter 4.

projectile charge). In Table 14 are listed the relevant X-ray production cross-sections by ∿ 5.2 MeV alpha-particles as derived from this compilation. Most of the data shown have been obtained through short extrapolations or interpolations (only between points from identical publications) followed by adjustments for fluorescence yields. Although the general trend of the data is apparent, so is the futility of trying to extract a reliable set of cross-sections from this source. Most of the authors quote uncertainties of < ± 30%, but between authors there are differences of up to a factor of six. Note also the absence of data between Si and Ca. There have been more recent measurements (50, 51, 52) but most of these are for alpha-particle energies or elements outside the range of interest here. In any case, small additional amounts of data would probably confuse the issue; a major experimental effort is needed to resolve the discrepancies.

Various theories (20, 53, 54), at least to a first approximation, allow a Z_1^2 scaling (i.e. x 4) of proton induced X-ray production cross-sections to obtain values

TABLE 14

K X-ray production cross-sections for 5.2 MeV alpha particles*

Element	Cross-section (barns/atom**)
Mg	5060 [a]
Al	5820 [a]
	3000 [b]
	835 [c]
Si	409 [c]
Ca	782 [d]
Sc	627 [d]
Ti	438 [d]
	121 [c]
Cr	243 [d]
	81 [c]
Mn	192 [d]
Fe	58 [c]

* Derived from the compilation by Rutledge and Watson (23)

** The superscripts indicate values from identical publications

for equal velocity alpha-particles (providing the particle energies are much greater than the electron binding energies). In Table 15 are listed the cross-sections obtained in this way from the Rutledge and Watson compilation, again mostly through short interpolations and extrapolations. The uncertainties quoted by the various authors are < ± 30%. Note once more the lack of data between Si and Ca. Also listed are Z_1^2 scaled values obtained from the universal curve for K shell ionization by protons as constructed by Johansson and Johansson (30) according to the theory of Garcia (54). The curve is based upon recent thin target measurements and cross-sections may be derived from it through a knowledge of the proton energy and the appropriate electron binding-energy. From Table 15 it appears to be reasonably valid for K shell ionization by 1-2 MeV protons for all elements of $Z \geq 8$.

The relative scaled cross-sections from Table 15 obtained from the curve of Johansson and Johansson are plotted in Fig. 24. Also plotted are the values obtained experimentally in the present work. The Z_1^2 scaling

TABLE 15

K X-ray production cross-sections for 5.2 MeV alpha-particles obtained by Z_1^2 scaling of proton values*

Element	Experimental cross-sections** (barns/atom)	Cross-sections derived from the universal curve of J and J (30) (barns/atom)	(Relative to Fe)
O	6528 [a]	6100	47.7
F	5760 [a]	5900	46.1
Na		4820	37.7
Mg	3500 [b]	4000	31.3
Al	2870 [b]	3350	26.2
	2160 [c]		
Si		2700	21.1
P		2160	16.9
S		1700	13.3
Cl		1360	10.6
K		820	6.4
Ca		640	5.0
Sc	3.2 [d]		
V		286	2.23
Fe	70 [e]	128	1.00

* The experimental values were derived from the compilation by Rutledge and Watson (23)

** The superscripts indicate values from identical publications

Figure 24. Measured relative X-ray production cross-sections compared to Z_1^2 scaled values for protons.

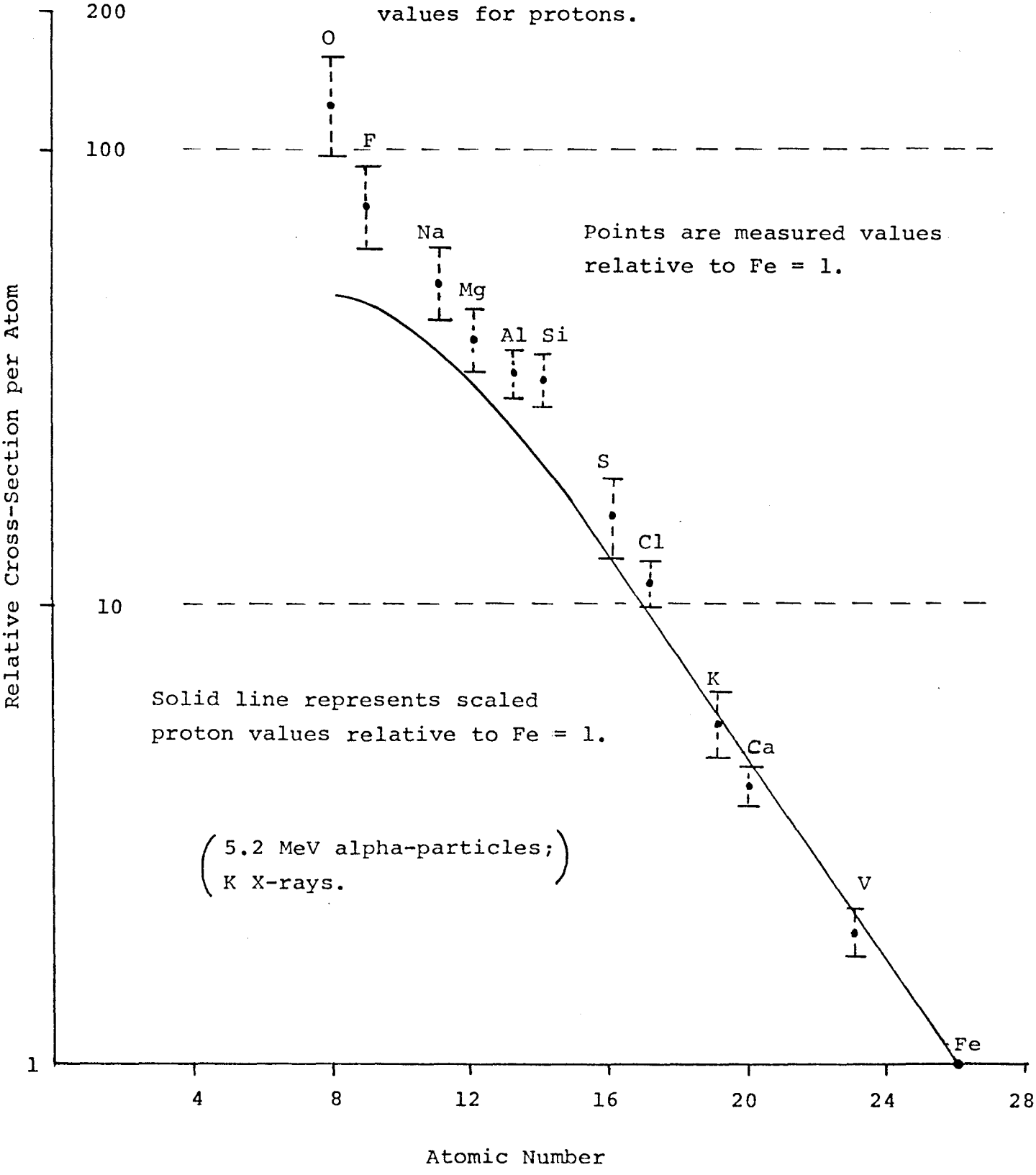

appears to work well only for atomic-numbers $\geq$ 16 (sulphur). Both Johansson and Johansson and Garcia et al. (22) indicate that Z_1^2 scaling between protons and alpha-particles should be valid within a few tens of percent, with no clearly defined constraints upon target atomic-numbers. But they considered essentially only heavy-element targets*. The present results are more consistent with their observations upon ionization by heavy ions (i.e. $Z_1 > 2$). Highly charged projectiles do not behave as point charges and thus violate their basic theoretical assumption. Polarization of the target atomic-shells and other effects occur, the net result being an enhancement of inner-shell ionization probabilities. This effect occurs for oxygen and heavier ions on high-Z targets and attempts have been made to exploit it for analytical purposes (55). It seems alpha-particles behave in a similar

---

* With the exception of the K shell ionization cross-section values for Mg and Al for 25-50 keV protons used by Johansson and Johansson, both they and Garcia considered only elements of $Z \geq 18$.

way on light-element targets. The present experimental values are also consistent with the line broadening effects noted in subsection 2.4.1.

Another possible reason for the apparently enhanced cross-sections for low-energy X-rays is the influence of secondary electrons. As pointed out in subsection 2.4.4, the maximum energy of these electrons produced by 5.2 MeV alpha-particles is $\sim$ 2.8 keV, i.e. the approximate X-ray energy below which the deviations occur. This idea is supported by calculations made by Van der Kam et al. (56) who suggest that enhancement of K X-ray emission by secondary electrons from 2.5 MeV protons is important for elements of $Z < \sim 25$, i.e. the element whose K shell electron-binding energy approximately corresponds to the maximum secondary-electron energy. The magnitude of the calculated effect was shown to increase with decreasing target-atom Z; and to increase with increasing average Z of the matrix in which the target atoms were contained, the heavier matrix elements making more fast electrons available.

The above argument is offset by calculations by Folkmann et al. (57) and Akselsson and Johansson (58) who indicate that the secondary-electron contribution to proton-induced X-ray production cross-sections is insignificant; the latter pair suggest that it is < 5% for proton energies around 2000 times that of the K-edge of the target element*. These calculations are supported by the data presented in Table 15. Extrapolations of the universal curve for protons from the heavy element region, where the experimental data for the curve were obtained and where no secondary-electron effects should occur, to the light elements, shows no significant conflict with the direct experimental measurements made in the light-element region.

3.5 Summary

The Si(Li) detector efficiency has been estimated. The silicon dead-layer thickness found, $\sim 0.2\ \mu m$, is within the normal range. The gold contact thickness measured, ~ 32 Å, is substantially less than the manufacturers

---

* Thin targets with respect to the proton energies - but thick enough to stop the 2^{o} electrons.

nominally stated 200 Å . But this latter figure is not to be taken too seriousy; to quote from a letter to the author from Kevex Corporation:- "..... As for the gold, the 200 Å value is the best we can say without explicit measurements (which we are not set up for here). Depending on the age of your detector, the gold may well be somewhat thinner. .." Furthermore, Campbell et al. (48) have also found a low value (90 Å) for a similar Kevex product.

The desired relative cross-sections for X-ray production by ~5 MeV alpha-particles have been measured.* The values deviate positively from those expected by Z_1^2 scaling of proton values. This may be caused by distortion of the atomic-electron orbits by the alpha-particles, or by secondary-electron enhancement. The general scarcity of experimental evidence leaves the matter open to question.

---

* The exception was phosphorus for which no suitable target-material was available.

CHAPTER 4

- EXPERIMENTS II -

ELEMENTAL ANALYSIS

4.1 Introduction

X-ray emission analysis is applicable to many materials consisting essentially of light elements. Among them may be listed rocks, minerals, glasses, ceramics, fertilizers, cements, biological tissues, organic compounds and so on. This chapter examines the capabilities of alpha-particle emitters in bringing these materials within the scope of radioisotope-based techniques. The major problems expected were those connected with the short ranges of the X-rays and alpha-particles, and with differences in composition and form between specimens. The associated questions of representative sampling, and absorption, enhancement and particle-size effects were studied experimentally through examples.

4.2 Qualitative and semi-quantitative measurements

Dry, powdered samples were presented for analysis as pressed discs 32 mm in diameter. The spectrometer was operated under high vacuum with the source-sample-detector

configuration as shown in subsection 2.2.3. Source I was used for excitation.

The spectrum of a vegetation sample, Bowen's Standard Kale (59), is shown in Fig. 25(a). According to Jones (60), at least half a million samples per year of this type are analyzed for light elements by a variety of methods, mainly with respect to the efficiency of fertilizers. As a trial of the present technique, mountain aspen leaves and a forage sample were analyzed for potassium. Values of 12,300 and 10,700 ppm respectively were obtained. Bowen's kale was used as comparator and no absorption corrections were applied. The corresponding results by neutron activation analysis were 12,600 and 9,900 ppm, the two methods agreeing within the statistical counting errors.

The prospects with regard to elemental analysis of organic compounds are indicated by Fig. 25(b). Destructive methods are now mainly used for these. The present approach, with refinement, may make possible rapid, non-destructive and simultaneous analyses for O, P, S, the halides etc. It is inherently a micro-method because of

Figure 25. Low-energy X-ray spectra of various sample types.

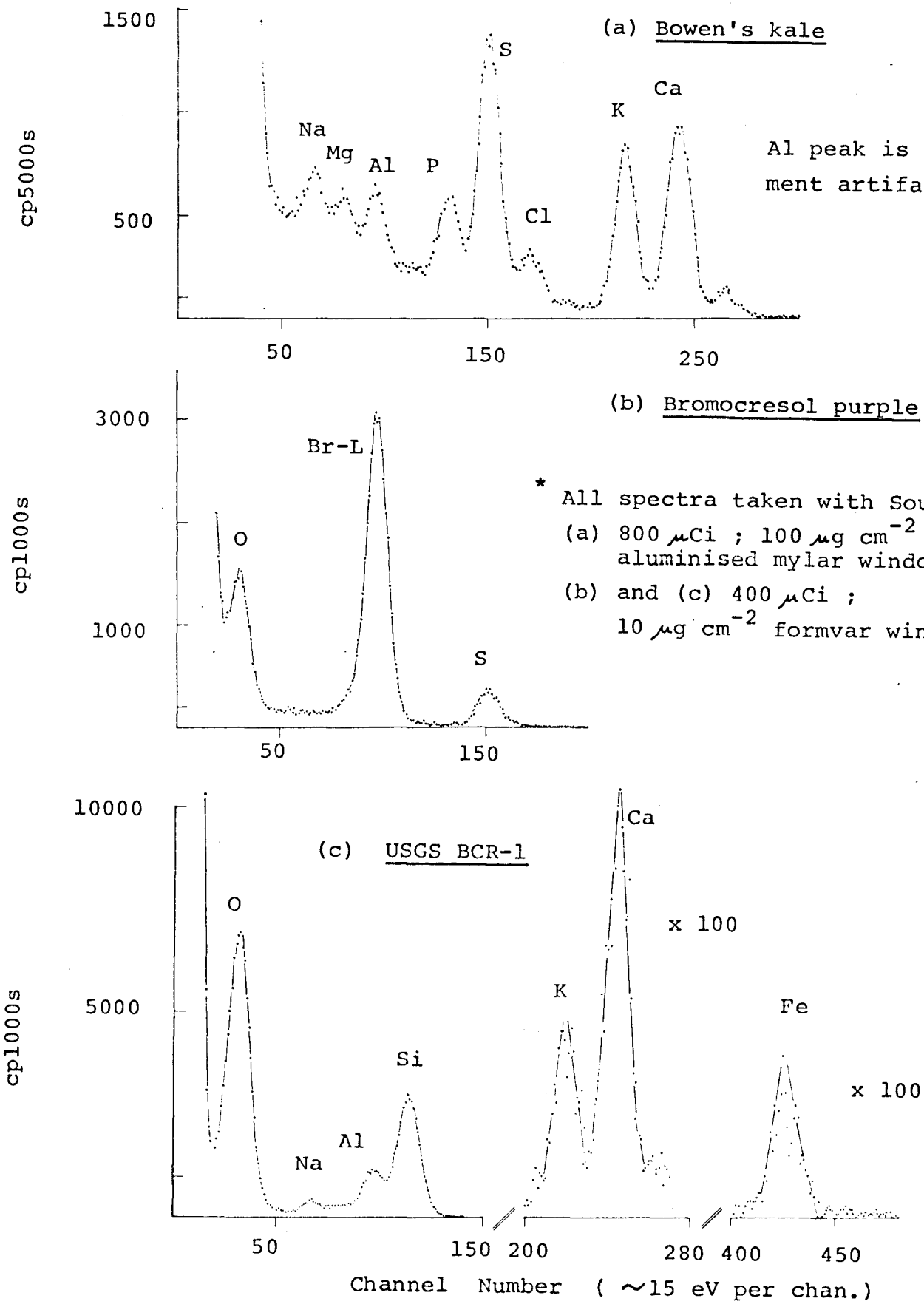

the short ranges of both the alpha-particles and the low-energy X-rays* and could well prove useful, especially for more precious samples where a non-destructive technique is desirable. The matter of sample-presentation is non-trivial but should not prove insurmountable.

The spectrum of a standard rock sample is shown in Fig. 25(c). Independent analyses of rocks for their oxygen content would be especially useful in view of possible anomalies in the stoichiometric ratios upon which calculated concentrations of the element are usually founded (61). The results of preliminary analyses of some standard rocks for oxygen and silicon are given in Table 16. The dispersion is largely attributable to differential absorption and enhancement effects. An attempt to correct for these is discussed in subsection 4.3.2.

---

* The range of 5 MeV alpha-particles in a carbon matrix is $\sim$ 4 mg cm^{-2}; the mean free path of S K_{α} X-rays is about the same. The effective sample size was therefore < 20 mg in the case shown.

TABLE 16

Preliminary analytical data for oxygen and silicon in some standard rocks

Rock*	%O	Found counts** per %O	% Si	Found counts** per % Si
USGS-BCR-1	44.8	1712	25.5	1709
USGS-GSP-1	47.8	1672	31.5	1880
NIM-D	42.5	2418	18.2	1460
NIM-G	49.1	1800	35.3	1837
NIM-L	44.2	1842	24.6	1743
NIM-N	45.2	1652	24.5	1617
NIM-P	43.4	2056	23.8	1607
		Mean = 1879		Mean = 1693
		Std.dev.= 15%		Std.dev.= 9%

* See subsection 4.3.1 for origins of samples

** Count-time = 1000s

4.3 Quantitative measurements

4.3.1 Samples:

Blast-furnace slags, iron ores and silicate rocks were studied. The first two represented cases often encountered or contrived in X-ray analysis, namely, nearly constant composition. They were analyzed directly without corrections for secondary effects. The silicate rocks were more difficult because of their widely disparate compositions. Here, an attempt was made to account for absorption and enhancement.

The slags and ores were provided by Dominion Foundries and Steel Limited (DOFASCO) of Hamilton, Ontario. Powdered samples of < 200 mesh (< 75μm) were homogeneously mixed with cellulose; the ratios were 20 g slag plus 2 g cellulose and 10 g ore plus 2 g cellulose. Smaller samples of a few grams were then pressed under 1000 kg cm^{-2} pressure into 32 mm pellets for analysis.

The rocks were standards issued by the United States Geological Survey (USGS)* and the South African National Institute of Metallurgy (NIM)**. Undiluted

---

* USGS., Washington, D.C. 20242, U.S.A.

** NIM, Auckland Park, South Africa

samples of a few grams of rock powder of < 200 mesh (< 75μm) were pressed into 32 mm pellets with an organic binder (< 0.1%) under ∿ 1500 kg cm^{-2} pressure.

In the analysis of all three sets of specimens, five samples were used for calibration. The major-element compositions of these are shown in Table 17. The values for the slags and ores were obtained by chemical methods in the Dofasco laboratories. Best values for the rocks have been summarized by Flanagan (62). The remaining samples, five slags, five ores and three rocks were treated as "unknowns". All samples were stored under vacuum dessication prior to use.

The elements analyzed for were S and Ca in the slags, Si and Fe in the ores, and O and Si in the rocks. These covered the effective elemental range of the spectrometer and suffered little spectral interference in the samples analyzed.

4.3.2 Preliminary studies - Secondary effects:

A: Absorption and enhancement corrections:

From the data presented in Table 16 it was

TABLE 17

Major components(%) of calibration standards used in elemental analysis

a) Rocks

	NIM-D	NIM-G	NIM-L	NIM-N	NIM-P
SiO_2	38.86	75.59	52.52	52.43	50.88
Al_2O_3	0.44	12.08	13.93	16.64	4.38
Total Fe as Fe_2O_3	16.97	2.02	9.77	9.00	12.29
MgO	43.30	0.10	0.36	7.43	25.19
CaO	0.31	0.80	3.30	11.55	2.68
Na_2O	0.10	3.32	8.27	2.44	0.37
K_2O	0.04	4.98	5.54	0.26	0.10
H_2O	0.4	0.6	2.4	0.4	0.3
TiO_2	0.04	0.09	0.5	0.20	0.20
P_2O_5	0.03	0.02	0.71	0.17	0.21
CO_2	0.4	0.1	0.2	0.1	0.1

b) Blast-furnace slags

	No. 14	No. 15	No. 16	No.17	No. 18
SiO_2	34.94	33.43	33.16	33.76	33.76
Al_2O_3	8.41	7.94	8.48	8.64	8.05
MgO	10.95	16.20	13.05	13.45	12.72
CaO	44.62	39.45	42.37	39.68	38.58
Fe	0.34	1.19	2.15	4.05	4.05
Mn	0.24	0.26	0.16	0.32	0.32
S	1.39	2.11	2.53	2.01	2.01

c) Iron ores

	No. 1	No. 6	No. 13	No. 19	No. 28
SiO_2	9.47	5.74	7.53	8.53	6.10
Al_2O_3	0.61	0.50	0.46	0.55	0.53
MgO	0.38	0.32	0.26	0.32	0.32
CaO	0.17	0.17	0.14	0.18	0.18
Fe	62.23	65.25	64.17	63.40	64.85
F_2O	0.15	0.11	0.06	0.09	0.11

apparent that in the rock analyses some account had to be taken of composition differences. For silicon, only absorption corrections were required; there were no intense X-rays above the Si absorption edge. For oxygen, enhancement also had to be considered.

The universal curve of Johansson and Johansson (30) indicates that the X-ray production cross-section of silicon for incident protons is almost linearly related to proton energy in the energy-range of interest. If the assumption is made that this relationship is maintained for equal velocity alpha-particles, the functional form of the cross-section is as represented in Fig. 26. The energy loss of $\sim$ 5 MeV alpha-particles is also quite linear and the two functions together indicate that the rate of production of Si K X-rays vs. sample penetration is approximately triangular in form. The transmission of X-rays from a target excited in this way is, as derived in Appendix 2,

Figure 26. Absolute silicon and oxygen X-ray production cross-sections, and alpha-particle energy vs. depth of penetration in SiO_2 matrix.*

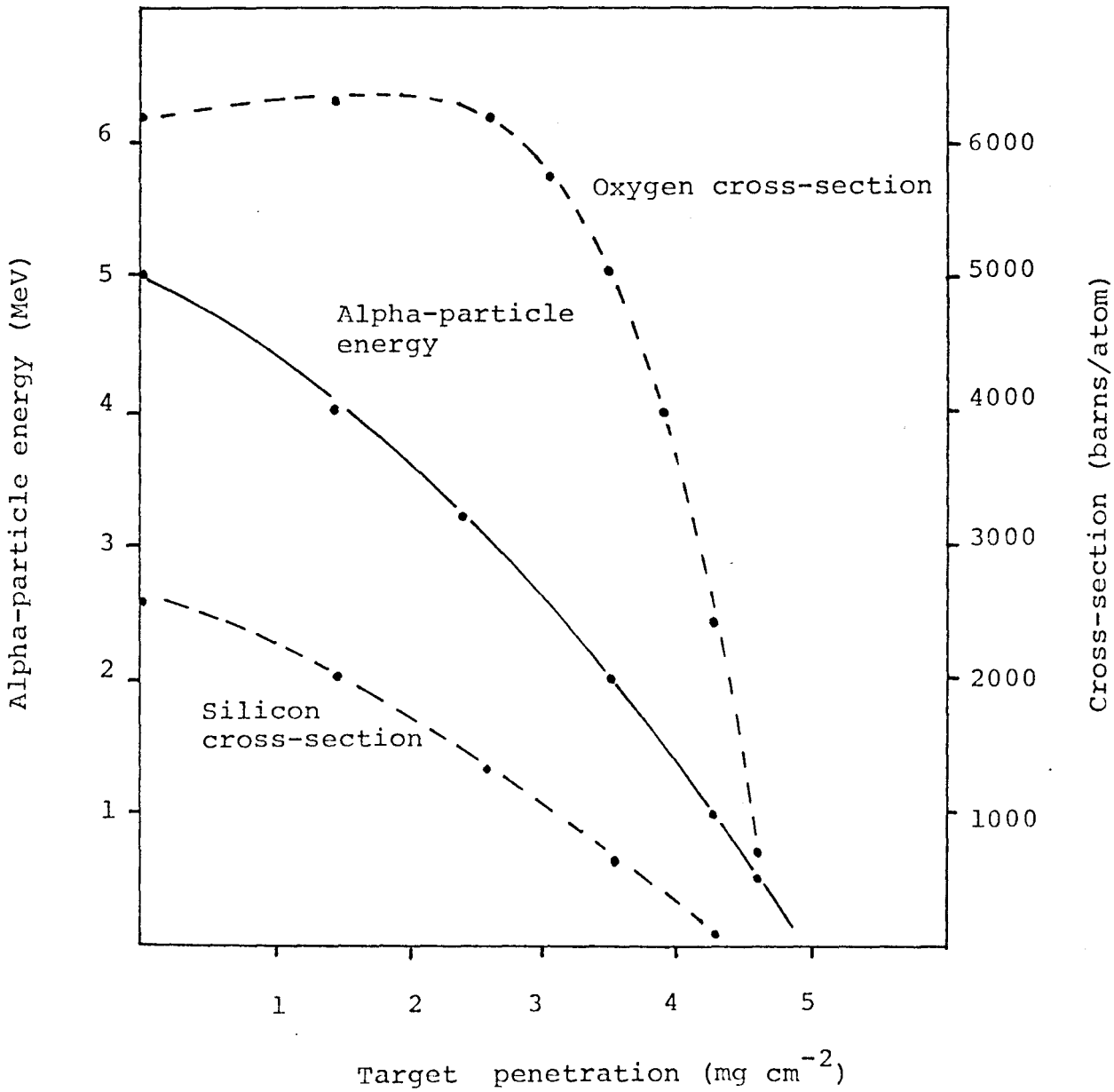

* Cross-sections Z_1^2 scaled from proton values according to Ref. 30.

$$T = \frac{2}{\mu R}(1 - e^{-\mu R}) - \frac{2}{(\mu R)^2}(1 - (\mu R+1)e^{-\mu R}) \quad *$$

where μ is the weighted mean mass-absorption coefficient and R is the alpha-particle range.

Based on the above arguments, the following model was used to account for Si X-ray absorption:

$$X_S = k_a \cdot \frac{T_S}{T_r} \cdot X_r$$

where X_S and X_r are the measured count-rates per percent silicon of a sample and a reference rock respectively; T_S and T_r are the corresponding transmission factors and may be calculated from a knowledge of the major elemental compositions of the rocks; and k_a is a weight to be assigned empirically to the ratio T_S/T_r . If the equation

---

* The picture is more complicated because of the varying angles of incidence of the alpha-particles and of the varying angles of emergence of the X-rays towards the detector. It has been calculated that the average alpha-particle penetration is $\sim$ 80% of the full range. This indicates that R above should be adjusted accordingly. But the non-normal X-ray emergence compensates for this. The expression as it stands should therefore give a reasonable first approximation to T.

is rewritten as $Y = k_a F_a$, where $Y = X_S/X_r$ and $F_a = T_S/T_r$, then it will be seen that k_a can be obtained from a straight line fit to a plot of Y vs. F_a for a series of calibration standards of known composition.

In oxygen determinations, a similar approach to absorption corrections was taken. Experimental and theoretical evidence (23, 30) indicates that the oxygen X-ray production cross-sections are almost constant between alpha-particle energies of 5.5 and 3.0 MeV (see Fig. 26). This means that the X-rays are produced in targets at constant intensity to a depth beyond which practically none of them escape. As shown in Appendix 2, the transmission in a case of this sort is $T = (1 - e^{-\mu R})/\mu R$. For present purposes R was taken as 1 mg cm^{-2}, a depth at which < 1% of the oxygen X-rays emerge.

Oxygen analysis was further complicated by enhancement effects. To a first approximation the degree of enhancement should be proportional to the efficiency with which X-rays above the oxygen absorption edge are produced, and to the photo-electric cross-sections of oxygen for these X-rays. Each rock was therefore assigned

an enhancement factor $E = \sum_i (C\sigma\beta)_i$, where the i's are the elements yielding X-rays capable of significantly enhancing oxygen X-rays (F, Na, Mg, Al, Si and Fe* in the present case); C_i is the concentration of element i; σ_i is the 5.2 MeV alpha-particle X-ray production cross-section of element i; and β_i is the photo-electric mass absorption coefficient of oxygen for the X-rays of element i.

The overall model used to account for oxygen X-ray absorption and enhancement was

$$X_S = k_a \cdot \frac{T_S}{T_r} \cdot X_r \left(1 + k_e \cdot \frac{E_S}{E_r}\right)$$

where X_S and X_r are the measured count-rates per percent oxygen of a sample and a reference rock respectively; T_S and T_r, and E_S and E_r are the corresponding transmission and enhancement factors; and k_a and k_e are weights to be assigned empirically to T_S/T_r and E_S/E_r respectively. The model may be rewritten as

$$\frac{Y}{F_a} = k_a k_e F_e + k_a \quad ,$$

---

* Only the Fe L X-rays need be considered

where $Y = X_S/X_r$, $F_a = T_S/T_r$ and $F_e = E_S/E_r$. It has the form $y = mx+b$ and k_a and k_e may be obtained from a straight-line fit to a plot of Y/F_a vs. F_e for a series of calibration standards.

Besides the approximations used, the above models have the obvious weakness of depending upon an essentially complete knowledge of the composition of the samples. When they are applied to real samples therefore, this knowledge will have to come from the recorded spectra; and corrections will need to be performed by a reiterative procedure.

In the present case advantage was taken of the known elemental compositions of the rocks as compiled by Flanagan (62). The mass-absorption coefficients were derived from the compilation of Veigele et al. (46). The alpha-particle ranges were obtained from the tables of Northcliffe and Schilling (63). The X-ray production cross-sections used were the relative ones (per unit weight) as measured in the present work and given in Table 13. NIM-D was used as the reference rock for the calculation of F_a and F_e factors. The results of actual analyses are reported in subsection 4.3.4.

B: Particle-size effects:

It is well known in X-ray emission analysis that the particle-size distribution of the sample material influences the emitted X-ray intensities. Experiments were therefore carried out to get some estimate of the magnitude of this effect in the present work. The relative intensities of O and Si X-rays from samples of SiO_2 of various particle-size ranges were measured. The samples were supported on 90 μg cm^{-2} mylar foils and presented to the spectrometer using the arrangement shown in Fig. 22 for the cross-section measurements. The results are given in Table 18. The influences of particle-size are pronounced for oxygen.

All that was known about the slags, ores and rocks to be analyzed was that they were < 200 mesh (75 μm). Because the samples were similarly prepared within sets, their distributions below 75 μm were probably similar, and particle-size effects small. However these effects cannot be ruled out entirely. Although they appear to be negligible for silicon, they may possibly amount to 1 - 2% for the oxygen analysis of rocks.

TABLE 18

Oxygen and silicon X-ray intensities vs. particle-size of 8 mm SiO_2 targets

	Oxygen (counts/1000s)*		Silicon (counts/1000s)*	
Particle-size (μm)	Run No. 1	Run No. 2	Run No. 1	Run No. 2
< 75	6772	6829	25706	25810
75 - 105	6311	6568	25767	25589
105 - 150	6390	6637	25033	25477
> 150	4637	4896	23831	24142

* Fresh samples and new mylar supports were used between runs. Background was subtracted using a mylar support backed by polyethylene. The counting statistical errors were $\sim \pm 1.5\%$ for oxygen and $< \pm 1\%$ for silicon.

4.2.3 Experimental arrangement:

The source-sample-detector configuration used for quantitative analysis was the same as that used for the cross-section measurements except that the 8 mm upper collimator was removed (see Fig. 22). The sampling diameter was < 20 mm. Source II was used for excitation; the ^{210}Po activity at the time of data collection was $\sim$ 1.2 mCi. The spectrometer was operated as usual under high vacuum in the completely windowless mode.

4.3.4 Experimental data, calculations and results:

The system gain was in all cases $\sim$ 15 eV per channel. Count times ranged from 500 to 2000s. Example spectra of the slags and ores are shown in Fig. 27. Appropriate total absorption peaks were integrated between channels at full-width one-tenth maximum.

The results obtained for the blast-furnace slags are summarized in Tables 19 and 20. Values for S and CaO were obtained from a single spectrum. The deviations from the "true" values can be largely attributed to counting statistical errors. The negative intercepts of the linear regression fits to the calibration data

Figure 27. Examples of spectra used in blast-furnace slag and iron ore analyses.

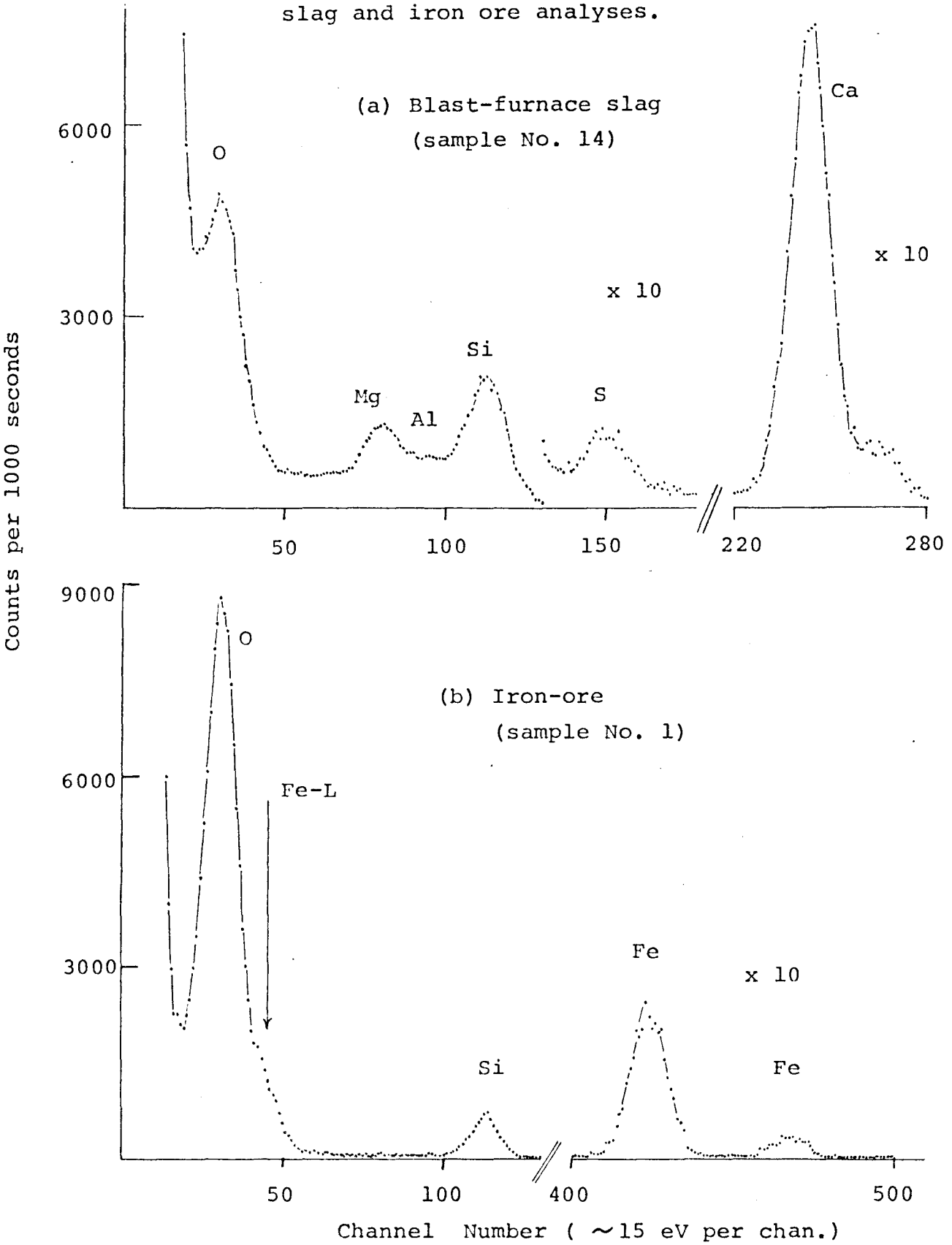

are puzzling; they seem to have no obvious physical explanation. A re-examination of the spectral data indicated background over-subtraction not to be the cause. Inclusion of the "zero-zero" point in the regression analysis slightly degrades the results.

The results of the iron ore analysis are given in Tables 21 and 22. The values for SiO_2 are reasonably good, bearing in mind the chemical method used to fix the "true" values, but again there is a negative intercept for the calibration data. The values found for Fe are not as good. In this case calibration was done simply by calculating the average counts per percent Fe from the standards; the small differences in Fe content and the counting errors did not sensibly allow a linear regression fit.

In an attempt to find a reason for the poor Fe results, the detector system was restored to its normal operating mode with the beryllium-windowed cap in place. And the ore samples were re-surfaced by polishing away the top few milligrams on felt cloths and by baking them for $\sim$ 20 hours at $110^{\circ}C$ in an effort to remove

TABLE 19

Results of blast-furnace slag analyses for sulphur

	Specimen	S content (%) Chemical analysis	Found values for "unknowns" Run No. 1	Run No. 2	Relative mean deviation of calibration points from regression fits/or mean found from wet-chem. value
Standards	14	1.39			- 2%
	15	2.11			- 2%
	16	2.53	Used for calibration		- 1%
	17	2.01			+ 3%
	18	2.01			+ 2%
"Unknowns"	4	2.09	2.22	2.27	+ 7%
	9	1.98	1.99	1.97	0%
	10	1.92	1.94	1.98	+ 2%
	19	2.22	2.17	2.31	+ 1%
	21	2.23	2.13	2.23	- 2%
	21		2.18	2.17	
	21		2.18	2.19	
	21		2.15	2.25	

The linear regression fits to the calibration points had slopes of 939 and 1061 counts per percent S and intercepts of -91 and -188 counts for runs 1 and 2 respectively.

The count-time was 1000s in each case.

The background was ∿ 100 counts and the counting statistical error associated with each measurement ± ∿ 2%.

The chemical analysis for sulfur was by furnace volatilization of sulphurous gases followed by their titration using the starch-iodide method. The precision (std. dev.) was ∿ 2%.

TABLE 20

Results of blast-furnace slag analyses for calcium oxide

	Specimen	CaO content (%) Chemical analysis	Found values for "unknowns" Run No. 1	Run No. 2	Relative mean deviations of calibration points from regression fits/or mean found from wet-chem. value
Standards	14	44.62			+ 0.6%
	15	39.45			- 0.2%
	16	42.27	Used for calibration		- 1.1%
	17	39.68			+ 0.2%
	18	38.58			+ 0.5%
"Unknowns"	4	38.9	39.1	39.5	+ 1.0%
	9	38.0	37.4	38.3	- 0.4%
	10	39.0	38.1	38.3	- 2.1%
	19	42.7	43.3	43.5	+ 1.6%
	21	39.9	39.5	39.8	0.0%
	21		39.5	39.7	
	21		40.1	40.4	
	21		40.7	39.8	

The linear regression fits to the calibration points had slopes of 245.2 and 304.4 counts per percent CaO and intercepts of -160 and -1270 counts for runs 1 and 2 respectively.

The count-time was 1000s in each case.

The background was ∿ 100 counts and the counting statistical error associated with each measurement ± ∿ 1.0%.

The chemical analysis for calcium was by atomic-absorption. The precision (std. dev.) was ∿1%.

TABLE 21

Results of iron ore analyses for silica

	Specimen	SiO_2 content (%) Chemical analysis	Found values for "unknowns" Run No. 1	Run No. 2	Relative mean deviation of calibration points from regression fits/or mean found from chem. value
Standards	1	9.47			+ 0.4%
	6	5.74			+ 1.0%
	13	7.53	used for calibration		- 1.8%
	19	8.53			+ 0.5%
	28	6.10			+ 0.1%
"Unknowns"	4	6.51	6.29	6.40	- 3.1%
	4		6.37	6.36	
	4		6.23	6.33	
	4		6.14	6.38	
	8	5.69	5.43	5.49	- 4.2%
	16	7.67	7.80	7.86	+ 2.1%
	22	8.78	9.05	8.96	+ 2.6%
	27	8.71	8.54	8.57	- 1.8%

The linear regression fits to the calibration points had slopes of 869 and 884 counts per percent SiO_2 and intercepts of -611 and -927 counts for runs 1 and 2 respectively.

The count-time was 1000s in each case. The background was ~250 counts and the counting statistical error associated with each measurement ± ~1.5%.

The chemical analysis for silica was by acid dehydration followed by HF volatilization of SiF_4 and the gravimetric determination of SiO_2 by difference. The precision (std. dev.) was ~1%.

TABLE 22

Results of iron ore analyses for iron

	Specimen	Fe content (%) Chemical analysis	Found values for "unknowns" Run No. 1	Run No. 2	Run No. 3	Mean	Relative error of mean
Standards	1	62.23	used for calibration				
	6	65.25					
	13	64.17					
	19	63.40					
	28	64.85					
"Unknowns"	4	65.50	63.2	65.4	62.4	63.4	- 3.3%
	4		63.0	61.9	63.0		
	4		63.8	64.3	64.4		
	4		63.7	63.4	63.3		
	8	65.50	65.5	66.9	66.0	66.1	+ 0.9%
	16	63.65	57.7	59.9	58.2	58.6	- 8.6%
	22	62.97	61.0	58.6	60.8	60.1	- 4.8%
	27	63.02	61.8	59.7	59.6	60.4	- 4.3%

The mean counts per percent iron (and associated standard deviations) for the standards were 52.1 (± 2.3%), 49.6 (± 3.6%) and 96.6 (± 1.4%) for runs 1, 2 and 3 respectively.

The count-time for runs 1 and 2 was 1000s, and for run 3 2000s. The background for runs 1 and 2 was ~80 counts and for run 3 ~160 counts. The counting statistical error associated with each measurement was ± ~2% for runs 1 and 2 and ± ~1.4% for run 3.

The chemical analysis for iron was by dichromate titration of Fe(II) to Fe(III). The precision (std. dev.) was < 0.5%.

surface-adsorbed contaminants. A series of experiments was then carried out using ^{109}Cd and ^{210}Po for X-ray excitation in an air path. The results are presented in Table 23. The figures for ^{109}Cd suggest strongly that the chemical analysis values are reliable. The figures for ^{210}Po suggest that the problem lies in the alpha-particle excitation but is not strongly related to alpha - particle energy or angle of entry. The results for Fe presented in Table 22 are all the more interesting since they have no correlation with the results for silica in Table 21 obtained from the same spectra (runs 1 and 2).

The calibration data for silicon in rocks and the results of the analyses are shown in Tables 24(a) and (b). The equivalent data for oxygen are in Tables 25(a) and (b). By comparing these tables with Table 16, it will be seen that the models used for photon absorption and enhancement corrections account for the major part of the previous discrepancies. Considerations of the alpha-particle and X-ray entry and emergence angles, and the different stopping-powers of the rocks for alpha-particles should yield further improvement.

TABLE 23

Fe K X-ray count-rates obtained from iron ore samples through excitation by ^{109}Cd and ^{210}Po in air paths

	Counts per percent Fe		
		^{210}Po*	
Specimen	^{109}Cd	Run No. 1	Run No. 2
1	560.6	312.9	201.1
4	547.7	299.6	193.0
6	555.7	307.5	206.9
8	556.1	307.2	202.8
13	561.4	323.1	210.3
16	555.8	283.6	191.1
19	558.8	296.5	196.8
22	556.5	297.8	194.3
27	554.6	291.4	196.4
28	554.8	297.8	198.2
Mean	556.2	301.7	199.1
Std. dev.	0.7%	3.7%	3.1%

* Source II, ∿ 1 mCi was used. In Run No. 1 the source-sample distance was ∿ 13 mm, and in Run No. 2 ∿ 4 mm. The sample detector distance was ∿ 15 mm in both runs.

TABLE 24

Results of silicate rock analyses for silicon

a) Calibration data

Rock	μ ($cm^2\ mg^{-1}$)	Fa	Counts/500s	% Si	Counts/%Si (actual)	Counts/%Si (from model)	Deviation of actual from model
NIM-D	1.57	1.00	13340	18.17	734	760	- 3.5%
NIM-G	1.01	1.45	39204	35.34	1109	1129	- 1.8%
NIM-L	1.23	1.23	23593	24.55	961	948	+ 1.4%
NIM-N	1.30	1.18	23324	24.51	952	907	+ 5.0%
NIM-P	1.31	1.17	21100	23.79	887	899	- 1.4%

The linear regression fit to Y vs. F_a according to the correction model (see subsection 4.3.2) yielded k_a = 1.12 and an intercept on the Y axis of -0.081

b) "Unknown" data

Rock	μ ($cm^2\ mg^{-1}$)	Fa	Counts/500s	Counts/% Si (from model)	% Si (found)	% Si (actual)	Relative error
BCR-1	1.27	1.20	24460	924	26.5	25.5	+ 3.9%
GSP-1	1.11	1.34	34431	1038	33.2	31.5	+ 5.4%
G-2	1.10	1.35	33963	1047	32.4	32.3	+ 0.3%

TABLE 25

Results of silicate rock analyses for oxygen

a) Calibration data

Rock	μ ($cm^2 mg^{-2}$)	F_a	F_e	Counts/500s	%O*	Counts/%O (actual)	Counts/%O (from model)	Deviation of actual from model
NIM-D	5.68	1.00	1.00	57362	42.5	1323	1351	-2.1%
NIM-G	5.61	1.02	0.39	53782	49.1	1096	1154	-5.0%
NIM-L	6.70	0.85	0.74	46270	44.2	1046	1069	-3.0%
NIM-N	7.20	0.79	0.57	45284	45.2	1003	946	+5.7%
NIM-P	5.69	1.00	0.73	56140	43.4	1295	1254	+3.2%

The linear regression fit to Y/F_a vs. F_e according to the correction model (see subsection 4.3.2) yielded $k_a = 0.75$ and $k_e = 0.27$.

b) "Unknown" data

Rock	μ ($cm^2 mg^{-1}$)	F_a	F_e	Counts/500s	Counts/%O (from model)	%O (found)	%O** (actual)	Relative error
USGS-BCR-1	7.30	0.78	0.69	43911	971	45.2	45.2	0.0%
USGS-GSP-1	6.18	0.92	0.40	49991	1045	47.8	48.0	-0.4%
USGS-G-2	5.90	0.97	0.39	50866	1094	46.5	48.3	-3.7%

* Calculated from stoichiometry.

** From direct measurements by neutron activation analysis by Volborth et al. (64). (In a study of eight USGS standard rocks, these authors found differences in the range 0.08 to 1.07% relative between stoichiometrically calculated and directly measured oxygen concentrations.)

4.4 Summary

The spectrometer and the general analytical approach have good potential for a variety of sample types. The accuracy of the method as applied has been mainly limited by counting statistics or the necessity for large absorption and enhancement corrections for photon processes. Other possible sources of errors such as non-representative sampling, particle-size effects and differences in alpha-particle stopping power appear to be small in comparison in the cases studied.

The results for Fe in the iron ore samples are disconcerting and no explanation has been found. Whether or not the problems are peculiar to the samples, to the element, or to heavier elements in general will only be determined through the analysis of many more samples.

CHAPTER 5

INFERENCES

5.1 Introduction

The previous chapters have indicated the capacity and limitations of the present experimental approach. The general inferences of the work however, need also to consider what may be reasonably achievable in the future. It is proposed in this chapter, therefore, to speculate upon the general features of an idealised system designed with respect to gained experience and recent or expected developments. The performance of the proposed equipment will be anticipated and comments made on possible improvements through better means of spectral analysis and absorption - enhancement corrections. Comparisons will be made with the work already carried out and methods of circumventing certain shortcomings will be indicated.

5.2 Future prospects

5.2.1. Equipment:

A. Excitation sources:

One of the most obvious misgivings associated with the method is its dependence upon potentially dangerous

radioisotopes. It is only through the useful and yet safe encapsulation of these that the method will find general application.

The problems encountered by this author and others with ^{210}Po are mentioned in Appendix 1. While ^{210}Po is convenient for basic studies, a better choice for more general use would be ^{244}Cm. Although less accessible, this isotope is more manageable than ^{210}Po (34,36), and its higher alpha-particle energies would allow thicker seals. ^{244}Cm also has a much more convenient half-life (17.6 years) and its photon output would increase sensitivity for elements between $Z \sim 20$ and 35, with little effect on lighter elements. There seems to be no obvious reason why safe and durable sources of the type shown in Fig. 28 should not be made with some technical effort; and with reasonable precautions used at room temperature.

B. Detection systems:

Good energy-resolution is crucial to the success of the method, especially where spectral interferences from L and M lines are present. While nothing better than Si(Li) detectors is in view, substantially better models than the one used in this work are now available.

Figure 28. Schematic diagram of idealised spectrometer system.

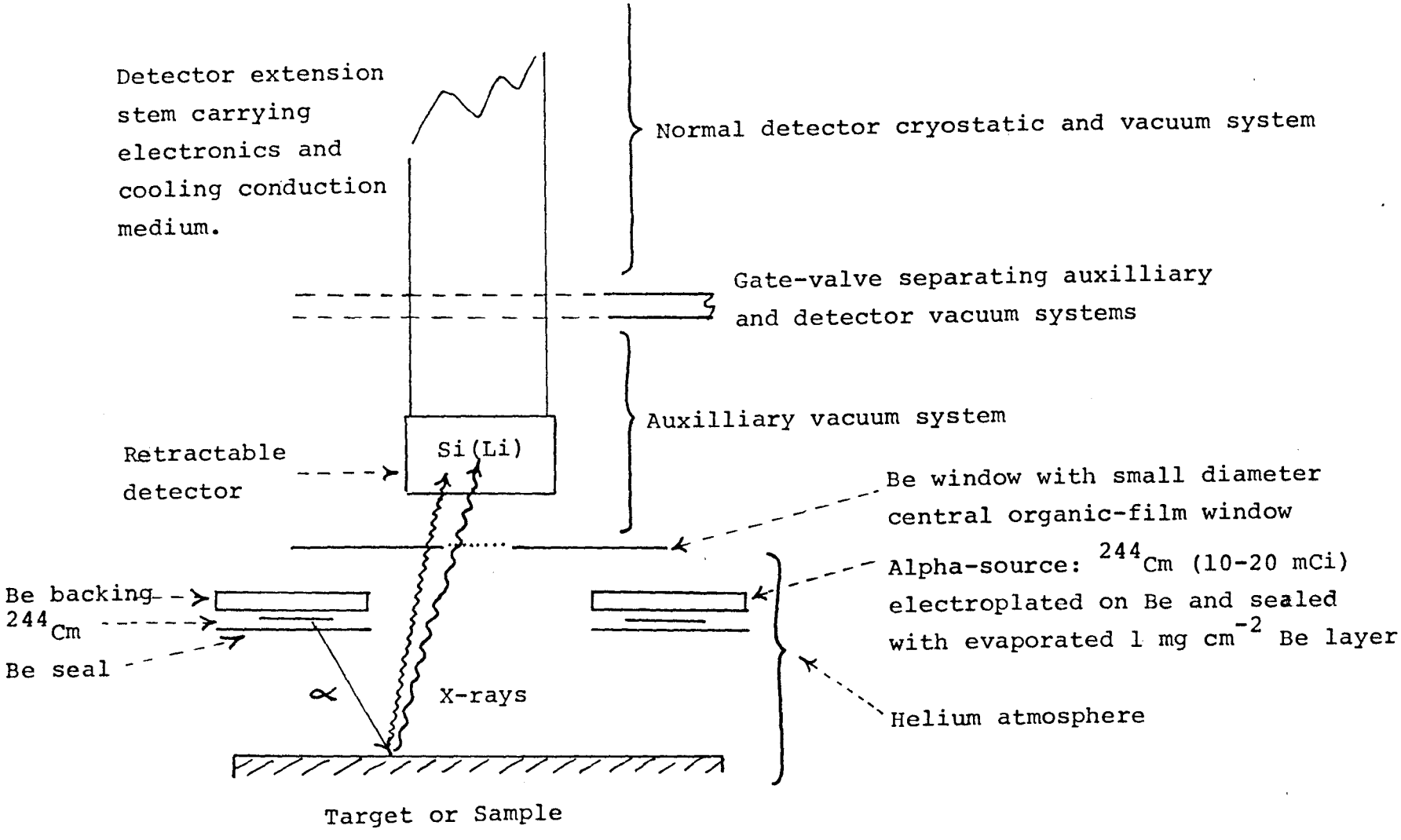

Windowless versions with resolutions of < 140 eV at 5.9 keV may be used as supplied* for the detection of X-rays to < 200 eV (44). The resolution of these detectors is < 100 eV at 1 keV and may be adequate for the separation of all elements above carbon. They usually operate through a gate-valve on a retractable stem. A system of this type is included in Fig. 28; the detector would only be moved into the secondary vacuum system during data acquisition.

The questions of silicon dead-layers and electrical contact layers remain. The former are responsible for reduced efficiency and sensitivity losses through background caused by incomplete charge-collection. There seems to be no complete remedy, and dead-layers $\ll 0.2$ μm are unlikely to be achieved. The latest evidence (65) suggests that at least this thickness is a fundamental property of detectors and is caused by their operation at liquid nitrogen temperature.

---

* Kevex Corporation, Burlingame, California, U.S.A.

Gold contacts, currently < 100 Å, are generally less problematic but leave room for improvement through the use of lighter metals. There seems to be a reluctance of manufacturers to move in this direction, but palladium, chromium and aluminum have been shown to be possible alternatives (66).

As to the long-term performance prospects of Si(Li) detectors, it has been suggested (40) that resolutions of ∿ 100 eV at 5.9 keV should be ultimately attainable, depending mainly on FET noise improvement. This would mean resolutions of < 60 eV at 1 keV and would considerably broaden the scope of the method.

C. Sample handling:

The presentation of samples under vacuum has drawbacks. It takes time; and certain materials sublime or outgas and need to be handled at very low temperatures. The use of a self-supporting very thin window as shown in Fig. 28 between samples and detector would obviate vacuum requirements and has been already suggested (40). Because of the very high production rates potentially achievable at low X-ray energies, the window need only be 1-2 mm

diameter and broader access to the detector could be via a standard beryllium window for higher energy X-rays. This would have the advantage of flattening the detector response across a wide range of the spectrum and of reducing the count-rate problems to be expected with the high-intensity excitation source proposed.

This author has shown 2 mm diameter 90 μg cm^{-2} mylar windows to be capable of sustaining a pressure differential of 1 atmosphere. Such windows may be used for elements down to carbon. But it is known that mylar is permeable to water vapour, and other materials may be better. Whatever is used is almost certain to be permeable to the helium atmosphere suggested. However, provided helium diffusion is not too fast, it should be easily removable from the detector vacuum system via an ion-pump. Other inert gases not susceptible to this problem may be used depending on the application.

5.2.2 Data treatment:

A. Spectral analysis:

In the present work energy-resolution was only barely adequate, and for quantitative analysis cases were selected where spectral interference was not severe.

With the potential improvements in detector performance suggested above, the situation should improve substantially.

In addition, computerized techniques of spectral analysis will be of great value. The excellent statistics attainable in the low-energy region where resolution is most critical presents a good situation for spectrum-stripping techniques, with only a small library of reference spectra required.

More recent techniques offer even better prospects. Fig. 29 shows the analysis of a blast-furnace slag spectrum by a method originated by Kennett (67). This approach requires only a knowledge of the peak shape and width, and offers great possibilities for improved resolution and data handling.

B. Absorption and enhancement corrections:

It has been shown that for elements down to silicon in samples of similar composition, absorption and enhancement effects are not severe. In such cases, the small corrections for these effects should be completely manageable with the fundamental data on mass-absorption coefficients and X-ray production cross-sections currently available

Figure 29. Improving resolution by a recent computerized technique of spectral analysis.

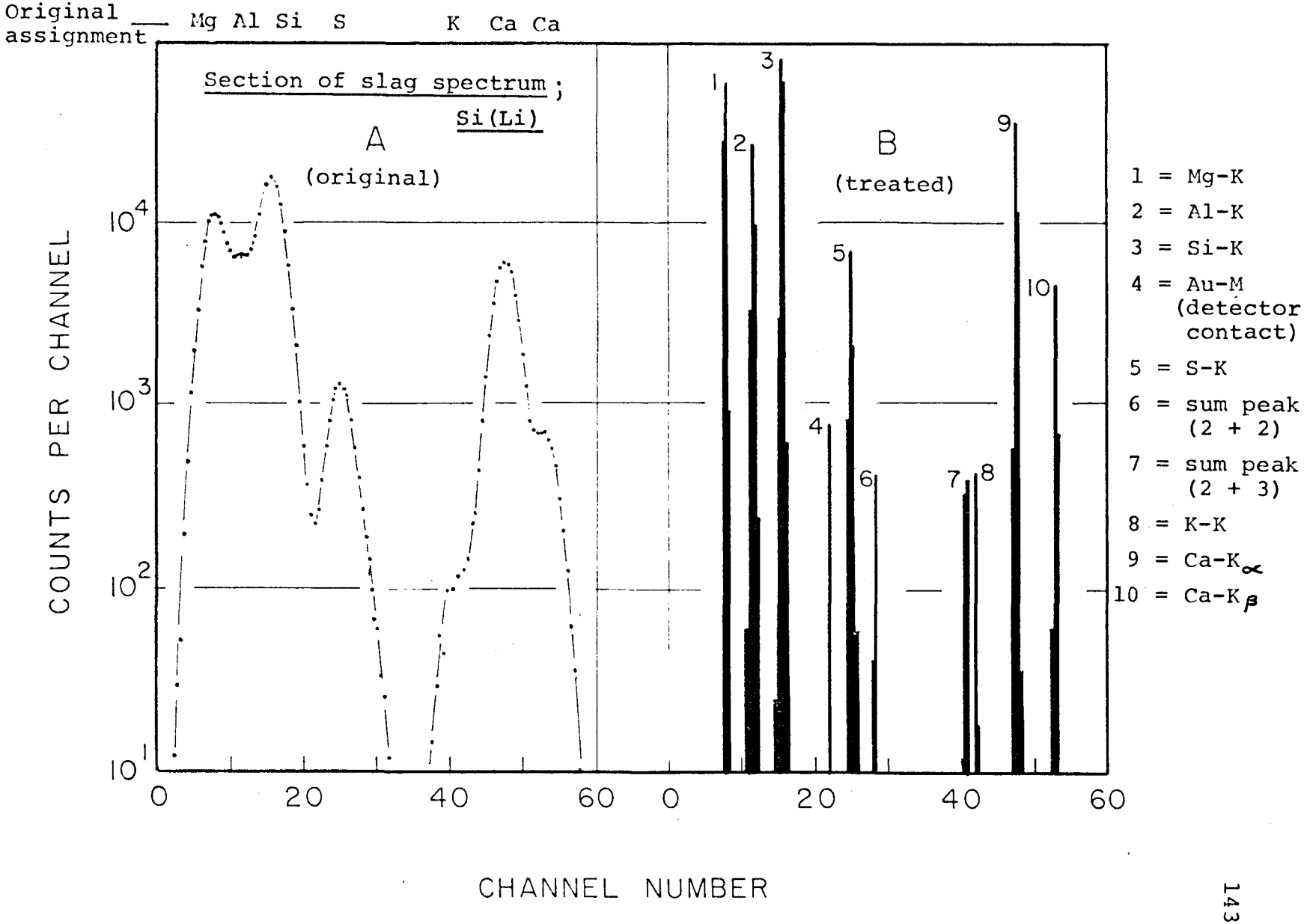

and with refined mathematical and computer techniques. For lighter elements in variable matrices the situation is quite different, especially with regard to the production cross-sections. Broadly speaking, the method will be hampered in the region where it is potentially of most value until accurate and comprehensive low-energy X-ray production cross-sections as a function of alpha-particle energies are available.

5.3 Concluding remarks

Some of the groundwork has been laid towards realizing the combined capabilities of alpha-particle emitters and semiconductor detectors as a practical analytical tool. And an attempt has been made to foresee the future prospects of the method.

Suggestions have been made for an improved spectrometer. Although some of these are speculative, applications to elements down to carbon at concentrations on the order of 0.1% in suitable circumstances should be within reach in the near future. With a completely windowless system, there may be scope for analytical work down to < 200 eV, but the difficulties of working in this region of the X-ray spectrum should not be underestimated.

Within the framework of X-ray spectrometry, a nuclear-particle accelerator and a multi-channel wavelength-dispersive system would no doubt offer the best prospects for light-element analysis. However, the simpler approach presented in this thesis may well match the above combination on a practical level in many cirumstances. Overall, the results are encouraging for a technique yet in its early stages of development.

6. APPENDIX 1

FABRICATION AND LEAK-TESTING OF ^{210}Po SOURCES

A1.1 General information

^{210}Po is a hazardous radioisotope and notorious for the complexity and unpredictability of its chemical and physical behaviour, particularly its predisposition to diffuse, migrate or volatilise. Bagnall (68) and Sellers et al. (34) have made some observations in this regard. It was therefore to be expected that some difficulties would be encountered in source preparation. This turned out to be so; although sources adequate for the present purposes were made, their suitability for general use cannot be claimed. The limited experiences of this author with ^{210}Po tend to confirm those of others.

Since the excitation sources were on the order of 1 mCi ^{210}Po, about 10^4 times the maximum permissible body-burden, all work in their fabrication was carried out in a "hotlab" glovebox. Pilot work with activities < 10 μCi was carried out in a radioisotope laboratory fumehood. All manipulations of the isotope were closely monitored by the McMaster University Health Physics group.

All counting of alpha-radioactivity was done with a gas-flow windowless proportional counter.

Carrier-free ^{210}Po was supplied in dilute HNO_3 solution from two vendors: The Radiochemical Centre Ltd., Amersham, Bucks, England; and New England Nuclear, Boston, Mass., U.S.A.

The beryllium source backings were machined to order by Magna Electronics of Toronto. The colloidal suspension of graphite in isopropanol used for sealing was product number 154 supplied by Acheson Colloids Co., Port Huron, Mich., U.S.A.

A1.2 Fabrication

There were several properties desirable in the excitation sources: a) easy fabrication with a minimum of chemical operations, b) backing and containment materials giving rise to little interfering secondary emissions, or greatly degrading the output alpha-particle energy, and c) good stability and integrity in vacuum ($< 10^{-6}$ mm Hg) over at least several months.

It was decided from the outset, in meeting points a) and b) above, to spontaneously electrodeposit

^{210}Po upon beryllium backings (spontaneous deposition may take place upon several less noble metals (68), and ^{210}Po - Be neutron sources can be made in this way (69)). It was hoped that point c) would be automatically met, i.e. that the deposit, presumably metallic Po, would strongly adhere to the substrate and not volatilise. The removal of ^{210}Po by abrasion was not considered a danger since sources would be stored in an inacessible place in the spectrometer.

In preliminary experiments, machined but otherwise unfinished beryllium backings were used. These were cup-shaped and designed to contain the deposition solution as well as provide the desired annular source distribution. The deposition solutions were dilute strong acids. Under these conditions deposition could occur very rapidly, e.g. $\sim$ 50% in 5 minutes upon a 2 cm^2 surface from 2 ml 0.1 M HCl. However the unsealed sources prepared in this way had two bad characteristics. Firstly, the rough and corrosion-pitted deposition surface led to considerable broadening of the output alpha-particle spectrum. And secondly, leak testing at room temperature showed potentially dangerous volatilisation of ^{210}Po, the extent of the losses

increasing rapidly with decreasing storage pressure.

From the above experiences it was evident that some changes in approach were needed. Further experiments showed that volatility losses could be substantially reduced at liquid-nitrogen temperature (77°K), even under high vacuum.* It was therefore decided that all future sources should be used under these conditions and that they should be sealed. It was further decided that the deposition should take place on a flat, polished surface under milder conditions of acidity to facilitate sealing and to decrease alpha-particle straggling.

After more preliminary experiments the procedure adopted for the preparation of source I (see subsection 2.2.2) was as follows: a) the HNO_3 solution in which the ^{210}Po was supplied was gently evaporated to dryness and the isotope then redissolved in 1 M acetic acid, b) the acetic acid solution was then placed

---

* This suggests that the loss mechanism is mainly sublimation rather than aggregate recoil.

inside the teflon-beryllium assembly shown in Fig. A1 - the beryllium having been polished* to a mirror finish and solvent (CCl_4) washed - and the deposition allowed to take its course. The results of three trial runs are shown in Table A1. Sealing was accomplished by three immersions of the sources in a ten-times dilution of the graphite suspension mentioned in section A1.1. A separate graphite suspension supply was used for each immersion and the solvent was allowed to completely evaporate between immersions.

Although the above procedure was reasonably satisfactory, some problems remained. Localised corrosion in a few spots was evident, leading to corresponding non-uniformities in the seal and alpha-particle straggling; the activity was not necessarily evenly deposited, although this was not a major shortcoming owing to the symmetry of the source-sample-detector arrangement; there was still

---

* Precautions were taken in this procedure owing to the toxicity of beryllium when in finely divided form. Polishing was done in a fume-hood on a felt cloth with 5 μm alumina grinding powder and ample water present to suppress Be dust. The cloths and alumina paste were disposed of in sealed containers with non-combustible radioactive waste for burial.

Figure A1. The teflon-beryllium assembly used for spontaneous electrodeposition of ^{210}Po.

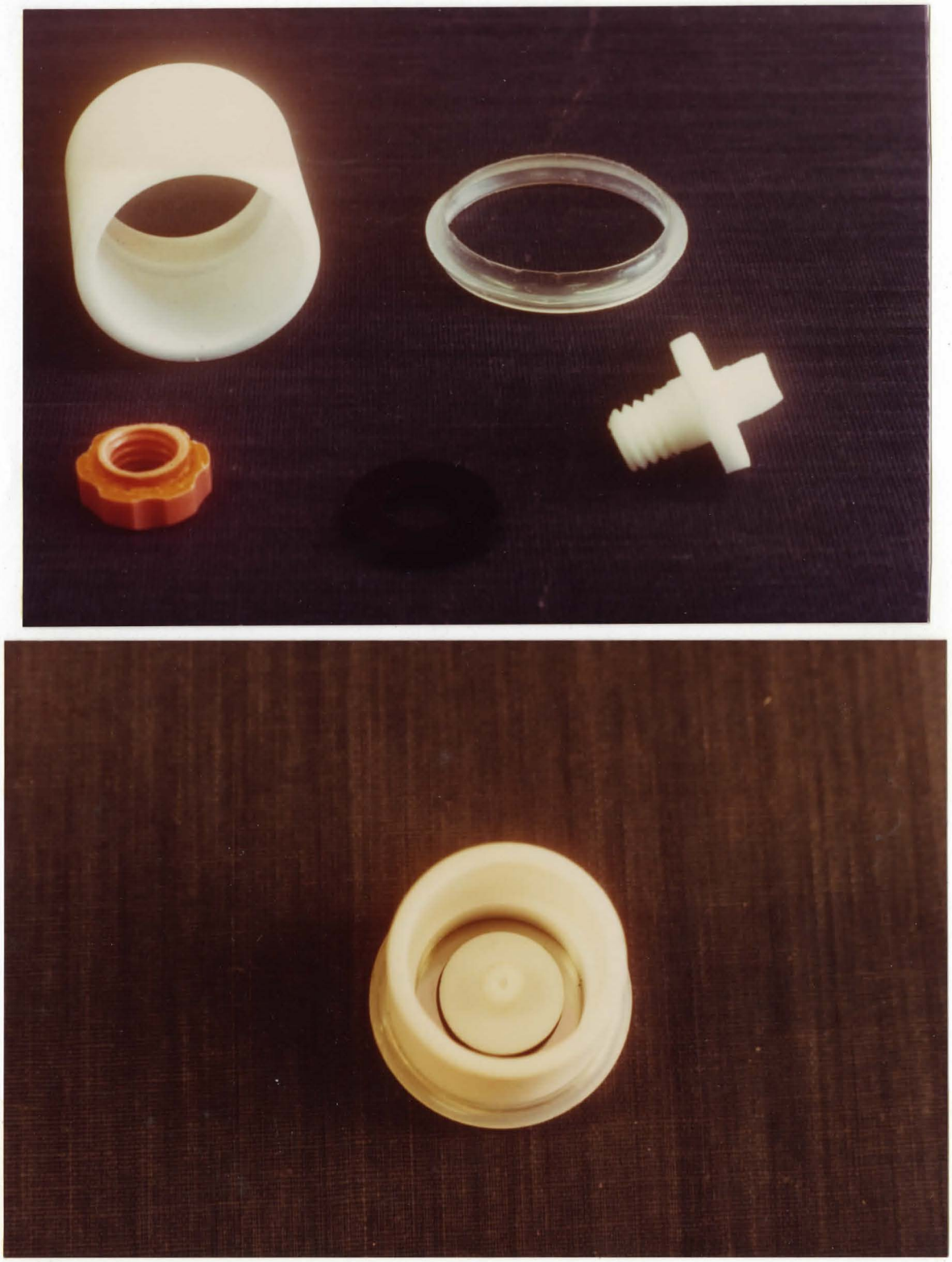

TABLE A1

Spontaneous electrodeposition of ^{210}Po upon beryllium annuli from 1 M acetic acid solution (see text p.)

Elapsed deposition time, hours	10 µℓ aliquot from 2 mℓ deposition solution, cp 5m*		
	Run No. 1	Run No. 2	Run No. 3
0.0	2054	2079	2687
0.25	1787		
1.0	1578		
2.0		1532	1861
2.5	1272		
3.8	1150		
8.0	734		
13.3		550	
14.7		460	
19.0			512
19.3		323	
21.0	74 (terminated)		
26.0			289
28.0		148	
39.0		83	
41.0		82 (terminated)	
43.0			85
45.0			59 (terminated
Total activity on Be annulus, cp 5 m*	412484	416066	586617

*50% counting efficiency

evidence of small ^{210}Po losses by volatilisation from sources stored under vacuum at liquid-nitrogen temperature.

Several further changes were made for the preparation of source II (see subsection 2.2.2) : a) the beryllium disc, after polishing and immediately before the start of the deposition process, was immersed in fuming nitric acid for 1 minute followed by water and methanol rinses, b) 10 µg of copper as the acetate was added to the deposition solution (compared to < 1 µg Po), c) the acetic acid solution concentration was reduced to 0.17 M from 1 M, and d) the solution was manually mixed by swirling gently for 1 minute every 5 minutes throughout the deposition process. The sealing procedure was identical to that used for source I except that only two immersions were used.

The variations were introduced with the following thoughts in mind : a) the HNO_3 treatment may give an electrochemically uniform surface and thereby aid uniform activity distribution, b) the incorporation of ^{210}Po within a Cu deposit may reduce its volatility and break

up aggregates, c) the reduced acid concentration may reduce corrosion and weaken complexation of ^{210}Po which could hinder its deposition, and d) active homogenisation of the solution should help uniform activity distribution, speed deposition, and disperse corrosion-promoting gas-bubbles.

The courses of three trials of the modified procedure are shown in Table A2. Visual inspection of the sources indicated the copper to be evenly distributed, and no significant corrosion of the beryllium surface. Fig. A2 shows a photomicrograph of a section of one weak source (Run No. 3) before sealing. Source II showed improvement over source I with respect to alpha-particle straggling and activity distribution; but showed little improvement with respect to activity leakage.

A1.3 Leak testing

Volatility-leak testing was carried out with the finished sources inside an obsolete Ge(Li) detector cryostat. Filter-paper swipes were suspended $\sim$ 2 mm above the deposition surface to catch volatilized ^{210}Po activity. Swipes taken from the inside walls of the

TABLE A2

Spontaneous electrodeposition of ^{210}Po upon beryllium annuli from 0.17 M acetic acid

(see text p.)

Elapsed deposition time, minutes	Run No. 1: 20 µℓ aliquot from 1 mℓ deposition solution, cp 10 m*	Run No. 2: 20 µℓ aliquot from 1.25 mℓ deposition solution, cp 10 m*
0	4571	4354
30		2134
45	2041	
65		990
90	627	540
120		273 (terminated)
135	346 (terminated)	
Total activity on Be annulus, cp 10 m*	209545	219216

*50% counting efficiency

Figure A2. Photomicrograph of ^{210}Po co-deposited with copper on beryllium backing.

(magnification X 6)

cryostat cavity after termination of each test always indicated negligible activity.

Table A3 summarizes the results from the testing of an unsealed source and sources I and II. It is suspected that most of the volatility-leakage shown for sources I and II at liquid nitrogen temperature occurred during the cool-down and warm-up periods of the storage cycle. The reasons for this thinking are twofold : a) long-term use of these sources in the spectrometer gave very little contamination of the detector surface and no alpha-particle activity was found inside the sample-chamber or on targets, and b) there is little difference between the short-term and long-term figures obtained for source II at liquid-nitrogen temperature.

Surface swipes with filter paper of source I showed that appreciable quantities of activity could be removed by abrasive contact, indicating entrainment of ^{210}Po within the carbon seal. Two such swipes gave count rates of 52 and 143 cp 2m. It was noticed that the graphite suspensions used for sealing were slightly contaminated with ^{210}Po after use. Presumably then,

TABLE A3

Volatility-leakage of ^{210}Po sources on beryllium backings

Test conditions	Activity on catcher swipe, cpm.* (duration of test)		
	400 μCi source, unsealed	800 μCi source I, 120 μg cm^{-2} carbon seal	1500 μCi source II, 80 μg cm^{-2} carbon seal
Room temperature and pressure	5330 (30 days)	740 (2 days)	589 (2 days)
Liquid-nitrogen temperature, < 10^{-6} mm Hg pressure	871 (14 days)	25 (2 days)	32 (2 days) 16 (10 days)

* 50% counting efficiency

during the drying periods after source immersion, some ^{210}Po goes into solution and is brought to the surface where the evaporation of the solvent is occurring. As mentioned earlier, this did not have serious consequences here but certainly makes the sources unfit for general routine use.

7. APPENDIX 2

DERIVATIONS OF EQUATIONS

A2.1 Escape peak intensity

Consider monochromatic radiation of intensity I_o

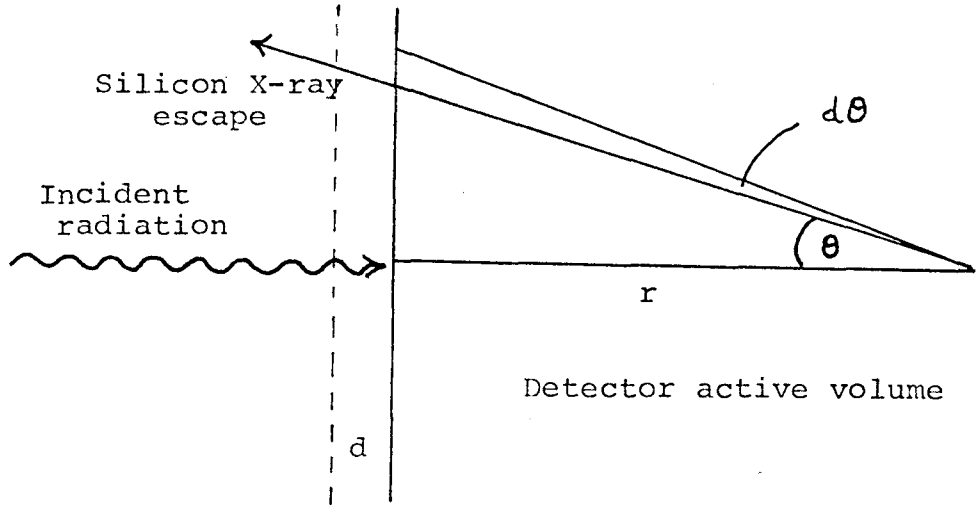

incident normally upon the Si(Li) detector surface, as shown. The change in intensity in traversing an increment of detector thickness, dr, located at depth r is $\mu_1 I_o e^{-\mu_1 r} dr$, where μ_1 is the mass absorption coefficient of silicon for the incident radiation. Of the events occurring at depth r, the fraction giving rise to Si K X-rays is $F\omega$, where F is the Si K-shell ionisation contribution to μ_1 and ω is the Si K-shell fluorescence yield. The transmission of these X-rays through an annular increment of detector surface-area defined by an angular increment d0 is $\sin 0 d0/2$,

assuming no attenuation. However attenuation along the path occurs in both the fully active detector material and the dead-layer of thickness d ; the appropriate transmission is $e^{-\mu_2(r+d)\sec\theta}$, where μ_2 is the mass absorption coefficient of silicon for Si K X-rays. The escape peak intensity therefore arising from depth increment dr, through a solid angle defined by $d\theta$ is

$$dI = \frac{\mu_1 I_o F_\omega}{2} \; e^{-\mu_1 r} e^{-\mu_2(r+d)\sec\theta} \sin\theta dr d\theta$$

The escape peak probability is given by integration of this expression and is

$$\frac{I_{\text{escape}}}{I_o} = \frac{\mu_1 F\omega}{2} \int_{r=o}^{\infty} \int_{\theta=o}^{\pi/2} e^{-\mu_1 r} e^{-\mu_2(r+d)\sec\theta} \sin\theta d\theta dr.$$

This in turn may be integrated numerically by recognizing that $\sin\theta d\theta = d\cos\theta$ and $1/\sec\theta = \cos\theta$; and by rewriting the equation as

$$\frac{I_{\text{escape}}}{I_o} \sim \frac{\mu_1 F\omega}{2} \int_{o}^{a} \int_{o}^{1} e^{-r\left(\mu_1 + \frac{\mu_2}{x}\right)} e^{-\frac{d\mu_2}{x}} dx dr.$$

Here, $x=\cos\theta$; and the limit, a, is taken for computing convenience to be the detector depth from which no significant fraction of Si X-rays escape.

A2.2 Self-absorption corrections

A: Homogeneously irradiated targets

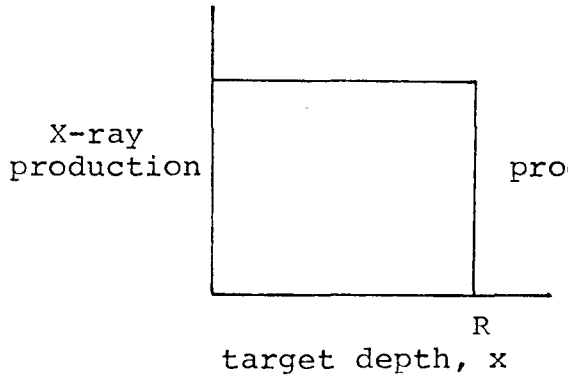

B: "Triangularly" irradiated targets

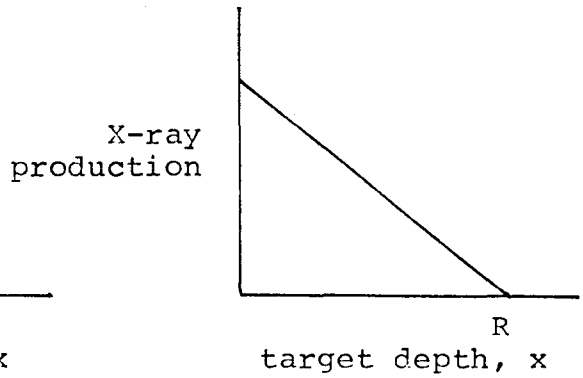

The fraction of photons escaping normally to the front surface of the target is in case A:

$$T = \frac{\int_0^R e^{-\mu x} dx}{\int_0^R dx} = \frac{1-e^{-\mu R}}{\mu R} ;$$

and in case B:

$$T = \frac{\int_0^R (1-\frac{x}{R}) e^{-\mu x} dx}{\int_0^R (1-\frac{x}{R}) dx}$$

$$= \frac{2}{\mu R}[(1-e^{-\mu R}) - \frac{2}{\mu R}(1-(1+\mu R)e^{-\mu R},]$$

8. REFERENCES

(1) R.D. EVANS, The Atomic Nucleus, McGraw-Hill Inc., New York/Toronto/London (1955).

(2) L.S. BIRKS, X-ray Spectrochemical Analysis (2nd. edition), John Wiley and Sons, New York/London/Sydney/Toronto (1969).
_____, Electron Probe Microanalysis (2nd. edition), same publisher (1971).

(3) R. WOLDSETH, X-ray Energy Spectrometry, Kevex Corporation, Burlingame, California (1973).

(4) E.P. BERTIN, Principles and Practice of X-ray Spectrometric Analysis (2nd. edition), Plenum Press, New York (1975).

(5) H.G.J. MOSELEY, Phil. Mag., 26 (1913), 1024; 27 (1914), 703.

(6) H.R. BOWMAN, E.K. HYDE, S.G. THOMPSON and R.C. JARED, Science, 151 (1966), 562.

(7) R.D. GIAUQUE, F.S. GOULDING, J.M. JAKLEVIC and R.H. PEHL, Anal. Chem., 45 (1973), 671.

(8) F.S. GOULDING, J.M. JAKLEVIC, B.V. JARRETT and D.A. LANDIS, in Advances in X-ray Analysis (K. Heinrich, Ed.), 15, 470-482, Plenum Press, New York (1972).

(9) B.L. HENKE, in Advances in X-ray Analysis (W. Mueller, Ed.), 7, 460-488, Plenum Press, New York (1964).

(10) J.I. GOLDSTEIN and J.W. COLBY, in Practical Scanning Electron Microscopy (J. Goldstein and H. Yakowitz, Eds.), 435-487, Plenum Press, New York/London (1975).

(11) A. HERBERT and K. STREET, Anal. Chem., 46 (1974), 203.

(12) J.R. RHODES, in Energy Dispersion X-ray Analysis, pp. 243-285 of publication STP 485 of the American Society for Testing and Materials, Philadelphia (1971).

(13) J.A. COOPER, Nucl. Instr. and Meth., 106 (1973), 525.

(14) T.J. KNEIP and G.R. LAURER, Anal. Chem., 44 (1972), 57A.

(15) A.R. HAWTHORNE and R.P. GARDNER, Anal. Chem., 48 (1976), 2130.

(16) J. CHADWICK, Phil. Mag., 24 (1912), 594.

(17) W. BOTHE and H. FRANZ, Zeit fur Phys., 49 (1928), 1.

(18) Ibid., 52 (1929), 466.

(19) W. HENNEBERG, Z. Physik, 89 (1933), 592.

(20) E. MERZBACHER and H.W. LEWIS, in Handbuch der Physik (S. Flugge, Ed.), 34, 166-192, Springer Verlag, Berlin (1958).

(21) J.M. KHAN, D.L. POTTER and R.D. WORLEY, Phys. Rev., 139 (1965), A1735.

(22) J.D. GARCIA, R.J. FORTNER and T.M. KAVANAGH, Rev. Mod. Phys., 45 (1973), 111.

(23) C. RUTLEDGE and R. WATSON, At. Data Nucl. Data Tables, 12 (1973), 195.

(24) Atomic Inner-Shell Processes, (B. Crasemann, Ed.), Academic Press, New York (1975).

(25) J.M. KHAN, D.L. POTTER and R.D. WORLEY, J. Appl. Phys., 37 (1966), 564.

(26) R.R. HART, N.T. OLSEN, H.P. SMITH Jr., and J.M. KHAN, J. Appl. Phys., 39 (1968), 5538.

(27) J.A. CAIRNS, D.F. HOLLOWAY and R.S. NELSON, in Advances in X-ray Analysis (C. Barret, Ed.), 14, 173-183, Plenum Press, New York (1971).

(28) T.B. JOHANSSON, R. AKSELSSON and S.A.E. JOHANSSON, Nucl. Instr. and Meth., 84 (1970), 141.

(29) F. FOLKMANN, J. Phys. E: Sci. Instr. 8 (1975), 429.

(30) S.A.E. JOHANSSON and T.B. JOHANSSON, Nucl. Instr. and Meth., 137 (1976), 473.

(31) Proceedings of the first international conference "Particle-Induced X-ray Emission (PIXE) and Its Analytical Applications", Lund, Sweden, August 1976, published in Nucl. Instr. and Meth., 142 (1977).

(32) A. ROBERT, Commissariat à ℓ' Energie Atomique, Rapport CEA-R 2539 (1964).

(33) H. IMAMURA, K. UCHIDA and H. TOMINAGA, Radioisotopes, 14 (1965), 286.

(34) B. SELLERS, United States Atomic Energy Commission Report NYO-3491-1 (1966).

(35) B. SELLERS, J. PAPADOPOULOS and H. WILSON, ibid. NYO-3491-2 (1967).

(36) B. SELLERS, H. WILSON and F.A. HANSER, ibid. NYO-3491-3 (1968).

(37) L. ADLER and J. TROMBKA, in Geochemical Exploration of the Moon and Planets, pp. 67-74, Springer Verlag, New York/Heidelberg/Berlin (1970).

(38) E. FRANZGROTE, in Advances in X-ray Analysis (K. Heinrich, Ed.), 15, 388-406, Plenum Press, New York (1972).

(39) R. HIGHT and C.L. FOSTER, in Advances in X-ray Analysis (W. Pickles, Ed.), 18, 333-342, Plenum Press, New York (1975).

(40) W.D. AITKEN and E. WOO, in Energy Dispersion X-ray Analysis, pp. 36-56 of publication STP 485 of the American Society for Testing and Materials, Philadelphia (1971).

(41) E. ELAD and D.A. GEDCKE, in Proceedings of the Sixth International Conference on X-ray Optics and Micro-analysis (G. Shimoda et al., Eds.), pp. 263-270, University of Tokyo Press (1972).

(42) S.T. THORNTON, R.H. McKNIGHT and R.R. KARLOWICZ, Phys. Rev., A10 (1974), 219.

(43) J. JAKLEVIC and F. GOULDING, IEEE Trans. Nucl. Sci., 18 (1971), 187.

(44) R.G. MUSKET, Nucl. Instr. and Meth., 117 (1974), 385.

(45) W. BAMBYNEK, B. CRASEMANN, R.W. FINK, H.U. FREUND, H. MARK, C.D. SWIFT, R.E. PRICE and P.V. RAO, Rev. Mod. Phys., 44 (1972), 716.

(46) W.J. VEIGELE, E. BRIGGS, B. BRACEWELL and M. DONALDSON, Report KN-798-69-2 (R) of Kaman Nuclear, a division of Kaman Sciences Corporation, 1700 Garden of the Gods Road, Colorado Springs, Colorado 80907, U.S.A.

(47) J.S. HANSEN, J.C. McGEORGE, D. NIX, W.D. SCHMIDT-OTT, I. UNUS and R.W. FINK, Nucl. Instr. and Meth., 106 (1973), 365.

(48) J.L. CAMPBELL and L.A. McNELLES, Nucl. Instr. and Meth., 117 (1974), 519.

(49) J.H. SCOFIELD, Phys. Rev., A9 (1974), 1041.

(50) C.G. SOARES, R.D. LEAR, J.T. SANDERS and H.A. VAN RINSEVELT, Phys. Rev., A13 (1976), 953.

(51) F.D. McDANIEL, T.J. GRAY and R.K. GARDNER, Phys. Rev., A11 (1975), 1607.

(52) R.H. McKNIGHT, S.T. THORNTON and R.R. KARLOWICZ, Phys. Rev., A9 (1974), 267.

(53) J.M. HANSTEEN and O.P. MOSEBEKK, Nucl. Phys., A201 (1973), 541.

(54) J.D. GARCIA, Phys. Rev., A1 (1970), 280.

(55) J.B. CROSS, R. ZEISLER and E.A. SCHWEIKERT, Nucl. Instr. and Meth., 142 (1977), 111.

(56) P.M.A. VAN DER KAM, R.D. VIS and H. VERHEUL, Nucl. Instr. and Meth., 142 (1977), 55.

(57) F. FOLKMANN, C. GAARDE, T. HUUS and K. KEMP, Nucl. Instr. and Metho., 116 (1974), 487.

(58) R. AKSELSSON and T.B. JOHANSSON, Z. Physik, 266 (1974), 245.

(59) H.J.M. BOWEN, in Advances in Activation Analysis (J. Lenihan and S. Thomson, Eds.), Volume 1, pp. 101-113, Academic Press, London/New York (1969).

(60) J. JONES, American Laboratory, March 1976, p. 15, (monthly publication of International Scientific communications Inc., 808 Kings Highway, Fairfield, Connecticut 06430, U.S.A.

(61) D.M. SHAW, McMaster University, Dept. of Geology, (personal communication).

(62) F.J. FLANAGAN, Geochimica and Cosmochimica Acta., 37 (1973), 1189.

(63) L.C. NORTHCLIFFE and R.F. SCHILLING, Nucl. Data Tables, 7 (1970), 233.

(64) A. VOLBORTH, G.E. MILLER and C.K. GARNER, Chemical Geology, 20 (1977), 85.

(65) F.S. GOULDING, Nucl. Instr. and Meth., 142 (1977), 213.

(66) C. INSKEEP, E. ELAD and R.A. SAREEN, IEEE Trans. Nucl. Sci., 21 (1974), 379.

(67) T.J. KENNETT, McMaster University, Dept. of Physics, (personal communication on work to be published in Nucl. Instr. and Meth.).

(68) K.W. BAGNALL, Chemistry of the Rare Radioelements, Butterworth Scientific Publications, London (1957).

(69) Polonium, (H.V. Moyer, Ed.), United States Atomic Energy Commission, Report TID-5221 (1956).